Comparative Analysis of Muscle Architecture and Myosin Heavy Chain Content in the Forelimbs of Geomyid and Heteromyid Burrowing Rodents

by

Jordan T. Fain

Submitted in Partial Fulfillment of the Requirements

for the Degree of

Master of Science

in the

Biological Sciences

Program

YOUNGSTOWN STATE UNIVERSITY

August, 2021

Comparative Analysis of Muscle Architecture and Myosin Heavy Chain Content in the Forelimbs of Geomyid and Heteromyid in Burrowing Rodents

Jordan T. Fain

I hereby release this thesis to the public. I understand that this thesis will be made available from the OhioLINK ETD Center and the Maag Library Circulation Desk for public access. I also authorize the University of other individuals to make copies of this thesis as needed for scholarly research.

Signature:

Jordan T. Fain, Student	Date

Approvals:

Dr. Michael T. Butcher, Thesis Advisor	Date
Dr. Thomas P. Diggins, Committee Member	Date
Dr. Alexis A. Moore-Crisp, Committee Member	Date
Dr. Salvatore A. Sanders, Dean, College of Graduate Studies	Date

ABSTRACT

Geomyid and heteromyid rodents demonstrate a range of limb morphology. In particular, subterranean/fossorial pocket gophers have hypertrophied forelimbs with large mechanical advantage (MA) for burrowing, whereas those of semi-fossorial pocket mice and kangaroo rats are smaller in size and lack MA, yet these taxa are capable of digging elaborate burrow systems similar to gophers. To better understand the functional capacity of their forelimb musculature, dissections of Botta's pocket gopher (*Thomomys bottae*; N=10), desert pocket mouse (*Chaetodipus penicillatus*; N=5), and Merriam's kangaroo rat (*Dipodomys merriami*; N=3) were conducted to quantify limb MA, muscle architectural properties, and myosin heavy chain (MHC) isoform content. As expected, metrics indicating MA varied significantly larger in *T. bottae* than in both *C. penicillatus* and *D. merriami*. With the exception of the humeral retractors, however, the latter two taxa generally have longer, parallel fascicles and shorter moment arms in the power stroke muscle functional groups resulting in larger facicle length to muscle length (L_F/ML) and facicle length to moment arm (L_F/r_m) ratios than pocket gophers. Nevertheless, the humeral retractors of *C. penicillatus* and *D. merriami* are observed to have large force per unit mass by physiological cross-section area to muscle mass (PCSA/MM) ratios nearly 2x those of *T. bottae*. PCSA/MM ranged from 1.0–3.0 in all pocket mouse and K-rat muscle groups analyzed. MHC content is also notably faster in *C. penicillatus* and was only species to express fast MHC-2B, whereas slow MHC-1 isoform expression was low, but specific to *T. bottae*. All three species mainly expressed fast MHC-2A and -2X with each isoform showing some relationship with body size. The findings provide evidence that pocket mice and K-rats compensate for their lack of MA by their forelimb muscles being capable of both large intrinsic contractile velocity and size-scaled force production, which match well with functional data that they not only cycle their limbs faster than specialized pocket gophers, but also may exert larger substrate reaction forces during scratch-digging. Future work is needed to identify MHC isoform expression in a broader diversity of burrowing taxa, which should include evaluations of recovery stroke muscles and their roles in scratch-digging.

ACKNOWLEDEMENTS

I sincerely thank my graduate advisor, Dr. Michael Butcher, for his guidance, patience, and mentoring throughout my Thesis research project and Masters Degree. I thank my graduate committee members, Drs. Thomas Diggins and Alexis Moore-Crisp, for their critical reviews of my Thesis, manuscript, and helpful comments. I am especially thankful for Dr. Diggins for help with statistics. I thank Dr. Rachel Olson and Zachary Glenn for initial dissection data from pocket gophers. I am also grateful to Dr. Rachel Olson for her guidance with DICE-CT protocols. A special thank you to Dr. Jesse Young (NEOMED) and Sharon Usip (NEOMED) access to and assistance with μ-CT scanning and visualization software. Thanks to Amelia Sprague and Branson Brownfield for help with 3D limb reconstructions. Thanks to Alexis Sullivan, Noah Chrestay, and Anna Turnbull for assistance with dissection and data entry. I am thankful for Dakota Morgan, Michael Deak, A.J. McKamy, and Dragan Juzbasich, who are terrific lab mates, and gave me support throughout my tenure at YSU. The Department of Chemical and Biological Sciences is additionally acknowledged. Finally, a Cushwa/Commercial Shearing Fellowship award funded my graduate assistantship AY 2020–2021.

DEDICATION

I dedicate this to my patient significant other that spent a lot of time supporting and helping me throughout this process. I also dedicate this to my friends that helped me continue to succeed. This would not have been possible without the guidance and help from my advisor, Dr. Michael Butcher. Lastly, I would like to thank my family for all their love and support that pushed me to strive for success.

TABLE OF CONTENTS

LIST OF TABLES

LIST OF FIGURES

INTRODUCTION

Pocket gophers are members of the family Geomyidae (order Rodentia) with populations concentrated in the desert biomes of the southwestern United States (Smith, 1998; Wilkins and Roberts, 2007). Burrowing behavior is critical to resource acquisition in pocket gophers and coupled with their subterreanean lifestyle, their functional habits are considered to be fossorial (Jones and Baxter, 2004). Fossorial is defined here as subterreanean mammals that have specializations for digging intricate burrows. Pocket gophers share their habitat with numerous other burrowing rodents, including pocket mice and kangaroo rats (K-rats) (Randall, 1993). Both latter taxa belong to the family Heteromyidae, which is a sister group of the Geomyidae (Lessa and Stein, 1992). Being sympatric relatives of pocket gophers (e.g., *Thymomys*), pocket mice and K-rats must burrow in very dry earth for protection from predators, despite their lack of obvious forelimb modifications for digging (Hidebrand, 1985).

Pocket mice (e.g., *Chaetodipus*) and K-rats (e.g., *Dipodymys*) are considered to be semi-fossorial-to-fossorial rodents. Semi-fossorial mammals typically construct less intricate burrows and display a continuum of morphofunctional modifications for digging habits (Montoya-Sanhueza, 2020). Notably, pocket mice have a generalized body plan with fore- and hindlimbs lengths that are equal in proportion (Djawdan, 1993), while K-rats have reduced forelimbs and elongate hindlimbs that are specialized for ricochetal leaping. A characteristic of *Chaetodipus* and *Dipodymys*, however, is their ability to construct complex burrow systems similar to those of *Thymomys* that consist of multiple entrances and exits, as well as relatively smaller pits for food storage (Leaver and Daly, 2001). Yet, neither pocket mice nor K-rats primarily rely on subterranean resources, and instead, spend considerable amounts of time above ground at night forgaing for seeds in support of their granivorous diet.

Aside from pocket gophers, musculoskeletal traits related to the functional morphology of the limbs across the three genera are not known. In particular, the forelimbs are employed for scratch-digging whereby earth is excavated by alternating power strokes (Lessa and Stein, 1992; Stein, 1993). Thus, scratch-digging taxa commonly have well-developed shoulder flexors, elbow extensors, and carpal/digital flexors (Moore et al., 2013; Rupert et al., 2015; Olson et al., 2016). Another trait that is common in fossorial and semi-

fossorial mammals are well-developed foreclaws (Samuels and Van Valkenburgh, 2008), as well as stout limb bones, and these features combined provide enhanced mechanical advantage (MA) for strong burrowing performance. Limited observations on muscular arrangements in pocket mice and K-rats include muscle insertions on a modestly enlarged deltopectoral crest of the humerus, epicondyles of the humerus, and olecranon process of the ulna (Price, 1993), the latter of which represents the in-lever (L_{in}) for extensor torque applied at the elbow joint and is a proportion of considerable significance as applied to digging behavior (Hildebrand, 1985).

The in-lever to out-lever (L_{in}/L_{out}) ratio represents an instantaneous measure of MA with which contractile force produced by a muscle (or functional group) can generate a moment at a limb joint (Williams et al., 2008). Moreover, L_{in}/L_{out} determines either a rotational force (torque) or velocity advantage. Therefore, this simple metric is often used to explain limb mechanics where large MA is expected. Burrowing performance in pocket mice and K-rats, however, has been shown to approximate, or even exceed, that of pocket gophers (Moore Crisp, 2018). These previous findings derived from recorded magnitudes of horizontal substrate reaction forces (SRF) and observed higher frequency components in the SRF signals suggest that pocket mice and K-rats (Moore Crisp et al., 2019) overcome potential limitations of reduced MA by both producing more muscle force and cycling their forelimbs more rapidly during burrowing. Importantly, these data further lead to hypotheses of variable modifcations for muscle contractile force coupled with excursion and velocity across burrowing rodents.

The force, torque, and power that muscles apply at limb joints are strongly influenced by muscle fiber architecture (Lieber and Ward, 2011). Due to having a greater number of short muscle fibers per unit area of muscle tissue (Gans, 1982), pennate-fibered muscles typically have large physiological cross-sectional area (PCSA) and isometric force production capacity (Alexander, 1984), but are less capable of performing mechanical work and power (Azizi et al., 2008; Williams et al., 2008). On the other hand, parallel-fibered muscles have long fascicles (Lieber, 2002) that are orientated at low angles (0–15°) relative to the line of action (Zajac, 1989, 1992) and provide the advantage of shortening ability (proportional to fascicle/muscle length) and contractile velocity, albeit they are less capable of producing large force. Long fascicles are thusly specialized for fast movements

or extensive rotations requiring a large range of motion (ROM) at the limb joints.

Contractile velocity is also dependent on myosin heavy chain (MHC) expression in muscle fibers. Four different adult isoforms of MHC are expressed in the skeletal muscles of mammalian limbs are ordered from slowest-to-fastest contracting by their intrinsic rate of ATP hydrolysis: MHC-1 (slow), MHC-2A (slowest fast), MHC-2X (intermediate fast), and MHC-2B (fastest) (Bottinelli, 2001; Toniolo et al., 2004). Whereas mammals across broad orders of body size may express fast MHC-2A and -2X isoforms in their skeletal muscles, expression of fast MHC-2B isoform is critically related to body size and thermoregulation in small mammals, and is cheifly expressed in rodents (Seow and Ford, 1991; Pellegrino et al., 2003). That said, several studies have found a predominant isoform expression of MHC-2A in the forelimbs of fossorial rodents (Goldstein, 1971; Alvarez et al., 2012; Rupert et al., 2015) that are phylogenetically and functionally similar to pocket gophers. Other studies performed on laboratory rats and mice, however, have found mainly MHC-2X and -2B isoforms in their hindlimb skeletal muscles (e.g., Bottinelli et al., 1994, 2001; Pellegrino et al., 2003; Mathewson et al., 2012; Eng et al., 2008). MHC isoform content has not been determined in pocket gophers, pocket mice, and K-rats.

Both fiber architecture and the composition slow *vs.* fast MHC fibers therefore reflect the functional specializations of muscles, and evaluations of these properties are essential to interpretation of limb function, yet they remain poorly understood for extremity muscles of animals adapted for burrowing. The aim of this study is to quantify muscle architectural properties and MHC isoform content in forelimbs of three burrowing rodents. To this end, diversity in functional use of rodent forelimbs for scratch-digging will be evaluated by a comparative analysis of muscle properties to explain how three sympatric species can burrow equally well despite each having marked differences in body form and forelimb size. It is hypothesized that the forelimb muscles of pocket mice and K-rats will have fast-contracting muscles related to powerful and rapid bursts of scratch-digging that compensate for their overall lack of limb muscle development, whereas pocket gophers will have stronger, slow-contracting muscles consistent with large MA and slower burrowing behavior.

Central to this hypothesis are the previous findings and interpretations put forth in Moore Crisp (2018). Based on these studies, specifically, it is expected that (1) the limb

retractors, elbow extensors, and carpal/digital flexors of pocket mice and K-rats will have a predominant expression of fast MHC-2X and -2B isoform fiber types, whereas those functional groups in pocket gophers will have a broader distribution of fast MHC-2A fibers. It is also predicted that (2) the muscles composing mainly those three functional groups will have long muscle fascicles and a large capacity for shortening excursion in pocket mice and K-rats. The well-developed muscles of pocket gophers are expected to have greater degrees of muscle fiber pennation with shorter fascicles and larger PCSA than of those observed in pocket mice and K-rats, in addition to obvious limb modifications for enhanced MA.

MATERIALS AND METHODS

Study specimens

The forelimbs of Botta's pocket gopher (*T. bottae: N*=10), the desert pocket mouse (*C. penicillatus: N*=5), and Merriam's kangaroo rat (*D. merriami: N*=3) were measured for this study. Frozen specimens of each species were supplied by Alexis Moore-Crisp, Ph.D. (Nevada Wildlife and Game Trapping Permit #372719), stored (-20ºC) until observation, and were allowed to thaw 24–36 hours at 4ºC prior to dissection. Limbs used for dissection, body mass, and total forelimb muscle mass for all specimens and species studied are reported in Table 1.

Dissection and muscle measurement

Myology and muscle nomenclature primarily followed that of Lessa and Stein (1992) and Thorington et al. (1997). Briefly, the forelimbs of each animal were skinned, muscles were identified, measured, and dissected along their origin and insertion with a dissection microscope (Olympus SCX7). Muscles were systematically exisced proximal-to-distal beginning with the extrinsic muscles of the limb. Phosphate buffered saline (PBS) was periodically applied to prevent muscle desiccation during dissection (Rupert et al., 2015). The right forelimb of each animal was a priori selected for dissection, muscle architecture measurements, and muscle harvesting. A suite of 10–15 limb retractor, elbow extensor, and carpal/digital muscles were harvested for MHC isoform fiber type analysis (see below).

Muscle architecture was quantified following the procedures used in previous studies (e.g., Moore et al., 2013; Rose et al., 2013; Rupert et al., 2015; Olson et al., 2016, 2018).

In situ muscle moment arm (r_m) and muscle belly length (ML) were measured three times using digital calipers (CD-4 CSX, Mitutoyo, Japan) with the limb joints placed in a neutral position (i.e., ~90°: angle at which agonist/antagonist muscle pairs could exert equal joint torque). Fascicle length (L_F) was measured from 5–10 random fascicles (depending on muscle size) using digital calipers, while pennation angle (θ, to the nearest degree) was also measured from 5–10 random sites along the muscle belly using a goniometer. Wet muscle mass (MM) was recorded with an analytical balance (Mettler Toledo, AB104-S/FACT, accurate to 0.0001g) after muscle excision and removal of any free tendons.

Upon completion of the muscle measurements, a suite of 16 osteological measurements were taken to the nearest 0.01 mm with digital calipers from the cleaned limb bones (humerus, radius, ulna, metacarpal III, and first phalanx and claw of digit III). Bones were measured for a series of length, width, and depth dimensions, and each metric was recorded three times and averaged. A total of 6 functional indices were calculated and analyzed from the raw osteological measurements (Rose et al., 2014), and these ratios were used to inform quantitative evaluations of MA for scratch-digging ability and specialization of the forelimb for fossorial habits. Abbreviations, formulae, and functional implications of each index are given in Table 2.

Architectural properties quantification

Calculations of muscle volume were determined by dividing MM by a muscle density of 1.06 g/cm^3 (Mendez and Keyes, 1960). PCSA was then calculated using the equation:

$$\frac{\text{muscle volume}}{\text{mean } L_F} \times \cos(\theta),$$

where cos θ was used to correct PCSA for the observed fiber architecture. Maximum isometric force (F_{max}) was determined by multiplying PCSA (in cm^2) by a maximum isometric stress of 30 N/cm^2 (Woledge et al., 1985; Medler, 2002). Joint torque was calculated as $F_{max} \times r_m$ (maximal value at joint angles of 90°). Last, instantaneous muscle power (P_{inst}) was determined according to Hill (1938) as $0.1(F_{max} \times V_{max})$, where V_{max} is maximum fiber shortening velocity (in fiber lengths per second, FL/s). A size-specific value of unloaded fiber shortening (V_0) of 2.70 FL s^{-1} for fast, MHC-2A fibers was used to estimate V_{max} for pocket gophers. This value was predicted using published body size scaling relationships of V_0 (Toniolo et al., 2007; Butcher et al., 2010) at 10–15°C, and

assuming a Q_{10} of 2–6 for V_{max} at physiologic temperature, resulted in a V_{max} of 10.8 FL s^{-1} for *T. bottae*. Values of V_0 for pocket mice (2.85 FL s^{-1}) and K-rats (2.52 FL s^{-1}) were taken from the literature from mice and rats, respectively (Pelligrino et al., 2003), and adjusted for body temperature by the same factor of four. The final values used for V_{max} were 11.4 FL s^{-1} for *C. pennicilatus* and 10.1 FL s^{-1} for *D. merriami*.

Raw and calculated metrics for each species were scaled to total forelimb muscle mass (TFMM). TFMM was used in favor of body mass due to the disproportinaly small forelimbs of *D. merriami*. Following the null hypothesis of isometry, length scales with TFMM to the one-third power ($TFMM^{0.33}$), area to the two-thirds power ($TFMM^{0.67}$), and volume/mass to the three-thirds power ($TFMM^{1.0}$) (Biewener, 1989, 2005). Estimates of F_{max}, joint torque, and P_{inst} were simply normalized to TFMM (in g). The mass distribution of each functional group was additionally determined as a percentage of TFMM. Muscles were placed in the following functional groups for this analysis: limb retractors (shoulder flexors), limb protractors (shoulder extensors), limb adductors, elbow flexors, elbow extensors, carpal/digital flexors, carpal/digital extensors, pronators, and supinators. Muscles with synergistic functions are combined into one functional group, though muscles with multiple actions (e.g., pectoralis superficialis) and biarticular muscles (e.g., triceps brachii long head) were placed in more than one functional group (Table 3). Several size-scaled ratios were also calculated and represent important muscle architectural indices (AI): fascicle length to muscle length ratio (L_F/ML), PCSA to muscle mass ratio (PCSA/MM), and fascicle length to muscle moment arm ratio (L_F/r_m). Each AI were averaged across muscles within functional groups.

Myosin heavy chain expression

Muscle tissue was harvested by sampling 10–15 selected forelimb muscles from a sub-set of $N = 3$ individuals from each species studied. Harvesting involved flash freezing entire muscles in micro-centrifuge tubes and storing them at –80ºC. SDS-PAGE proceeded by placing a small block of muscle tissue in a bath of liquid nitrogen, grinding to powder, homogenizing 50 mg of muscle powder in 800 µL (1:16 ratio) of Laemmli buffer (Laemmli, 1970; Toniolo et al., 2008), and centrifugation of the homogenates at 13k rpm for 10 min (Rupert et al., 2014). For small muscle yielding significantly less freeze-dried muscle powder (e.g., 10-20 mg), the volume of Laemmli buffer was lowered accordingly

to maintain the same ratio. Prior to loading samples on gels, they were most commonly diluted 2:498 in gel sample buffer (GSB) (Mizunoya et al., 2008) to a final protein concentration of ~0.25 mg/mL and were heated for 5 min at 90°C. Dilutions in GSB were also adjusted accordingly based on protein band expression in gels, but were standardized for each species (working range- 2:498–5:495). MHC isoforms were resolved on SDS-PAGE gels using established methods (Talmadge and Roy, 1993) which were performed with slight modifications (Mizunoya et al., 2008) as previously described (Hazimihalis et al., 2013; Rupert et al., 2014, 2015; Thomas et al., 2017). Briefly, gels were loaded with a total of ~2.5 μg of protein per lane, stained with silver (Bio-Rad, Hercules, CA), and photographed using a Nikon digital camera mounted on a copystand and set to a standard focal length.

MHC isoform content was quantified by densitometry in Image J (v.1.43, NIH) using the brightness area product (BAP) method of densitometry similar to Toniolo et al. (2008). The sum of the band intensity values in each gel lane was used to calculate a percentage for each MHC isoform expressed in a single muscle. Pooled percentages of the MHC isoforms for each muscle and individual were taken across 2–3 independent gel runs (3 replicates were most common) to provide an overall percentage composition of slow and fast MHC isoforms. Means of percent MHC (% MHC) content were then determined for each species (Rupert et al., 2015).

Statistics

Descriptive statistics for all measurements were reported as means±s.d. (standard deviation), unless otherwise specified. A MANOVA (in SPSS) was used to determine statistical differences among suites of experimental variables among the three species sampled, with particular interest focused on statistical differences in %MHC content and selected functional osteological indices. ANOVA and Tukey's *post-hoc* tests were used to determine all pairwise differences following significant results from MANOVA. Pearson-Moment correlations were also used to determine the strength of the relationships between MHC isoform content and body size across in a small sample of burrowing rodents. For these tests, data for talus tuco-tucos (*Ctenomys talarum*) was taken from Alvarez et al. (2012). Significance for all statistical tests was accepted at $p \leq 0.05$.

RESULTS

Functional Osteological Indices

Box-whisker plots for selected osteological indices are shown in Fig. 1. In general, *T. bottae* has large scores for indices that indicate large limb mechanical advantage; however, *C. penicillatus* and *D. merriami* both have bone proportions indicative of a joint rotational velocity advantage. Scores on leverage-related indices, including SMI, IFA, and TMOI are significantly larger ($p<0.001$) for *T. bottae* than those for both *C. penicillatus* and *D. merriami* (Fig. 1a, d, e). In contrast, BI for *D. merriami* is greater ($p<0.001$) than that of either *T. bottae* or *C. penicillatus* due to its disproportionately long radius and short humerus (Fig. 1b), but RLI is significantly smaller ($p<0.001$) than both. *C. penicillatus* and *D. merriami* (Fig. 1c). The index CLAW is also large for *T. bottae* and the differences between its scores and those of both *C. penicillatus* and *D. merriami* are significant ($p<0.001$). The index CLAW for *D. merriami* is also significantly greater ($p=0.02$) than that of *C. penicillatus,* which has notably reduced claws (Fig. 1f).

Functional distribution of forelimb muscle mass

The digging apparatus of a pocket gopher, pocket mouse, and K-rat forelimb contains 44, 36, and 40 muscles (excluding the muscles intrinsic to the manus), respectively, for which muscle architecture is quantified. Mean values of TFMM for *T. bottae*, *C. penicillatus*, and *D. merriami* are 5.69±1.5g, 0.58±0.1g, and 0.65±0.1g, respectively, and these account for 4.31±0.5%, 3.04±0.6%, and 1.94±0.2% of body mass per forelimb. The distribution of muscle functional group mass is shown in Fig. 2. The limb retractors and scapular stabilizers/rotators are the two functional groups that account for the largest %TFMM in all three species. However, the limb protractors and adductors (mostly muscles with synergistic functions) are also relatively well-developed (Fig. 2). The humeral retractors of *C. penicillatus* have overall the greatest %TFMM at a mean of 43.4±3.0%, while across species, the scapular elevators/rotators in *D. merriami* notably have the largest %TFMM with a mean of 26.5±1.4% compared with averages of 22% for both *T. bottae* and *C. penicillatus*. Among the intrinsic limb muscles, the elbow extensors and digital flexors have appreciable %TFMM. Specifically, the elbow extensors of *T. bottae* have the largest relative mass across species with a mean value of 15.9±0.2%. The digital flexors are relatively the most well-developed in *D. merriami* (Fig. 2).

Muscle architectural properties

Raw data for measured architectural properties from all extrinsic and intrinsic muscles for each species are presented in Tables 4–9. Overall, the forelimb of *T. bottae* contains an even distribution of parallel and pennate-fibered muscles, whereas 69% and 63%, of muscles in *C. penicillatus* and *D. merriami*, respectively, have parallel-fibered archietecture. Moreover, all extrinsic muscles of the forelimb in *C. penicillatus* and *D. merriami* demonstrate parallel fascicles and the two muscles among all three species that absolutely have the longest fascicles are m. trapezius thoracica (TT) and m. latissimus dorsi (LAT) (Tables 4, 5, 6).

The metric L_F/ML indicates muscle shortening capacity and it is shown for selected functional groups associated with the power/recovery strokes of scratch-digging in Fig. 3. Correpsonding with the observed greater pennation of the musculature, *T. bottae* has relatively lower L_F/ML than both *C. penicillatus* and *D. merriami* for all muscle groups analyzed. Among functional groups, the scapular rotators/stabilizers and elbow extensors have the greatest L_F/ML with values $\geq$0.7 and show a species-specific trend of *T. bottae* having the lowest ratios, *C. penicillatus* intermediate, and *D. merriami* having the largest (Fig. 3). The limb retractors notably have similar L_F/ML across all species, whereas both the limb protractors (average ratio: 0.66) and carpal flexors (average ratio: 0.47) show greater values for *C. penicillatus* and *D. merriami,* with those of pocket mice being slighty larger between the two species. This trend was most apparent for the digital flexors of *C. penicillatus* having a mean ratio of 0.49±0.1 versus a similarly lower, but equivalent, L_F/ML for *T. bottae* and *D. merriami* (Fig. 3).

PCSA to muscle mass (MM) ratio represents the ability of force production per unit mass and is shown in Fig. 4. Overall, *C. penicillatus* and *D. merriami* have larger ratios than *T. bottae* across all functional groups. Specifically, pocket mice and K-rats have similarly large PCSA/MM for all functional groups (all values above 1.0) except for the carpal flexors where *C. penicillatus* has the single largest ratio at a mean of 3.07±0.1. Beyond the carpal flexors, values for PCSA/MM were high for humeral protractors (range: 1.7–2.9) and digital flexors (range: 1.9–2.9) of each species (Fig. 4). Similar species-specifc trends were observed between the humeral protractors and retractors but with PCSA/MM ratios for the latter muscles for *C. penicillatus* and *D. merriami* being nearly

double that of *T. bottae* (average ratio: 0.91). The scapular rotators/stabilizers have the lowest values among the functional groups analyzed (Fig. 4).

The contractile ability of muscle fascicles to rotate a joint through a large range of motion is given by the metric L_F/r_m and it is shown in Fig. 5. Most if not all the muscles in the forelimbs of *C. penicillatus* and *D. merriami* have smaller L_F/r_m compared with *T. bottae*, and no muscle functional group across all three species had an average ratio less than 2.0. Moreover, the same trends evident for L_F/ML are replicated in L_F/r_m ratios by the influence of relatively long fascicles. In particular, the limb retractors have similarly elevated L_F/r_m across species (average ratio: 4.0), whereas the elbow extensor group has the overall lowest mean ratio at 2.3±0.6 for *T. bottae*, with that for *C. penicillatus* being intermediate, and the mean value for *D. merriami* being the largest (Fig. 5). This species-specific trend is also observed for the humeral protractors. In general, the carpal flexors have the largest L_F/r_m with a value of 5.4 for *C. penicillatus* being the single greatest followed by a ratio of 4.9 for *D. merriami*. A similar pattern is seen in the digital flexors, albeit values for L_F/r_m are somewhat lower (range: 3.9–4.3) for *C. penicillatus* and *D. merriami* (Fig. 5).

Normalized values of PCSA and L_F for selected power/recovery stroke muscles are plotted in Fig. 6a. The majority of muscles in all three species are shown to be more generalized in their functional capacity by their position in the lower left quadrant of the plot. Nonetheless, the m. serratus ventralis (SV) for *D. merriami* is the only muscle that is capable of high power output, while TT and LAT are two muscles shared among species which have the ability for large contractile excursion and shortening velocity. Specifically, the LAT of *D. merriami* has the longest relative fascicle lengths across all species (Fig. 6a). In contrast, m. subscapularis (SUB) of *T. bottae* has a shorter normalized L_F and the largest capability of force production of any muscle and species. Along with SUB, the m. infraspinatus (ISP) is the other large force-producing muscle shared among the three species. The m. triceps brachii long head (TBLO) for *T. bottae* likewise has the capacity to produce substantial force. Several of the same muscles across species (e.g., SV and TBLO), in addition to the m. pectoralis superficialis (PS), also have intermediate size-scaled PCSA and L_F and similarly have the capacity to generate moderate power, most notably in *C. penicillatus* and *D. merriami* (Fig. 6a).

Normalized PCSA and r_m for selected power/recovery stroke muscles are plotted in Fig. 6b. The only muscle capable of applying large torque at both the shoulder and elbow joints is TBLO in *T. bottae* by its position in the upper right quadrant of the plot. Smaller values of normalized r_m limit the ability of SUB and ISP to apply joint torque despite their consistently large PCSA across all species. PS and TBLO (at the elbow joint) are the two muscles that have a moderate capacity to apply joint torque, again namely in *C. penicillatus* and *D. merriami*. Last, normalized L_F and r_m for selected power/recovery stroke muscles are plotted in Fig. 6c. Most muscles analyzed across species have modest size-scaled values of L_F and r_m and generalized ability to affect joint rotation. Only LAT in *C. penicillatus* and *D. merriami* has the capacity for fast joint rotational velocity by occupying the upper left quadrant of the plot; however, the LAT in *T. bottae* appears to be modified for relatively greater joint torque (has an appreciable r_m) despite its long fascicles (Fig. 6c). Moreover, again the PS and TBLO (at the elbow joint), as well as the m. teres major (TMJ), also have the capacity for intermediate joint torque that is shared among species, whereas TBLO (at the shoulder joint) and m. triceps brachii lateral head (TBLA) have the ability for moderate fast joint rational velocity.

MHC Isoform Content

MHC content for individual muscles involved in the power stroke of scratch digging for each species are presented in Table 10. The forelimb musculature of *T. bottae* shows expression of three MHC isoforms: MHC-1, MHC-2A, and MHC-2X. The species *C. penicillatus* expressed all the three fast MHC isoforms (-2A, -2X, and -2B) but no slow MHC-1, while *D. merriami* expressed only fast MHC-2A and MHC-2X. Figure 7 displays the %MHC content across the muscle functional groups humeral retractors, elbow extensor, and carpal/digital flexors. Consistently, *T. bottae* has the largest expression of fast MHC-2A (range: 62–87% MHC content) along the forelimb (Table 10). The distal limb muscles in both *T. bottae* and *D. merriami* also become slower-contracting by increased relative expression of MHC-1 (12.3%) and MHC-2A (86.2%), respectively, whereas in *C. penicillatus*, the greatest %MHC content of fast MHC-2B (31.1%) is seen in the carpal/digital flexors (Fig. 7). Additionally, relationships between %MHC content and body mass are demonstrated in Fig. 8. MHC-2A shows a positive correlation (correlation

coefficient: 0.96, p=0.036) with body mass (Fig. 8a). Conversely, MHC-2X has a negative correlation (correlation coefficient: 0.92, p=0.076) with body mass (Fig. 8b).

DISCUSSION

The muscle architectural properties observed indicate that the muscles of pocket mice and K-rats are capable of more rapid limb cycling by their forelimbs demonstrating longer, parallel fascicles, shorter moment arms, greater expression of fast MHC isoforms, and lower limb mechanical advantage (MA) than pocket gophers as hypothesized. However, pocket mice and K-rats also have very large force production capability in their forelimb musculature, which was unexpected, and may further reveal how burrowing performance in these taxa may approximate or exceed that of fossorial pocket gophers. This study is the first to compare force production capacity among multiple sympatric rodents and the key findings of this study are adressed in relation to hypothesized muscle (or group) function with comparisons to available data for burrowing performace in each taxa.

Whereas muscle architectural properties are unavailable for many fossorial mammals, numerous studies have reported that bone proportions of the forelimbs of burrowing taxa confer a sizable MA (e.g., Hildebrand, 1985; Lagaria and Youlatos, 2006; Elissamburu and De Dantis, 2011; Warburton et al., 2013; Reese et al., 2013; Olson et al., 2016). *T. bottae* exhibits hypertrophied, strong muscles coupled with forelimb morphology (large SMI and IFA) that provides them with signifcant MA as predicted. On the other hand, *C. penicillatus* distinctly lacks these features, having little-to-no modification for MA, whereas K-rats display elongate distal forelimbs with a short humerus (large BI) and appreciable foreclaws (index: CLAW). An increase in out-lever length lowers MA while increasing the velocity of joint rotation (i.e., velocity advantage) in the forelimbs of K-rats. Thus, *C. penicillatus* and *D. merriami* are limited by two major factors: 1.) the lack of limb MA and 2.) the small size of their forelimb muscles. Consequently, their musculature must be capable of producing appreciable size-scaled force (in-force) to compensate for reduced leverage for burrowing, and the PCSA/MM data reported here help explain previous findings that these two taxa exert markedly greater horizontal substrate reaction forces (SRF) than pocket gophers during scratch-digging in both loose and compact soil types (Moore-Crisp, 2018).

Remarkably, isometric force production capacity in all functional groups in the forelimbs of pocket mice and K-rats is larger than that of Botta's pocket gopher with ratios

broadly ranging from 1–3. This finding is notable because with the exception of moles (Rose et al., 2013), which burrow via humeral-rotation digging, PCSA/MM ratios often do not exceed a value of 1.0 as shown for both scratch-digging (Moore et al. 2013; Rupert et al., 2015) and cursorial (Zarucco et al., 2004) taxa. Talpid moles are reknowned for their strength with an ability to exert an estimated 10–20 times their body mass in out-force (Rose et al., 2013), or greater (Lin et al., 2017, 2019), by their forelimbs. And while scratch-digging *C. penicillatus* and *D. merriami* are not expected to reach those levels of force, their carpal and digital flexors appear to be quite strong and similarly had the largest capacity for force production in the forelimbs among the power stroke functional groups analyzed. Distal forelimb muscles in scratch-digging taxa have been shown to have increased pennation (smaller L_F/ML and L_F/r_m) accounting for their appreciable PCSA, and thus enhanced force/torque production ability for purchase of the substrate and the strength to sustain flexion of the carpus and digits through the power stroke (Moore et al., 2013; Rupert et al., 2015). But, the humeral protractors, which are the primary recovery stroke muscles, also have appreciable force production ability that rivals that of the limb retractor and elbow extensor muscles, particularly in *C. penicillatus* and *D. merriami*. This finding may suggest a near equal requirement of large muscle force for the recovery stroke of scratch-digging in small burrowers that might be less important for other, larger semi-fossorial diggers (Martin et al., 2019). In addition, it may point to the need for intrinsic power properties of the muscle fibers in the humeral protractors and this should be addressed in future studies.

One of the more peculiar findings of this study is that, on avergae, L_F/ML and L_F/r_m ratios in humeral retractors are identical across species. In particular, LAT is a muscle capable of large contractile excursion and velocity due to its equally long fascicles, although it is also capable of fast joint rotational velocity due to its short moment arm in pocket mice and K-rats. *T. bottae* does not have any muscles that are capable of joint rotational velocity ability which complements their hypertrophied forelimb structure and slow, constant burrowing behaviors Pocket gophers are active throughout the day/night and spend most, if not all, of their time in or around their burrow and forage strictly underground (Vleck, 1979). However, except for LAT, the intrinsic force production ability of the humeral retractors in *C. penicillatus* and *D. merriami* is nearly double that in

T. bottae. Specific humeral retractors are indeed force specialized (e.g., SUB, ISP, and TBLO at the shoulder joint). The combination of architectural properties observed in these muscles may represent functional compartmentalization in the limb/humeral retractors for actions performed during the power stroke of stratch-digging. For example, in combination with its short r_m and pennate fascicles, SUB may act to stabilize the shoulder joint during limb humeral retraction. Coversely, the bi-pennate ISP with its short r_m may initiate shoulder flexion while the long fascicles of LAT shorten substantially to move the forelimb through an appreciable range of limb retraction. Each taxa sampled here may additionally depend on activation of a combination muscles that are capable of either appreciable force or excursion to achieve moderate power output, and such a feature might be critical to their burrowing performance. In the distal limb, the muscle with greatest force production and power ability among the carpal/digital flexors is the m. flexor digitorum profundus humeral medial head (FDPHM). Pocket mice and K-rats, in contrast to *T. bottae*, are nocturnal and spend considerable time above ground foraging in shrubs and brush (Leaver and Daly, 2001). Rapid scratching of the substrate to unearth and cache seeds is essential to their foraging behavior (Moore Crisp, 2018), which could be accomplished primarily by actions of the carpal/digital flexors.

Architectural properties indicative of rapid limb cycling would also allow pocket mice and K-rats to excavate similar amounts of earth (in aggregate) as pocket gophers per unit time during burrow construction. The forelimbs of burrowing mammals have been generally shown to have well-developed extrinsic muscles with parallel fiber architecture. In addition, these muscles typically have elevated PCSA due to large muscle mass. Mathewson et al. (2012) reported overall large PCSA in the flexors, but long facicle lengths in the extensors of the forelimb of the common house mouse (*Mus musculus*), which broadly agree with observations made in *C. penicillatus* and *D. merriami*. In that same study, TBLO also notably had both large PCSA, but long fascicle lengths, thus indicating that this muscle could also be capable of either large joint torque at the shoulder joint or high power output and may be important to forelimb function in rodents by providing propulsion for either running or burrowing. Pocket mice and K-rats do not have any muscles that are obviously capable of large joint torque, whereas in *T. bottae* TBLO at both the shoulder and elbow joints is the only muscle with this capability.

The TBLO is one of the moderately high power generating muscles studied herein, along with PS and SV. These data agree with those of scratch-digging bandicoots (Warburton et al., 2013) and quendas (Martin et al., 2019) and suggest a synergistic functional of these three muscles to retract the forelimb and rotate the scapula. In particular, SV in pocket gophers (29.6 mW/g), pocket mice (21.4 mW/g), and K-rats (48.1 mW/g) has the greatest capacity for power. Burrowing rodents may rely on the ability of SV for rapid rotation of the scapula to initiate forelimb protraction/retraction during scratch-digging. Powerful muscle function may be most critical in *D. merriami* to overcome the velocity of limb cycling contraints imposed by its gracile, but elongate distal forelimbs. Moroever, intermittent digging in *C. penicillatus* and *D. merriami* may allow them to generate high power output during burrowing. Correspondingly, bandicoots have powerful muscles for quick bursts of burrowing for aquistion of shallow subterranean food or nest contruction (Martin et al., 2018) and may not require on force-specialized muscles, which might be necessary for prolonged burrowing and construction of intricate burrow systems.

Overall, fossorial rodents have been shown to have little-to-no muscles specialized for high power output. Most of the forelimb muscles for which architectural properties were analyzed similarly to those herein are classified as generalized with some muscles that are specialized for either force or contraction excursion and/or velocity. Remarkably, the muscles previously found to be force and velocity specialized in groundhogs (Rupert et al., 2015) overlap with those in pocket gophers, pocket mice, and K-rats. Also consistent with previous reports in borrowing rodents is broad expression of the fast MHC-2A isoform in the forelimb musculature. Compared with *C. penicillatus* and *D. merriami*, pocket gophers express a larger percentage of MHC-2A fibers in their forelimbs, as was observed in tuco-tucos (Alvarez et al., 2012) and groundhogs (Rupert et al., 2015). Although muscle fiber architecture and limb lever mechanics constrain fiber contractile properties (Lieber, 2009), intrinsic muscle power is chiefly dependent on fast MHC expression (Shiaffino and Reggiani, 2011). Coupling large MA in the distal limbs of *T. bottae* with a faster- to slower-contracting MHC isoform distribution along the forelimb reflects a slower, stronger mode of burrowing. Distal limb muscles may be expected to contract more slowly since they serve postural roles during weight-bearing, and while the pattern observed for pocket gohers is mostly comparable to that of K-rats, which use primarily bipedal leaping

locomotion without forelimb support, *D. merriami* does not express slow MHC-1 and retains a greater expression of MHC-2A in its distal forelimb.

Having faster-contracting muscles with long fascicles and short moment arms concentrated proximally (i.e., shoulder and elbow joints) paired with an elongated distal forelimb are likely the major factors giving K-rats their ability to cycle their limbs fast during scratch-digging. The condition in *C. penicillatus* is the opposite of this pattern by comparison. The distal muscles of pocket mice have large contractile excursion properties and faster-contracting MHC isoforms, including expression of fast MHC-2B, possibly to compensate for their short claws (lowest score on CLAW index). Coupling the general lack of MA in their shoulder, elbow, and carpal joints and expression of fast MHC-2B may also be a means to amplify distal limb joint rotational velocity to keep their feet moving faster than their proximal limb segments. For example, *C. penicillatus* may rely on large and fast rotation in the distal limb segments whereby their carpal/digital flexors have moderate L_F and r_m properties appropriate for appreciable joint rotational velocity. Regardless of the exact limb mechanics employed, variation in MHC between pocket mice and K-rats versus pocket gophers matches well with differences in frequency components of SRF application observed across these three taxa (Moore Crisp, 2018). Specifically, *C. penicillatus* and *D. merriami* demonstrate properties of the SRF above the designated digging frequency of (15±2Hz) established in *T. bottae* (Moore Crisp et al., 2019).

It was expected that pocket mice and K-rats would have appreciable expression of MHC-2B in accordance with previous studies that reported large expression of the MHC-2B isoform in the limbs of laboratory mice (Mathewson et al., 2012) and rats (Eng et al., 2008). The expression of slower MHC isoforms in the burrowing rodents studied here, however, could be attributed to their functional need for increased intrinsic force in the case of *C. penicillatus* and *D. merriami* and prolonged contractions for steady burrowing in *T. bottae*. Goldstein (1971) previously reported considerable amounts of slow "red" fibers in the forelimb muscles (e.g., LAT, TBLO, TBLA) of a diverse sample of burrowing ground squirrels; however, the methods used in that study were not capable of determining comparable MHC expression. In addition, the observed variation in our sample may be representative of differences in MHC between wild type and captive animals or that related

to muscle fiber composition for rodents classified in different sub-orders (i.e., sciuromorphic and castoromorphic rodents vs. myomorphic rodents).

Variability in MHC isoform expression in *T. bottae*, *C. penicillatus*, and *D. merriami* may also be a function of body size based on established relationships showing decreasing fiber shortening velocity with increases in body mass (Seow and Ford, 1991; Pellegrino et al., 2003; Toniolo et al., 2007; Butcher et al., 2010). Evidence of size-related trends are present in the data, although it is acknowledged that the sample is small with means of MHC isoform content from only four species. Nonetheless, fast MHC-2X was negatively correlated with body mass as expected, whereas MHC-2A showed a positive correlation. Moreover, across just one order of magnitude in body size a lack (or loss) of expression of fast MHC-2B in K-rats and the expression of slow MHC-1 in pocket gophers is indicative of a reduction in contractile velocity.

Despite the potential affects of body size influencing MHC expression in burrowing rodents, it does not appear to constrain MHC-2A content in the power stroke musculature. For example, expression of fast MHC-2A between a 134 g pocket gopher (range: 62–87%) and a 4.7 kg groundhog (range: 63–80%; Rupert et al., 2015) are quite similar across the functional groups humeral retractors, elbow extensors, and carpal/digital flexors. Expression of fast MHC-2X is further identical between pocket gophers (1–25%) and groundhogs (0–21%). Few studies, however, have reported MHC isoform expression in burrowing rodents and additional data are needed to support the assertion that MHC isoform expression may be strongly related to burrowing behavior in the order Rodentia. Future studies should aim to focus on MHC isoform content in power stroke musculature in a variety of of ground squirrels to more thoroughly test this hypothesis that adresses the relative influence of lifestyle (i.e., functional signal) versus body size scaling. These evlauations should also sample musculature involved in the recovery stroke as these muscles are required for rapid limb cycling.

One last consideration is that small rodents are expected to counter the limitation of their large surface area to volume ratios with fast-contracting muscle fibers to assist in maintaining core body temperature. Burrowing behavior may then be a critical means of staying warm to compensate for the small expression (or lack thereof) of fast MHC-2B in the forelimbs. Futhermore, there may be strong links among the slow, steady burrowing

behavior in *T. bottae,* their subterrean lifestyle, and diet of fibrous vegetation. Constant activity agrees with their resource acquisition habits and likewise a means to stay warm. By contrast, small *C. penicillatus* and *D. merriami* appear to require much greater contractile effort to burrow effectively. A great deal of energetic exertion during burrowing would incur a large metabolic expense that likely offset by their high energy diet. Thus, it is possible that they support their short bouts of high frequency/large force stratch-digging by performing this activity at night and subsisting on protein and oils from seeds.

Conclusions

The power stroke muscles studied here in three species of burrowing rodents provide novel evidence on their architectural properties and MHC content as well as the ways pocket mice and K-rats must compensate for their lack of forelimb MA and muscle size. With the exception of a few muscles specialized for either force production and/or application of joint torque, the properties of the forelimb musculature in pocket gohpers, pocket mice, and kangaroo rats is surpisingly similar by displaying long fascicles and modest muscle moment arm lengths. However, selective pressures for subterranean lifestyle in *T. bottae* have strongly influenced limb mechanics and hyperptophied musculature to apply large out-force with less contractile effort. These specializations are absent or opposite (i.e., joint velocity advantage) in pocket mice and K-rats, which have forelimbs that are either generalized or reduced, respectively. Therefore, these two sympatric taxa must use their musculature in functionally different ways to approximate the burrowing performance of pocket gophers. *C. penicillatus* and *D. merriami* are capable of overcoming their morphological limitations by cycling their forelimbs at higher frequencies and producing greater magnitudes of intrinsic, size-scaled muscle force. These functions are largely faciliated by faster-contracting MHC isoforms providing the muscles of pocket mice and K-rats with higher intrinsic power. Overall, the burrowing habits each species corresponds with their ecology and resource acquisition behaviors.

REFERENCES

Alexander, R. MCN. (1984). Elastic Energy Stores in Running Vertebrates. *Am. Zool.* **24**, 85–94.

Alvarez, G. I., Díaz, A. O., Longo, M. V. Becerra, F. and Vassallo, A. I. (2012). Histochemical and morphometric analyses of the musculature of the forelimb of the subterranean rodent *Ctenomys talarum* (Octodontoidea). *Anat, Histol, Embryol.* **41**, 317–325.

Azizi, E., Brainerd, E. L. and Roberts, T. J. (2008). Variable gearing in pennate muscles. *Proc. Nat. Acad, Sci.* **105,** 1745–1750.

Biewener, A. A. (1989). Scaling body support in mammals: limb posture and muscle mechanics. *Science* **4913,** 45–48.

Biewener, A. A. (2005). Biomechanical consequences of scaling. *J. Exp. Biol.* **208,** 1665–1676.

Bottinelli, R. (2001). Functional heterogeneity of mammalian single muscle fibres: do myosin isoforms tell the whole story? *Pflügers Arch.* **443,** 6–17.

Butcher, M. T., Chase, P. B., Hermanson, J. W., Clark, A. N., Brunet, N. M. and Bertram, J. E. A. (2010). Contractile properties of muscle fibers from the forelimb deep and superficial digital flexors of horses. *Am. J. Physiol. Regul. Integr. Comp. Physiol.* **299,** R996–R1005.

Chikuni, K., Muroya, S. and Nakajima, I. (2004). Myosin heavy chains expressed in bovine skeletal muscles. *Meat Sci.* **67**, 87–94.

Contreras, L. C. and McNab, B. K. (1990). Thermoregulation and energetics in subterranean mammals. In *Evolution of Subterranean Mammals at the Organismal and Molecular Levels* (eds. E. Nevo and O. A. Reig), pp. 231–250. New York: Wiley-Liss.

Davis, J. L., Santana, S. E., Dumont, E.R. and Grosse, I. R. (2010). Predicting bite force in mammals: two-dimensional versus three-dimensional lever models. *J. Exp. Biol.* **213**, 1844–1851.

DeMont, M. (1996). Measuring how muscles function in levers. *Am. Biol. Teach.* **58**, 490–492.

Dickinson, E., Stark, H. and Kupczik, K. (2018). Non-destructive determination of muscle architectural variables through the use of diceCT. *Anat. Rec.* **301**, 363–377.

Dickinson, E., Basham, C., Rana, A. and Hartstone-Rose, A. (2019). Visualization and quantification of digitally dissected muscle fascicles in the masticatory muscles of *Callithrix jacchus* using nondestructive diceCT. *Anat. Rec.* **302**, 1–10.

Djawdan, M. (1993). Locomotor performance of bipedal and quadrupedal heteromyid rodents. *Funct. Ecol.* 7, 195–202.

Elissamburu, A. and De Santis, L. (2011). Forelimb proportions and fossorial adaptations in the scratch-digging rodent *Ctenomys* (Caviomorpha). *J. Mammal.* **92,** 683–689.

Eng, C. M., Smallwood, L. H., Rainiero, M. P., Lahey, M., Ward, S. R. and Lieber, R. L. (2008). Scaling of muscle architecture and fiber types in the rat hindlimb. *J. Exp. Biol.* **211,** 2336–2345.

Gans, C. (1982). Fiber architecture and muscle function. *Exerc. Sport Sci. Rev.* **10**, 160–207.

Gettinger, R. D. (1984). A field study of activity patterns of *Thomomys bottae*. *J. Mammal.* **65,** 76–84.

Goldstein, B. (1971). Heterogeneity of muscle fibers in some burrowing mammals. *J. Mammal.* **52,** 515–527.

Hildebrand, M. (1985). Digging of quadrupeds. In *Functional Vertebrate Morphology* (eds. M. Hildebrand, D. M. Bramble, K. F. Liem, and D. B. Wake), pp. 89–109. Cambridge: Harvard University Press.

Hildebrand M. and Goslow G. E. J. (2001). Digging, and crawling without appendages. In *Analysis of Vertebrate Structure*, 5th ed (eds. M. Hildebrand and G. Goslow), pp. 455–474. New York, NY: John Wiley & Sons.

Hill, A. V. (1938). The heat of the shortening and the dynamic constants of muscle. *Proc. R. Soc. B.* **126,** 136–195.

Hepple, R. T. (2014). Mitochondrial involvement and impact in aging skeletal muscle. *Front. Aging Neurosci*. **6,** 1–13.

Jones, C. A. and Baxter, C. N. (2004). *Thomomys bottae*. *Mammal. Spec*. **742**, 1–14.

Klieber, M. (1947). Body size and metabolic rate. *Physiol. Rev.* **27**, 511–541.

Kohn, T. A. (2014). Insights into the skeletal muscle characteristics of three southern african antelope species. *Biol. Open* **3**, 1037–1044.

Kotler, B. P. (1984). Risk of predation and the structure of desert rodent communities. *Ecology* **65**, 689–701.

Krupa, J. J. and Geluso. K. N. (2000). Matching the color of excavated soil: cryptic coloration in the plains pocket gopher (*Geomys bursarius*). *J. Mammal*. **81**, 86–96.

Lagaria, A. and Youlatos, D. (2006). Anatomical correlates to scratch digging in the forelimb of european ground squirrels (*Spermophilus citellus*). *J. Mammal*. **87**, 563–570.

Leaver, L. A. and Daly, M. (2001). Food caching and differential cache pilferage: a field study of coexistence of sympatric kangaroo rats and pocket mice. *Oecologia* **128**, 577–584.

Lessa, E. P. and Thaeler, C. S. (1989). A reassessment of morphological specializations for digging in pocket gophers. *J. Mammal*. **70**, 689–700.

Lessa, E. P. and Stein, B. R. (1992). Morphological constraints in the digging apparatus of pocket gophers (Mammalia: Geomyidae). *Biol. J. Linn. Soc*. **47**, 439–453.

Lieber, R. L. (2009). Skeletal muscle, structure, function, and plasticity: the physiological basis of rehabilitation 3rd ed (ed. R. L. Lieber), pp. 369. Baltimore, MD: Lippincott Williams & Wilkins.

Lieber, R. L. and Fridén, J. (2002). Spasticity causes a fundamental rearrangement of muscle-joint interaction. *Muscle Nerve.* **25**, 265–270.

Lin, Y., Chappuis, A., Rice, S. and Dumont, E. R. (2017). The effects of soil compactness on the burrowingperformance of sympatric eastern and hairy-tailed moles. **301**, 310–319.

Lin, Y., Konow, N. and Dumont, E. R. (2019). How moles destroy your lawn: the forelimb kinematics of easternmoles in loose and compact substrates. *J. Exp. Biol.* **222**, 1–10.

Longland, W. S. and Price, M. V. (1991). Direct observations of owls and heteromyid rodents: can predation risk explain microhabitat use? *Ecology* **72**, 2261–2273.

Martin, M. L., Warburton, N. M., Travouillon, K. J. and Fleming, P. A. (2018). Mechanical similarity across ontogeny of digging muscles in anAustralian marsupial (*Isoodon fusciventer*). *J. Morphol.* **280**, 1-13.

Martin, M. L., Travouillon, K. J., Sherratt, E., Fleming, P. A. and Warburton, N. M. (2019). Covariation between forelimb muscle anatomy and bone shape in an Australian scratch-digging marsupial: Comparison of morphometric methods. *J. Morphol.* **280**, 1900–1915.

Mascarello, F., Maccatrozzo, L., Patruno, M., Toniolo, T. and Reggiani, C. (2004). 2B myosin heavy chain isoform expression in bovine skeletal muscle. *Vet. Res. Comm.* **28**, 201–204.

Mathewson, M. A., Chapman, M. A., Hentzen, E. R., Fridén, J. and Lieber, R. L. (2012). Anatomical, architectural, and biochemical diversity of the murine forelimb muscles. *J. Anat.* **221**, 443–451.

Medler, S. (2002). Comparative trends in shortening velocity and force production in skeletal muscles. *Am. J. Physiol., Regul. Integr. Comp. Physiol.* **283**, R368–R378.

Mondal, M. and Tabassum, F. (2016). Scientific aspects of lever. *Int. J. Sci. Res.* **5**, 326–330.

Montoya-Sanhueza, G. (2020). Functional Anatomy, Osteogenesis and Bone Microstructure of the Appendicular System of African Mole-Rats (Rodentia: Ctenohystrica: Bathyergidae). Ph. D. Dissertation, University of Cape Town, South Africa.

Montoya-Sanhueza, G., Wilson, L. A. B. and Chinsamy, A. (2019). Postnatal development of the largest subterranean mammal (*Bathyergus suillus*): morphology, osteogenesis, and modularity of the appendicular skeleton. *Dev. Dyn.* **248**, 1101–1128.

Moore, A. L., Budny, J. E., Russell, A. P. and Butcher, M. T. (2013). Architectural specialization of the intrinsic thoracic limb musculature of the American badger (*Taxidea taxus*). *J. Morphol.* **274**, 35–48.

Moore Crisp, L. (2018). Digging Mechanics in Geomyid Rodents. Ph. D. Dissertation, University of Nevada, Las Vegas.

Moore Crisp, A., Barnes, J. C. and Lee, D. V. (2019). Tunnel-tube and Fourier methods for measuring three-dimensional medium reaction force in burrowing animals. *J. Exp. Biol.* **222**, 1–5.

Morgan, K. R. and Price, M. V. (1992). Foraging in heteromyid rodents: the energy costs of scratch-digging. *Ecology* **73**, 2260–2272.

Nader, I. A. (1978). Kangaroo rats: intraspecific variation In *Dipodomys spectabilis* Merriam and *Dipodomys deserti*, pp. 1–132. Champaign: Stephens University of Illinois Press.

Nevo, E. (1979). Adaptive convergence and divergence of subterranean mammals. *Ann. Rev. Ecol. System*. **10**, 269–308.

Olson, R. A., Glenn, Z. G., Cliffe, R. N. and Butcher, M. T. (2018). Architectural properties of sloth forelimb muscles (Pilosa: Bradypodidae). *J. Mammal. Evol*. **25,** 573–588.

Olson, R. A., Womble, M. D., Thomas, D. R., Glenn, Z. D. and Butcher, M. T. (2016). Functional morphology of the forelimb of the nine-banded armadillo (*Dasypus novemcinctus*): comparative perspectives on the myology of Dasypodidae. *J. Mammal. Evol.* **23**, 49–69.

Ørtenblad, N., Nielsen, J., Boushel, R., Söderlund, K., Saltin, B. and Holmberg, H-C. (2018). The muscle fiber profiles, mitochondrial content, and enzyme activities of the exceptionally well-trained arm and leg muscles of elite cross-country skiers. *Front. Physiol*. **9**, 1–11.

Pellegrino, M. A., Canepari, M., D'Antona, G., Reggiani, C. and Bottinelli, R. (2003). Orthologous myosin isoforms and scaling of shortening velocity with body size in mouse, rat, rabbit and human muscles. *J. Physiol*. **546**, 677–689.

Price, M. V. (1993). A functional-morphometric analysis of forelimbs in bipedal and quadrupedal heteromyid rodents. *Biol. J. Linn. Soc. Lond*. **50**, 339-360.

Randall, J. A. (1993). Behavioural adaptations of desert rodents (Heteromyidae). *Anim. Behav.* **45**, 263–287.

Reig, O. A., Busch C., Contreras J. and Ortells, M. (1990). An overview of evolution, systematic, population biology and molecular biology in Ctenomys. In *Biology of Subterranean Mammals* (eds. E. Nevo and O. A. Reig), New York: Allan Liss.

Rose, J. A., Sandefur, M., Huskey, S., Demler, J. L. and Butcher, M. T. (2013). Muscle architecture and out-force potential of the thoracic limb in the Eastern mole (*Scalopus aquaticus*). *J. Morphol.* **274,** 1277–1287.

Rose, J., Moore, A., Russell, A. and Butcher M. T. (2014). Functional osteology of the forelimb digging apparatus of badgers. *J. Mammal.* **95,** 543–558.

Rourke, B. C., Yokoyama, Y., Milsom, W. K. and Caiozzo, V. J. (2004). Myosin isoform expression and MAFbx mRNA levels in hibernating golden-mantled ground squirrels (*Spermophilus lateralis*). *Physiol. Biochem. Zool*. 77, 582–593.

Rupert, J. E., Rose, J. A., Organ, J. M. and Butcher, M. T. (2015). Forelimb muscle architecture and myosin isoform composition in the groundhog (*Marmota monax*). *J. Exp. Biol.* **218**, 194–205.

Samuels, J. X. and Valkenburgh, B. V. (2008). Skeletal indicators of `locomotor adaptations in living and extinct rodents. *J. Morphol*. **269**, 1387–1411.

Schiaffino, S. and Reggiani, C. (2011). Fiber types in mammalian skeletal muscles. *Physiol. Rev.* **91**, 1447–1531.

Scott, W., Stevens, J. and Binder–Macleod, S. A. (2001). Human skeletal muscle fiber type classifications. *Phys. Therapy* **81**, 1810–1816.

Seow, C. Y. and Ford, L. E. (1991). Shortening velocity and power output of skinned muscle-fibers from mammals having a 25,000-fold range of body-mass. *J. Gen. Physiol*. 97: 541–560.

Smerdu, V. and Erzen, I. (2001). Dynamic nature of fibre-type specific expression of myosin heavy chain transcripts in 14 different human skeletal muscles. *J. Mus. Res. Cell Motil.* **22**, 647–655.

Smith, M. F. (1998). Phylogenetic relationships and geographic structure in pocket gophers in the genus *Thomomys*. *Mol. Phylogen. Evol.* **9**, 1–14.

Spainhower, K. B., Cliffe, R. N., Metz, A. K., Barkett, E. M., Kiraly, P. M., Thomas, D. R., Kennedy, S. J., Avey-Arroyo, J. A. and Butcher, M. T. (2018). Cheap labor: myosin fiber type expression and enzyme activity in the forelimb musculature of sloths (Pilosa: Xenarthra). *J. Appl. Physiol.* **125**, 799–811.

Spainhower, K. B., Metz, A. K., Yusuf, A-R. S., Johnson, L. E., Avey-Arroyo, J. and Butcher M. T. (2021). Coming to grips with life upside down: how myosin fiber type and metabolic properties of sloth hindlimb muscles contribute to suspensory function. *J. Comp. Physiol. B.* **191**, 207–224.

Stein, B. R. (1993). Comparative hind limb morphology in geomyine and thomomyine pocket gophers. *J. Mammal.* **74**, 86–94.

Stein, B. R. (2002). Morphology of subterranean rodents. In *Life Underground* (eds. E. A. Lacey, J. L. Patton, and G. N. Cameron). pp. 19–61. Chicago: University of Chicago Press.

Sullivan, S. P., McGechie, F. R., Middleton, K. M. and Holliday, C. M. (2019). 3D muscle architecture of the pectoral muscles of european starling (*Sturnus vulgaris*). *Integr. Org. Biol.* **1**, 1–18.

Thomas, D. R., Chadwell, B. A., Walker, G. R., Budde, J. E., VandeBerg, J. L. and Butcher, M. T. (2017). Ontogeny of myosin isoform expression and prehensile function in the tail of the gray short-tailed opossum (*Monodelphis domestica*). *J. Appl. Physiol.* **123**, 513–525.

Thorington, R. W., Darrow, K. and Betts A. D. K. (1997). Comparative myology of the forelimb of squirrels. *J. Morphol.* **234**, 155–182.

Toniolo, L., Patruno, M., Maccatrozzo, L., Pellegrino, M. A., Canepari, M., Rossi, R., Antona, G. D., Bottinelli, R., Reggiani, C. and Mascarello, F. (2004). Fast fibres in

a large animal: fiber types, contractile properties and myosin expression in pig skeletal muscles. *J. Exp. Biol.* **207**, 1875–1886.

Toniolo, L., Patruno, M., Maccatrozzo, L., Pellegrino, M. A., Canepari, M., Rossi, R., D'Antona, G. D., Bottinelli, R., Reggiani, C. and Mascarello, F. (2007). Fiber types in canine muscles: myosin isoform expression and functional characterization. *Am. J. Physiol., Cell Physiol.* **292**, C1915–C1926.

Vleck, D. (1979). The energetic cost of burrowing by the pocket gopher *Thomomys bottae*. *Physiol. Zool.* **52**, 122–136.

Warburton, N. M., Grégoire, L., Jacques, S. and Flandrin, C. (2013). Adaptations for digging in the forelimb muscle anatomy of the southern brown bandicoot (*Isoodon obesulus*) and bilby (*Macrotis lagotis*). *Aust. J. Zool.* **61,** 402–419.

Webster, D. B. (1962). A function of the enlarged middle-ear cavities of the kangaroo rat, Dipodomys. *Physiol. Zool.* **35**, 248–255.

Whitford, M. D., Freymiller, G. A. and Clark, R. W. (2017). Avoiding the serpents tooth: predator–prey interactions between free-ranging sidewinder rattlesnakes and desert kangaroo rats. *Anim. Behav.* **130**, 73–78.

Wilkins, K. T. and Roberts, H. R. (2007). Comparative analysis of burrow systems of seven species of pocket gophers (Rodentia: Geomyidae). *Southwest. Nat.* **52**, 83–88.

Williams, S. B., Wilson, A. M., Rhodes, L., Andrews, J. and Payne, R. C. (2008). Functional anatomy and muscle moment arms of the pelvic limb of an elite sprinting athlete: the racing greyhound (*Canis familiaris*). *J. Anat.* **213**, 361–372.

Woledge, R. C., Curtin, N. A. and Homsher, E. (1985). Energetic aspects of muscle contraction. *Monogr. Physiol. Soc.* **41**: 1–357.

Zajac, F. E. (1989). Muscle and tendon: properties, models, scaling, and application to biomechanics and motor control. *Crit. Rev. Biomed. Eng.* **17**, 359–411.

Zajac, F. E. (1992). How musculotendon architecture and joint geometry affect the capacity of muscles to move and exert force on objects: a review with application to arm and forearm tendon transfer design. *J. Hand Surg. Am.* **17**, 799–804.

Zarucco, L., Taylor, K. T. and Stover, S. M. (2004). Determination of muscle architecture and fiber characteristics of the superficial and deep digital flexor muscles in the forelimbs of adult horses. *Am. J. Vet. Res*. **65**, 819–828.

TABLE 1. Morphometric data for the species sampled and dissected.

Animal	Limb (R/L)	Body Mass (g)	Total Forelimb Muscle Mass (g)	Femur Length (mm)	Radius Length (mm)	Ulna Length (mm)	Olecranon Length (mm)	MC3 Length (mm)	Claw III (mm)
Tb1	R	146.2	6.62						
Tb2	R	137.3	6.22						
Tb3	R	186.5	7.90						
Tb4	R	118.4	6.03						
Tb5	R	160.9	6.85						
Tb6	R	99.7	4.10						
Tb7	R	138.2	4.58	20.8	20.5	27.9	6.2	3.7	14.7
Tb8	R	185.8	7.09	22.8	22.0	29.8	7.6	3.6	15.4
Tb9	R	92.6	4.06	20.6	19.2	27.0	6.5	3.4	11.5
Tb10	R	70.5	3.28	18.8	17.7	24.0	6.1	3.2	11.4
Cp1	R	30.5	0.75	13.6	13.3	15.7	2.8	2.7	2.2
Cp2	R/L	17.2	0.55	10.6	12.1	14.1	2.3	2.2	2.7
Cp3	R	17.2	0.51	12.1	11.4	14.6	2.7	2.2	1.4
Cp4	R	15.7	0.65	12.1	12.7	14.7	2.8	2.1	1.6
Cp5	R/L	17.1	0.54	11.5	12.2	14.8	2.3	2.1	1.1
Dm1	R	30.6	0.55	12.5	16.3	20.2	2.8	2.3	3.9
Dm2	R	36.1	0.69	12.3	16.7	19.3	3.1	2.0	3.2
Dm3	R	33.4	0.68	12.1	16.3	19.4	2.8	2.1	4.9

TABLE 2. Forelimb bone indices: formulae and functional significance.

Index	Definition
Shoulder Moment Index (SMI)	Delto-pectoral crest proximodistal length (or deltoid tubercle) divided by greatest humerus length (DCL/HL). Indicates degree of mechanical advantage of the shoulder joint musculature and the ability to strongly retract the humerus.
Brachial Index (BI)	Greatest radius length divided by greatest humerus length (RL/HL). Indicates distal out-lever length and overall mechanical (or velocity) advantage of the forelimb.
Radial Length Index (RLI)	Greatest radius length divided by greatest ulna length (RL/UL). Indicates relative size and the area available for muscle attachment between the radius and ulna.
Fossorial Ability Index (IFA)	Olecranon length divided by functional ulna length [OL/(FUL)]. Indicates in-lever length and mechanical advantage of elbow extensors to apply large out-force during elbow extension.
Triceps Metacarpal Out-force Index (TMOI)	Functional olecranon length divided by the sum of the functional ulna and metacarpal III length (FOL/FUL+MCL). Indicates amount of out-force applied at distal end of metacarpals per unit triceps in-force.
Relative Manus Claw Length (CLAW)	Manus claw length of digit III divided by the sum of metacarpal III length and proximal phalanx length of digit III [CL/(MCL+PPL)]. Indicates relative proportions of the manus.

TABLE 3. Functional muscle groups analyzed for mass distribution in the forelimbs of a pocket gopher, pocket mouse, and kangaroo rat.

Functional Groups and Muscles Studied
EXTRINSIC MUSCLES:
Scapula elevator/rotators
Trapezius (parts: cervical, thoracic), Rhomboideus (heads: capital, cervical, thoracic), Serratus ventralis Omocervicalis[a]
Scapula/limb retractors
Trapezius thoracica, Rhomboideus thoracis, Latissimus dorsi, Pectoralis superficialis, Pectoralis profundus[a], Pectoralis abdominis[a]
Scapula/limb protractors
Rhomboideus cervicis , Rhomboideus capitis, Omocervicalis[a]
Limb adductors
Pectoralis superficialis, Pectoralis abdominis[a]
INTRINSIC MUSCLES:
Limb retractors (shoulder flexor/stabilizers)
Spinodeltoideus, Teres major, Teres minor, Infraspinatus, Triceps brachii (long head), Subscapularis
Limb protractors (shoulder extensor/stabilizers)
Coracobrachialis, Deltoideus pars acromio-clavicularis, Supraspinatus, Biceps brachii (heads: long, short)
Humeral adductors (shoulder stabilizers)
Coracobrachialis, Subscapularis, Deltoideus pars acromio-clavicularis
Elbow flexors
Biceps brachii (heads: long, short), Brachialis
Elbow extensors
Triceps brachii (heads: long, lateral, medial), Anconeus, Tensor fasciae antebrachii[a]
Carpal flexors
Flexor carpi radialis, Flexor carpi ulnaris
Carpal extensors
Extensor carpi radialis, Extensor carpi ulnaris
Digital flexors
Flexor digitorum superficialis, Flexor digitorum profundus (heads: humeral medial, humeral lateral[b], radial, ulnar)
Digital extensors
Extensor digitorum communis, Extensor digitorum lateralis[b], Abductor digiti I longus, Extensor digiti II[b]
Pronators
Pronator teres
Supinators
Supinator

[a]m. omocervicalis, m. pectoralis profundus, m. pectoralis abdominis, and m. tensor fasciae antebrachia were only observed in the pocket gophers. [b]FDPHL, EDL, and ED2 were only observed in the pocket gopher and K-rat

Table 4. Architectural properties data for pocket gopher forelimb muscles.

Muscle	Abbrev.	*N*	Muscle mass (g)	Belly length (mm)	Fascicle length (mm)	Pennation angle (°)	PCSA (mm^2)	F_{max} (N)	Power (mW)	Fiber architecture
Trapezius pars cervicalis	TC	10	0.19±0.07	23.7±3.8	17.0±4.9	0	10.4±2.6	3.1±0.8	57.9±19.8	parallel
Trapezius pars thoracica	TT	10	0.25±0.32	41.7±5.8	29.4±6.3	0	7.5±8.6	2.3±2.6	76.5±97.6	parallel
Rhomboideus capitis	RCP	10	0.16±0.06	23.9±2.5	18.0±4.2	0	8.6±2.9	2.6±0.9	50.5±18.1	parallel
Rhomboideus cervicis	RCR	10	0.16±0.05	13.8±3.4	10.7±3.3	0	14.4±5.1	4.3±1.5	48.1±16.6	parallel
Rhomboideus thoracis	RT	4	0.09±0.05	14.3±4.0	7.6±1.6	0	10.5±5.2	3.2±1.6	10.5±16.0	parallel
Omocervicalis	OC	9	0.04±0.01	15.1±5.1	10.0±2.7	0	4.3±1.7	1.3±0.5	12.0±5.0	parallel
Latissimus dorsi	LAT	10	0.33±0.11	46.0±6.0	36.6±10.7	0	8.8±3.1	2.7±1.0	102±33.7	parallel
Pectoralis superficialis	PS	10	0.36±0.13	26.1±3.8	20.4±5.3	20±8	15.9±6.1	4.8±1.8	104±38.4	unipennate
Pectoralis profundus	PP	10	0.09±0.02	22.5±3.3	17.3±4.5	0	4.8±1.0	1.4±0.3	26.7±6.6	parallel
Pectoralis abdominis	PA	10	0.25±0.17	39.7±10.9	33.7±10.2	18±5	6.4±2.9	1.9±0.9	73.7±48.8	unipennate
Serratus Ventralis	SV	10	0.54±.01	34.3±5.1	22.4±5.1	0	22.7±4.0	6.8±1.2	167±46.4	parallel
Deltoideus scapularis	DS	10	0.07±0.03	21.5±4.6	11.9±5.9	19±7	5.3±2.2	1.6±0.7	20.1±10.0	unipennate
Deltoideus acromialis clavicularis	DAC	10	0.09±0.03	11.4±1.3	7.9±1.7	0	10.7±4.9	3.2±1.5	26.5±9.6	parallel
Teres major	TMJ	10	0.11±.04	19.7±2.4	14.4±3.5	0	6.9±1.8	2.1±0.6	32.4±11.8	parallel
Teres minor	TMN	9	0.03±0.02	12.0±3.4	6.9±2.8	18±8	4.0±1.5	1.2±0.5	8.6±6.8	unipennate
Infraspinatus	ISP	10	0.21±0.07	20.7±1.9	5.0±1.6	22±6	37.2±15.5	11.2±4.7	58.4±19.9	bipennate
Supraspinatus	SSP	10	0.24±0.06	20.5±2.2	9.0±3.3	23±6	24.7±7.5	7.4±2.2	67.6±17.1	bipennate
Subscapularis	SUB	10	0.24±0.07	19.6±3.2	4.4±1.7	20±5	50.5±15.8	15.1±4.7	69.9±19.4	multipennate
Coracobrachialis	CCB	10	0.01±0.00	14.3±2.5	3.3±2.3	22±5	3.2±2.1	1.0±0.6	2.8±0.9	bipennate
Biceps brachii - long	BBL	10	0.07±0.02	15.2±1.6	7.9±3.3	18±7	8.6±3.6	2.6±1.1	19.9±4.0	unipennate
Biceps brachii - short	BBS	10	0.04±0.02	16.8±1.8	6.3±2.9	19±6	5.5±1.5	1.7±0.5	11.3±6.2	unipennate
Brachialis	BCH	10	0.07±0.03	16.3±2.2	11.6±2.7	0	5.8±2.2	1.7±0.7	21.4±8.8	parallel

Triceps brachii – long	TBLO	10	0.49±0.14	20.9±2.3	14.4±4.2	19±7	31.2±8.9	9.4±2.7	144±39.7	unipennate
Triceps brachii – lateral	TBLA	10	0.2±0.07	21.0±2.1	15.3±3.0	0	12.1±3.4	3.6±1.0	60.9±21.4	parallel
Triceps brachii – medial	TBM	10	0.11±0.05	17.0±2.3	10.1±2.5	18±7	10.0±4.3	3.0±1.3	32.3±13.5	unipennate
Anconeus	ANC	9	0.03±0.02	8.4±2.5	5.7±1.7	0	4.4±2.3	1.3±0.7	7.7±6.8	parallel
Tensor fasciae antebrachii	TFA	9	0.04±0.01	20.5±4.1	16.1±3.6	0	2.5±0.5	0.8±0.1	11.7±4.9	parallel
Pronator teres	PT	10	0.03±0.01	11.3±1.1	7.3±1.9	0	4.6±1.9	1.4±0.6	10.7±3.8	parallel
Palmaris longus	PL	10	0.05±0.02	16.3±2.0	11.0±2.4	0	4.6±2.1	1.4±0.6	16.4±7.3	parallel
Flexor carpi radialis	FCR	10	0.01±0.00	11.2±1.6	4.6±2.7	18±8	1.8±0.9	0.5±0.3	2.2±0.9	unipennate
Flexor carpi ulnaris	FCU	10	0.07±0.04	17.4±2.6	6.9±2.6	18±4	10.3±5.8	3.1±1.8	21.5±12.3	unipennate
Flexor digitorum superficialis	FDS	10	0.06±0.02	16.3±2.4	4.3±2.1	19±5	12.6±4.4	3.8±1.3	16.4±5.3	bipennate
Flexor digitorum profundus – humeral lateral	FDPHL	10	0.02±0.00	12.7±2.9	5.5±3.1	0	3.0±1.2	0.9±0.4	4.8±1.3	parallel
Flexor digitorum profundus – humeral medial	FDPHM	10	0.07±0.02	15.9±1.5	3.4±0.9	19±5	17.4±3.2	5.2±1.0	19.2±4.3	bipennate
Flexor digitorum profundus – radial	FDPR	10	0.03±0.01	12.2±2.5	4.4±1.3	25±5	5.7±2.4	1.7±0.7	7.9±3.5	unipennate
Flexor digitorum profundus – ulnar	FDPU	10	0.07±0.02	19.3±3.2	4.8±2.1	20±5	15.2±7.7	4.6±2.3	20.8±7.0	unipennate
Extensor carpi radialis – longus	ECRL	10	0.05±0.02	16.6±1.8	12.9±1.9	0	3.4±1.5	1.0±0.4	14.4±6.6	parallel
Extensor carpi radialis – brevis	ECRB	10	0.05±0.01	15.5±2.4	12.5±2.3	0	4.1±0.7	1.2±0.2	16.7±4.4	parallel
Extensor carpi ulnaris	ECU	10	0.03±0.01	16.1±2.2	4.0±2.2	19±5	8.8±5.0	2.7±1.5	9.7±3.3	bipennate
Extensor digitorum communis	EDC	10	0.03±0.01	15.1±2.4	5.6±1.8	17±3	5.5±1.8	1.7±0.5	9.8±2.5	bipennate
Extensor digitorum lateralis	EDL	10	0.01±0.01	12.2±1.6	6.2±2.9	0	2.7±2.2	0.8±0.7	3.6±1.5	parallel
Extensor digiti II	ED2	10	0.01±0.01	10.5±1.5	3.9±1.8	17±5	1.6±1.5	0.5±0.4	2.0±1.6	unipennate
Abductor digiti I longus	ADL1	10	0.02±0.01	13.3±2.9	2.9±1.2	18±4	7.5±3.4	2.2±1.0	6.9±2.4	bipennate
Supinator	SUP	10	0.01±0.00	8.1±1.2	5.3±1.5	0	1.3±0.3	0.4±0.1	2.3±1.0	parallel

Table 5 Architectural properties data for pocket mouse forelimb muscles.

Muscle	Abbrev.	*N*	Muscle mass (mg)	Belly length (mm)	Fascicle length (mm)	Pennation angle (°)	PCSA (mm^2)	F_{max} (N)	Power (mW)	Fiber architecture
Trapezius pars cervicalis	TC	5	20.6±13.0	10.9±2.2	9.1±2.5	0	2.1±0.8	0.6±0.3	6.7±4.2	parallel
Trapezius pars thoracica	TT	5	16.2±7.4	14.1±2.2	10.4±2.6	0	1.5±0.4	0.4±0.1	5.2±2.4	parallel
Rhomboideus capitis	RCP	4	34.2±19.8	12.7±3.3	9.9±3.1	0	3.4±1.6	1.0±0.5	8.8±7.4	parallel
Rhomboideus cervicis	RCR	5	11.1±4.2	8.0±1.9	6.2±1.1	0	1.7±0.5	0.5±0.2	3.6±1.4	parallel
Rhomboideus thoracis	RT	5	18.6±4.9	9.9±1.1	7.3±1.5	0	2.4±0.7	0.7±0.2	6.0±1.6	parallel
Latissimus dorsi	LAT	5	38.2±14.6	26.5±3.9	15.5±4.6	0	2.4±1.1	0.7±0.3	12.3±4.7	parallel
Pectoralis superficialis	PS	5	66.7±19.7	16.4±2.9	10.7±2.5	0	5.8±1.2	1.7±0.4	21.5±6.4	parallel
Serratus Ventralis	SV	5	40.8±18.5	17.9±1.7	10.4±2.9	0	3.9±2.1	1.2±0.6	13.2±6.0	parallel
Deltoideus scapularis	DS	5	5.0±4.7	7.4±0.7	5.1±1.1	0	0.9±0.9	0.3±0.3	1.6±1.5	parallel
Deltoideus acromialis clavicularis	DAC	5	5.5±2.1	5.5±0.7	4.7±0.9	0	1.1±0.4	0.3±0.1	1.8±0.7	parallel
Teres major	TMJ	5	32.7±5.8	10.7±0.9	8.7±1.0	0	3.6±0.7	1.1±0.2	10.6±1.9	parallel
Teres minor	TMN	5	16.4±12.7	10.4±1.4	8.7±1.2	0	1.8±1.3	0.5±0.4	5.3±4.1	parallel
Infraspinatus	ISP	5	19.8±4.1	10.2±0.6	2.5±0.8	20±4	7.1±1.8	2.1±0.5	6.0±1.3	bipennate
Supraspinatus	SSP	5	23.4±4.6	10.6±0.6	7.9±1.3	0	2.8±0.5	0.8±0.1	7.5±1.5	parallel
Subscapularis	SUB	5	17.3±4.5	10.1±1.1	2.4±0.9	19±4	6.9±2.5	2.1±0.8	5.3±1.3	multipennate
Coracobrachialis	CCB	5	2.0±0.6	7.2±1.4	1.2±0.4	18±5	1.5±0.4	0.5±0.1	0.6±0.2	bipennate
Biceps brachii - long	BBL	5	9.1±1.4	8.8±0.8	6.6±0.7	0	1.3±0.2	0.4±0.1	2.9±0.4	parallel
Biceps brachii - short	BBS	5	3.9±0.9	8.2±0.9	6.9±0.6	0	0.5±0.1	0.2±0.04	1.3±0.3	parallel
Brachialis	BCH	5	10.4±1.1	7.4±0.2	5.5±1.1	0	1.8±0.4	0.6±0.1	3.4±0.4	parallel
Triceps brachii – long	TBLO	5	55.1±2.7	11.1±0.7	9.7±0.7	0	5.4±0.5	1.6±0.2	17.8±0.9	parallel
Triceps brachii – lateral	TBLA	5	21.0±4.1	10.9±0.7	8.6±1.3	0	2.3±0.5	0.7±0.2	6.8±1.3	parallel
Triceps brachii – medial	TBM	5	3.7±1.8	7.6±1.0	5.0±1.4	0	0.7±0.4	0.2±0.1	1.2±0.6	parallel

Anconeus	ANC	5	2.1±0.9	5.1±0.2	3.5±0.6	0	0.6±0.3	0.2±0.1	0.7±0.3	parallel
Pronator teres	PT	5	2.1±0.7	5.3±0.6	3.6±0.8	0	0.5±0.2	0.2±0.1	0.7±0.2	parallel
Flexor carpi radialis	FCR	5	3.1±1.9	7.7±1.8	4.5±1.2	0	0.9±1.1	0.3±0.3	1.0±0.6	parallel
Flexor carpi ulnaris	FCU	5	4.7±1.8	8.3±1.7	3.0±1.5	17±4	1.8±1.0	0.5±0.3	1.4±0.6	bipennate
Flexor digitorum superficialis	FDS	5	6.4±2.7	9.5±2.4	3.6±2.3	14±3	1.7±0.6	0.5±0.2	2.0±0.9	bipennate
Flexor digitorum profundus – humeral medial	FDPHM	5	13.2±4.7	9.6±1.1	3.6±2.2	14±2	4.3±3.0	1.3±0.9	4.1±1.5	bipennate
Flexor digitorum profundus – radial	FDPR	5	5.5±2.7	7.7±1.7	4.7±1.2	16±2	1.0±0.4	0.3±0.1	1.7±0.8	unipennate
Flexor digitorum profundus – ulnar	FDPU	5	4.3±1.5	7.2±1.7	3.4±1.9	12±3	1.2±0.5	0.4±0.2	1.4±0.5	unipennate
Extensor carpi radialis – longus	ECRL	5	5.5±1.4	8.3±1.4	6.8±1.5	0	0.8±0.4	0.3±0.1	1.8±0.5	parallel
Extensor carpi radialis – brevis	ECRB	5	5.9±0.6	8.7±0.9	6.7±1.0	0	0.8±0.2	0.3±0.1	1.9±0.2	parallel
Extensor carpi ulnaris	ECU	5	1.8±0.6	8.6±1.9	3.5±2.2	13±3	0.6±0.4	0.2±0.1	0.6±0.2	bipennate
Extensor digitorum communis	EDC	5	4.4±1.2	9.7±1.3	2.7±1.9	16±3	2.0±1.4	0.6±0.4	1.4±0.4	bipennate
Abductor digiti I longus	ADL1	5	2.5±0.5	8.6±0.7	3.4±1.6	17±4	0.8±0.3	0.2±0.1	0.8±0.2	bipennate
Supinator	SUP	4	0.4±0.3	5.5±1.3	3.6±1.1	0	0.1±0.1	0.03±0.02	0.1±0.1	parallel

Table 6. Architectural properties data for kangaroo rat forelimb muscles.

Muscle	Abbrev.	*N*	Muscle mass (mg)	Belly length (mm)	Fascicle length (mm)	Pennation angle (°)	PCSA (mm^2)	F_{max} (N)	Power (mW)	Fiber architecture
Trapezius pars cervicalis	TC	3	21.9±7.8	12.7±1.6	10.8±2.3	0	1.9±0.4	0.6±0.1	6.3±2.2	parallel
Trapezius pars thoracica	TT	3	13.1±5.9	18.0±3.2	15.1±2.6	0	0.9±0.5	0.3±0.1	3.8±1.7	parallel
Rhomboideus capitis	RCP	3	9.5±3.3	8.7±2.9	8.0±2.0	0	1.1±0.2	0.3±0.1	2.7±0.9	parallel
Rhomboideus cervicis	RCR	3	10.7±5.6	7.1±0.5	5.6±1.2	0	1.9±1.2	0.6±0.4	3.1±1.6	parallel
Rhomboideus thoracis	RT	3	13.6±9.7	8.8±2.2	7.5±1.8	0	2.0±1.6	0.6±0.5	3.9±2.8	parallel
Latissimus dorsi	LAT	3	34.4±5.7	25.4±3.2	22.9±2.0	0	1.4±0.1	0.4±0.04	9.8±1.6	parallel
Pectoralis superficialis	PS	3	57.9±7.8	15.9±1.1	12.2±1.9	0	4.5±0.5	1.3±0.2	16.6±2.2	parallel
Serratus Ventralis	SV	3	105.5±13.2	22.5±5.4	14.3±6.2	0	7.9±3.0	2.4±0.9	30.2±3.8	parallel
Deltoideus scapularis	DS	3	6.3±1.7	8.8±0.4	6.0±1.7	0	1.0±0.2	0.3±0.1	1.8±0.5	parallel
Deltoideus acromialis clavicularis	DAC	3	6.2±2.1	4.9±0.6	4.0±0.7	0	1.6±0.7	0.5±0.2	1.8±0.6	parallel
Teres major	TMJ	3	38.7±5.5	12.5±0.4	9.7±0.8	19±5	3.5±0.6	1.1±0.2	10.4±1.6	unipennate
Teres minor	TMN	3	2.4±0.8	6.6±1.2	2.7±1.7	0	0.7±0.4	0.2±0.1	0.7±0.2	parallel
Infraspinatus	ISP	3	18.2±2.2	11.9±1.3	2.8±1.4	16±4	6.4±2.4	1.9±0.7	5.0±0.5	bipennate
Supraspinatus	SSP	3	22.0±6.6	11.5±0.3	7.0±2.6	0	2.9±0.3	0.9±0.1	6.3±1.9	parallel
Subscapularis	SUB	3	30.1±3.8	12.2±0.4	2.7±1.0	16±4	10.8±3.8	3.3±1.2	8.3±0.9	multipennate
Coracobrachialis	CCB	3	1.3±0.2	6.9±0.5	1.1±0.3	12±3	1.1±0.04	0.3±0.01	0.4±0.1	bipennate
Biceps brachii - long	BBL	3	13.4±3.3	9.1±0.9	7.1±0.8	0	1.8±0.5	0.5±0.2	3.8±1.0	parallel
Biceps brachii - short	BBS	3	6.5±3.2	8.0±0.3	6.9±0.5	0	0.9±0.5	0.3±0.2	1.9±0.9	parallel
Brachialis	BCH	3	10.4±2.3	7.7±0.9	6.2±0.8	0	1.60.4	0.5±0.1	3.0±0.6	parallel
Triceps brachii – long	TBLO	3	41.6±4.6	11.0±0.3	9.8±0.9	0	4.0±0.4	1.2±0.1	11.9±1.3	parallel
Triceps brachii – lateral	TBLA	3	13.4±2.8	11.0±1.0	9.3±1.5	0	1.4±0.4	0.4±0.1	3.8±0.8	parallel
Triceps brachii – medial	TBM	3	6.9±2.4	7.3±1.0	5.2±1.5	0	1.4±0.8	0.4±0.2	2.0±0.7	parallel

Anconeus	ANC	3	3.4±1.6	5.8±0.6	4.4±0.7	0	0.7±0.3	0.2±0.1	1.0±0.5	parallel
Pronator teres	PT	3	3.3±1.5	6.5±1.2	4.9±1.2	0	0.7±0.4	0.2±0.1	1.0±0.4	parallel
Palmaris longus	PL	3	6.8±0.8	11.2±0.4	6.4±1.7	0	1.0±0.2	0.3±0.1	1.9±0.3	parallel
Flexor carpi radialis	FCR	3	4.3±0.7	7.9±0.6	3.3±1.0	13±2	1.2±0.3	0.4±0.1	1.2±0.2	bipennate
Flexor carpi ulnaris	FCU	3	2.6±0.7	8.3±1.4	4.3±1.4	12±3	0.6±0.4	0.2±0.1	0.7±0.2	bipennate
Flexor digitorum superficialis	FDS	3	6.0±1.0	10.9±0.5	2.7±1.2	11±3	2.2±0.6	0.7±0.2	1.7±0.3	multipennate
Flexor digitorum profundus – humeral lateral	FDPHL	3	2.0±1.2	6.4±3.0	3.6±0.8	0	0.5±0.4	0.2±0.1	0.6±0.3	parallel
Flexor digitorum profundus – humeral medial	FDPHM	3	13.9±3.0	11.6±1.6	3.0±1.1	15±4	4.5±1.6	1.3±0.5	3.8±0.8	bipennate
Flexor digitorum profundus – radial	FDPR	3	7.3±1.3	9.8±0.9	3.0±1.4	22±3	2.2±0.3	0.7±0.1	1.9±0.4	unipennate
Flexor digitorum profundus – ulnar	FDPU	3	8.6±2.5	11.7±1.4	3.2±0.6	13±3	2.6±0.9	0.8±0.3	2.4±0.7	unipennate
Extensor carpi radialis – longus	ECRL	3	8.0±1.8	10.9±0.2	9.1±0.6	0	0.8±0.2	0.3±0.1	2.3±0.5	parallel
Extensor carpi radialis – brevis	ECRB	3	9.6±1.3	11.0±0.9	5.1±0.8	12±3	1.8±0.3	0.5±0.1	2.7±0.4	bipennate
Extensor carpi ulnaris	ECU	3	2.4±1.0	9.6±1.2	3.1±0.8	11±3	0.7±0.3	0.2±0.1	0.7±0.3	bipennate
Extensor digitorum communis	EDC	3	5.0±3.7	8.6±0.9	3.0±1.0	14±3	1.8±1.4	0.5±0.4	1.4±1.0	bipennate
Extensor digitorum lateralis	EDL	3	0.5±0.3	9.0±1.1	2.6±1.1	8±3	0.3±0.3	0.08±0.08	0.1±0.1	bipennate
Extensor digiti II	ED2	3	1.5±0.3	8.7±0.9	4.4±1.2	0	0.4±0.3	0.1±0.1	0.4±0.2	parallel
Abductor digiti I longus	ADL1	3	4.1±1.2	9.8±0.7	2.3±1.1	17±4	1.9±1.1	0.6±0.3	1.1±0.3	bipennate
Supinator	SUP	3	0.8±0.3	6.4±0.3	4.1±1.4	0	0.2±0.05	0.06±0.02	0.2±0.1	parallel

Table 7. Muscle moment arms (r_m), joint torques, and architectural indices (AI) for pocket gopher forelimb muscles.

Muscle	Joint	Mean r_m (mm)	Joint Torque (N.mm)	L_F/r_m	L_F/ML
Latissimus dorsi	Shoulder	**6.4±2.9**	16.9	6.46	0.79
Pectoralis superficialis		**5.0±1.7**	24.3	4.57	0.78
Pectoralis profundus		**3.7±1.3**	5.2	5.00	0.77
Pectoralis abdominis		**4.0±0.9**	7.6	8.39	0.82
Scapulodeltoideus		**4.8±1.7**	8.2	2.87	0.58
Acromio-clavicular deltoideus		**3.9±1.3**	13.2	2.19	0.70
Teres major		**5.0±1.1**	10.6	3.01	0.73
Teres minor		**3.1±0.7**	3.6	2.47	0.60
Infraspinatus		**2.0±0.7**	22.6	2.93	0.24
Supraspinatus		**3.2±1.4**	24.4	3.89	0.43
Subscapularis		**2.6±0.8**	39.3	1.87	0.23
Coracobrachialis		**1.9±0.6**	1.8	2.33	0.27
Triceps brachii – long		**9.1±3.0**	86.0	2.10	0.69
Biceps brachii - long		**3.2±1.5**	7.4	3.14	0.53
Biceps brachii – long	Elbow	**3.1±0.4**	8.1	2.75	0.53
Biceps brachii – short		**2.3±0.3**	3.9	2.85	0.40
Brachialis		**2.8±0.9**	4.8	4.76	0.71
Triceps brachii – long		**7.4±1.3**	70.6	2.00	0.69
Triceps brachii – lateral		**4.7±0.9**	17.5	3.33	0.73
Triceps brachii – medial		**5.6±0.8**	16.8	1.80	0.59
Anconeus		**2.9±1.1**	4.4	2.09	0.69
Tensor fasciae antebrachii		**7.1±1.2**	5.6	2.34	0.80
Flexor carpi radialis	Carpal	**1.3±0.5**	0.7	4.42	0.41
Flexor carpi ulnaris		**2.6±0.9**	8.7	2.81	0.39
Palmaris Longus		**2.4±0.7**	3.5	4.87	0.68
Flexor digitorum superficialis		**2.0±0.8**	7.9	2.37	0.27
Flexor digitorum profundus – humeral medial		**1.3±0.5**	6.9	2.93	0.22
Flexor digitorum profundus – humeral lateral		**1.6±0.6**	1.5	3.73	0.44
Flexor digitorum profundus – radial		**1.7±0.7**	3.1	3.19	0.38
Flexor digitorum profundus – ulnar		**1.9±0.4**	8.4	2.79	0.28

In bold are mean ± s.d.
L_F is mean fascicle length
r_m is mean moment arm
ML is muscle belly length
L_F/r_m ratios >2.0 indicate a high ability of the muscle to move a joint through a large range of motion
L_F/ML ratios >0.6 indicate a high ability of the muscle to shorten and contract at appreciable velocity

Table 8. Muscle moment arms (r_m), joint torques, and architectural indices (AI) for pocket mouse forelimb muscles.

Muscle	Joint	Mean r_m (mm)	Joint Torque (N.mm)	L_F/r_m	L_F/ML
Latissimus dorsi	Shoulder	**2.2±0.1**	1.6	7.13	0.58
Pectoralis superficialis		**2.8±0.8**	4.8	4.15	0.66
Scapulodeltoideus		**1.6±0.5**	0.4	3.40	0.69
Acromio-clavicular deltoideus		**2.7±0.5**	0.9	1.75	0.84
Teres major		**2.9±0.9**	3.1	3.36	0.82
Teres minor		**1.9±0.7**	1.0	5.51	0..84
Infraspinatus		**1.2±0.3**	2.4	2.20	0.25
Supraspinatus		**1.4±0.3**	1.2	5.82	0.75
Subscapularis		**1.0±0.2**	1.9	2.44	0.23
Coracobrachialis		**0.9±0.3**	0.4	1.44	0.18
Triceps brachii – long		**2.3±0.5**	3.6	4.38	0.87
Biceps brachii – long		**1.9±0.3**	0.7	3.58	0.75
Biceps brachii – long	Elbow	**1.8±0.2**	0.7	3.79	0.75
Biceps brachii – short		**0.9±0.1**	0.1	7.93	0.85
Brachialis		**1.2±0.3**	0.7	4.74	0.74
Triceps brachii – long		**3.1±0.9**	5.0	3.35	0.87
Triceps brachii – lateral		**1.9±0.2**	1.4	4.54	0.79
Triceps brachii – medial		**1.9±0.3**	0.4	2.73	0.67
Anconeus		**1.4±0.5**	0.2	2.93	0.70
Flexor carpi radialis	Carpal	**0.7±0.1**	0.2	6.85	0.58
Flexor carpi ulnaris		**0.8±0.1**	0.4	3.98	0.36
Flexor digitorum superficialis		**1.0±0.1**	0.5	3.69	0.40
Flexor digitorum profundus – humeral medial		**1.0±0.2**	1.2	4.65	0.43
Flexor digitorum profundus – radial		**0.9±0.3**	0.3	5.60	0.64
Flexor digitorum profundus – ulnar		**1.1±0.2**	0.4	3.21	0.51

In bold are mean ± s.d.
L_F is mean fascicle length
r_m is mean moment arm
ML is muscle belly length
L_F/r_m ratios >2.0 indicate a high ability of the muscle to move a joint through a large range of motion
L_F/ML ratios >0.6 indicate a high ability of the muscle to shorten and contract at appreciable velocity

Table 9. Muscle moment arms (r_m), joint torques, and architectural indices (AI) for kangaroo rat forelimb muscles.

Muscle	Joint	Mean r_m (mm)	Joint Torque (N.mm)	L_F/r_m	L_F/ML
Latissimus dorsi	Shoulder	**2.3±0.5**	1.0	10.31	0.90
Pectoralis superficialis		**3.3±0.1**	4.4	3.68	0.77
Scapulodeltoideus		**2.2±0.2**	0.7	1.32	0.68
Acromio-clavicular deltoideus		**3.0±0.1**	1.4	2.71	0.81
Teres major		**3.2±0.1**	3.4	3.05	0.78
Teres minor		**1.3±0.5**	0.4	2.11	0.44
Infraspinatus		**1.2±0.3**	2.4	2.62	0.24
Supraspinatus		**1.4±0.7**	1.2	6.17	0.61
Subscapularis		**1.1±0.2**	3.5	2.39	0.22
Coracobrachialis		**0.6±0.1**	0.2	1.91	0.17
Triceps brachii – long		**1.8±0.2**	2.2	5.41	0.90
Biceps brachii – long		**2.5±0.2**	1.3	2.88	0.79
Biceps brachii – long	Elbow	**2.4±0.4**	1.2	3.05	0.79
Biceps brachii – short		**1.3±0.5**	0.4	6.25	0.86
Brachialis		**1.6±1.0**	0.7	4.79	0.80
Triceps brachii – long		**2.8±0.6**	3.3	3.71	0.90
Triceps brachii – lateral		**1.8±0.2**	0.8	5.32	0.87
Triceps brachii – medial		**1.6±0.4**	0.7	3.38	0.72
Anconeus		**1.4±0.3**	0.3	3.32	0.75
Flexor carpi radialis	Carpal	**0.7±0.3**	0.2	5.62	0.42
Flexor carpi ulnaris		**1.0±0.1**	0.2	4.13	0.50
Palmaris Longus		**1.3±0.1**	0.4	4.96	0.57
Flexor digitorum superficialis		**1.2±0.6**	0.7	2.49	0.24
Flexor digitorum profundus – humeral medial		**1.1±0.1**	1.5	2.66	0.25
Flexor digitorum profundus – humeral lateral		**0.9±0.3**	0.1	4.91	0.67
Flexor digitorum profundus – radial		**0.9±0.1**	0.6	3.52	0.30
Flexor digitorum profundus – ulnar		**0.7±0.2**	0.5	5.21	0.27

In bold are mean ± s.d.
L_F is mean fascicle length
r_m is mean moment arm
ML is muscle belly length
L_F/r_m ratios >2.0 indicate a high ability of the muscle to move a joint through a large range of motion
L_F/ML ratios >0.6 indicate a high ability of the muscle to shorten and contract at appreciable velocity

Table 10. Mean percentage MHC isoform content for power stroke muscles in the forelimbs of a pocket gopher, pocket mouse, and kangaroo rat.

Muscle	Species	Myosin Heavy Chain Isoform (%)			
		MHC-1	MHC-2A	MHC-2X	MHC-2B
Latissimus dorsi	*Tb*	15.2±5.4	83.8±4.9	0.9±1.6	0.0
	Cp	--	--	--	--
	Dm	0.0	43.8±9.7	56.2±9.7	0.0
Pectoralis superficialis	*Tb*	16.6±3.5	80.5±7.6	2.9±4.5	0.0
	Cp	0.0	49.1±7.6	50.9±7.6	0.0
	Dm	0.0	41.6±25.3	58.4±25.3	0.0
Deltoideus	*Tb*	19.2±1.4	71.3±8.6	9.5±7.5	0.0
	Cp	0.0	40.7±3.1	46.7±3.4	12.6±6.4
	Dm	0.0	36.5±14.1	63.5±14.1	0.0
Teres major	*Tb*	11.1±0.5	78.6±5.3	10.2±4.8	0.0
	Cp	0.0	46.1±6.2	46.3±3.4	7.6±7.7
	Dm	0.0	33.4±23.4	66.6±23.4	0.0
Infraspinatus	*Tb*	13.4±5.3	61.5±12.2	25.1±9.9	0.0
	Cp	0.0	34.6±11.6	33.3±9.3	33.2±20.8
	Dm	0.0	41.5±9.8	58.5±9.8	0.0
Subscapularis	*Tb*	11.0±2.6	78.4±17.0	10.6±18.4	0.0
	Cp	0.0	51.1±18.1	35.0±15.3	13.9±5.6
	Dm	0.0	52.5±2.5	47.5±2.5	0.0
Triceps brachii long	*Tb*	14.4±2.2	78.1±0.6	7.4±2.2	0.0
	Cp	0.0	47.7±3.4	46.1±7.3	6.2±6.0
	Dm	0.0	37.8±28.7	62.2±28.7	0.0
Triceps brachii lateral	*Tb*	0.0	76.4±16.6	23.6±16.6	0.0
	Cp	0.0	48.5±3.9	47.7±2.9	3.8±3.7
	Dm	0.0	24.3±20.9	75.7±20.9	0.0
Flexor carpi ulnaris	*Tb*	11.4±1.4	85.7±4.1	3.0±5.1	0.0
	Cp	--	--	--	--
	Dm	--	--	--	--
Flexor digitorum superficialis	*Tb*	14.5±7.0	81.6±4.5	4.0±5.5	0.0
	Cp	--	--	--	--
	Dm	--	--	--	--
Flexor digitorum profundus	*Tb*	11.1±5.6	87.2±6.4	1.7±1.5	0.0
	Cp	0.0	33.5±15.4	35.4±11.8	31.1±21.8
	Dm	0.0	86.2±4.7	13.8±4.7	0.0

All data are mean ± s.d. for each muscle listed in order: pocket gopher, pocket mouse, and k-rat; means for each muscle were computed from 3 independent gel experiments per individual.

Mm. flexor carpi ulnaris and *flexor digitorum superficialis* were too small to sample in pocket mice and k-rats.

M. latissimus dorsi had low band resolution and was not quantifiable in pocket mice.

Fig. 1. Box and whisker plots for osteological indices. Boxes show the range of each index (whiskers), mean (horizontal bars), and data quartiles (boxes). **a**. SMI, shoulder moment index; **b**. BI, brachial index; **c**. RLI, radial length index; **d**. IFA, fossorial ability index; **e**. TMOI, Triceps Metacarpal Out-force Index; **f**. CLAW, Relative Manus Claw Length. Black boxes are pocket gopher; white boxes are pocket mouse; grey boxes are kangaroo rat. Significance levels: $*p<0.05$ and $**p<0.001$.

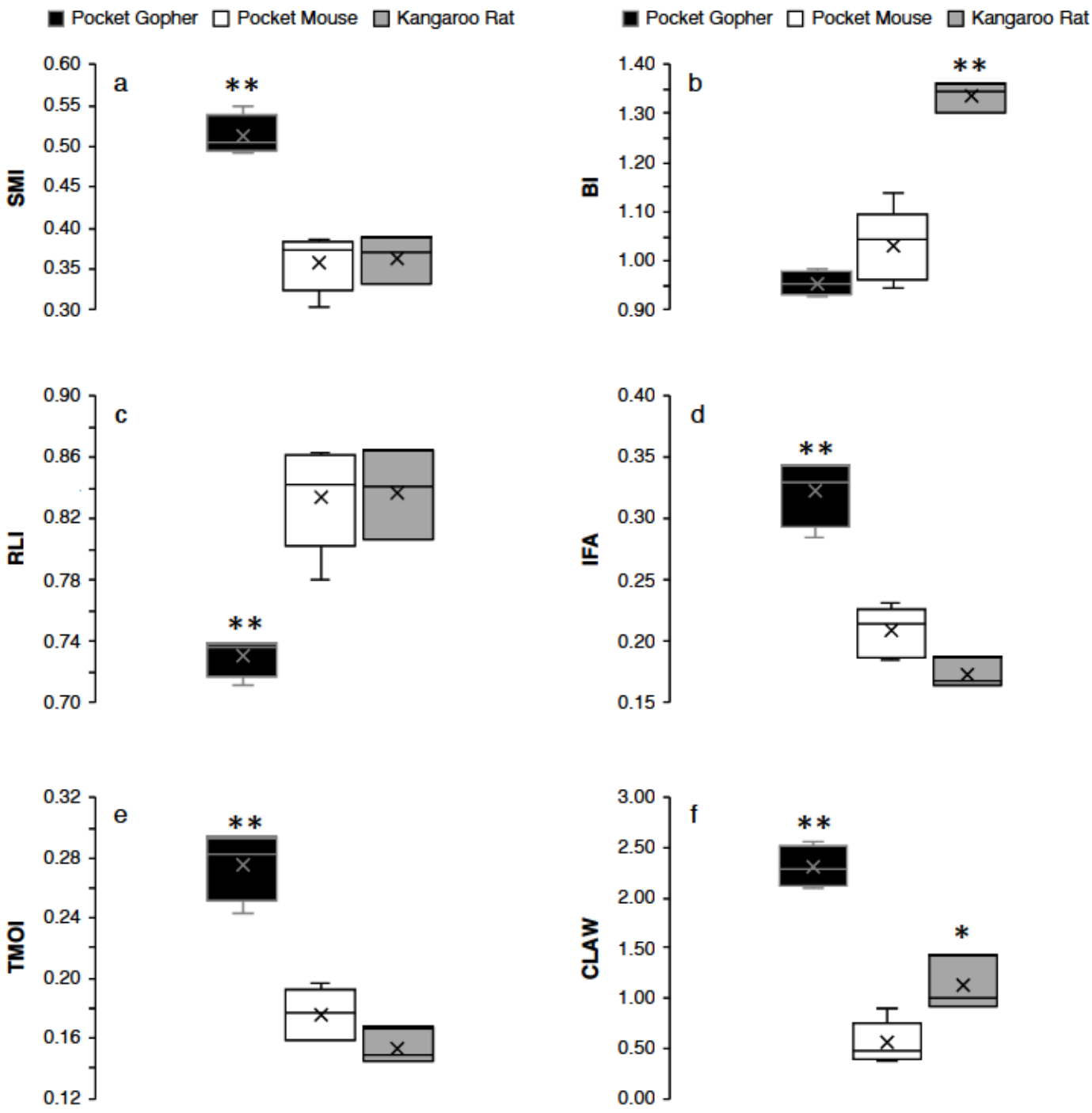
Pocket Gopher
Pocket Mouse
Kangaroo Rat
a
SMI
0.60
0.55
0.50
0.45
0.40
0.35
0.30
**
b
BI
1.40
1.30
1.20
1.10
1.00
0.90
**
c
RLI
0.90
0.86
0.82
0.78
0.74
0.70
**
d
IFA
0.40
0.35
0.30
0.25
0.20
0.15
**
e
TMOI
0.32
0.28
0.24
0.20
0.16
0.12
**
f
CLAW
3.00
2.50
2.00
1.50
1.00
0.50
0.00
**
*

Fig. 2. Distribution of functional group muscle mass to total forelimb muscle mass in pocket gopher, pocket mouse, and K-rat forelimbs. Total forelimb muscle mass was calculated as the summed mass of all individual muscles studied per limb. Proximal-to-distal muscle group mass is expressed as a percentage, with bars representing means for each functional group: N=10, *T. bottae*; N=5, *C. penicillatus*; and N=3, *D. merriami*. Error bars represent the standard deviation (s.d.). Muscles with synergistic functions are combined in one functional group. Biarticular muscles are included in more than one functional group. Black bars are pocket gopher, white bars are pocket mouse, and grey bars are kangaroo rat.

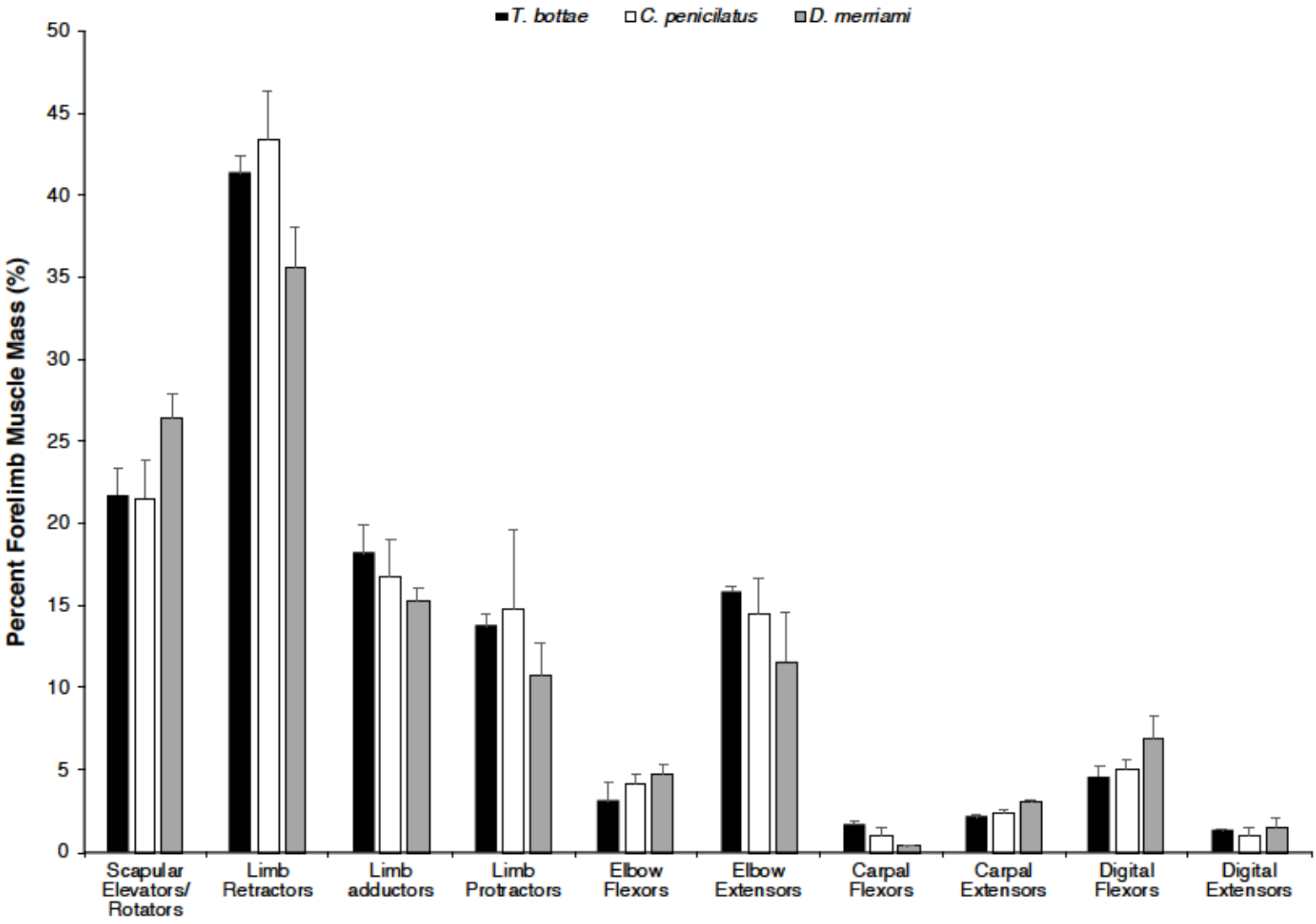
T. bottae
C. penicillatus
D. merriami
Percent Forelimb Muscle Mass (%)
50
45
40
35
30
25
20
15
10
5
0
Scapular Elevators/ Rotators
Limb Retractors
Limb adductors
Limb Protractors
Elbow Flexors
Elbow Extensors
Carpal Flexors
Carpal Extensors
Digital Flexors
Digital Extensors

Fig. 3. Architectural index of fascicle length (L_F) to muscle length (ML) ratios for pocket gopher, pocket mouse, and K-rat functional groups. A ratio closer to 1.0 indicates greater fascicle shortening capability and velocity of contraction. Bars are means±s.d. and are color-coded by species the same as illustrated in Figure 2. Functional groups are Scapular rotators/stabilizers: TC, TT, RCP, RCR, RT, SV, and OC[a]; Humeral protractors: DAC, CCB, SSP, BBL, and BBS; Humeral retractors: LAT, PS, PA[a], PP[a], DS, TMJ, ISP, TMN, SUB, and TBLO; Elbow extensors: TBLO, TBLA, TBM, ANC, and TFA[a]; Carpal flexors: FCU and FCR; Digital flexors: FDPHL[ab], FDPU, FDPHM, FDPR, FDS, and PL[ab]. Muscle abbrieviations are defined in Tables 4–6. a, muscles found in only *T. bottae*. ab, muscles found in both *T. bottae* and *D. merriami*.

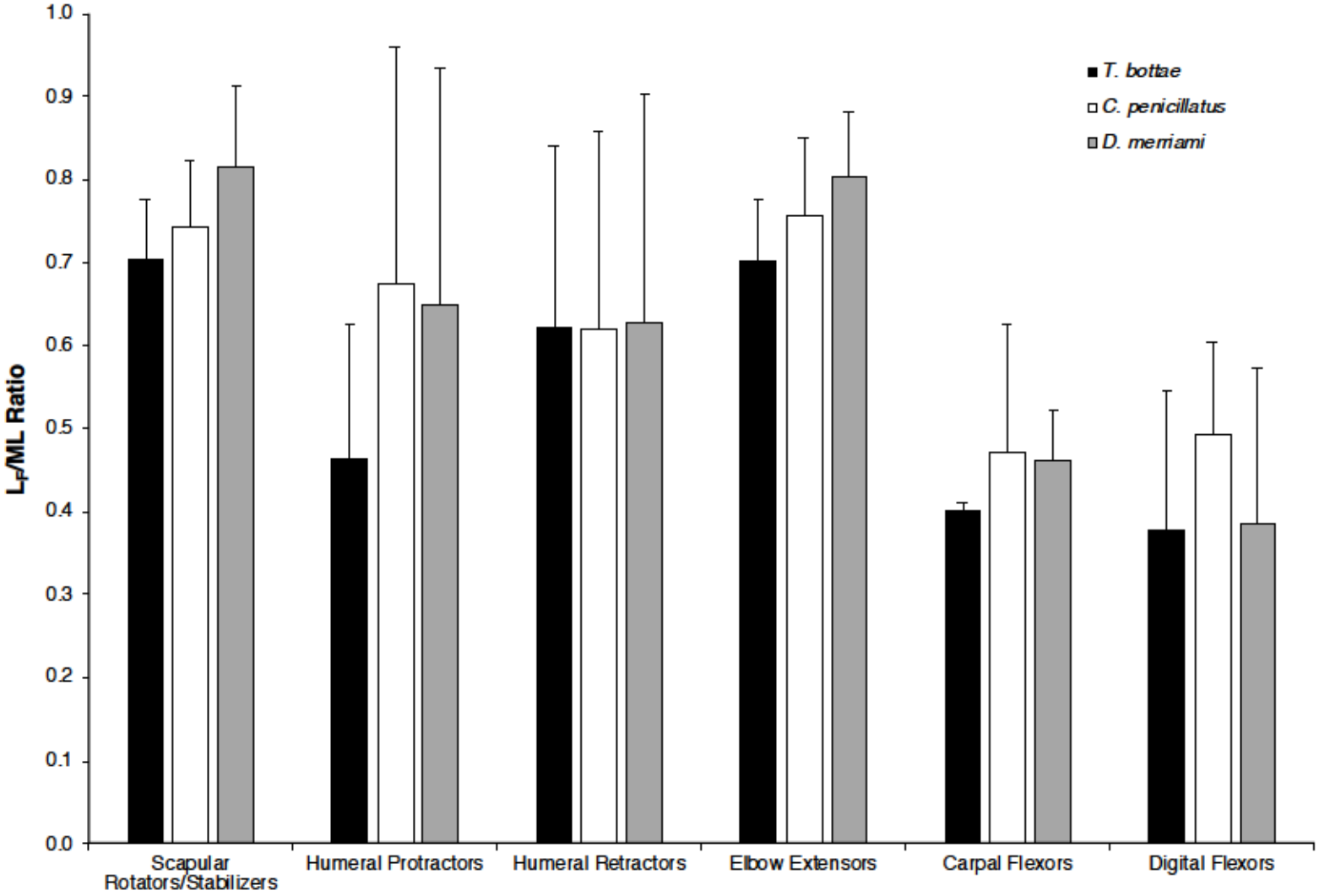
1.0
0.9
0.8
0.7
0.6
0.5
0.4
0.3
0.2
0.1
0.0
L_F/ML Ratio
T. bottae
C. penicillatus
D. merriami
Scapular Rotators/Stabilizers
Humeral Protractors
Humeral Retractors
Elbow Extensors
Carpal Flexors
Digital Flexors

Fig. 4. Architectural index of physiological cross-section area (PCSA) to muscle mass (MM) for pocket gopher, pocket mouse, and K-rat functional groups. A ratio closer to 1.0 indicates larger force production capability (per unit mass). Bars are means±s.d. and are color-coded by species the same as illustrated in Figure 2. The muscles in each functional group are the same as those classified in Figure 3. Coracobrachialis excluded from humeral protractors due to large variability in degree of pennation.

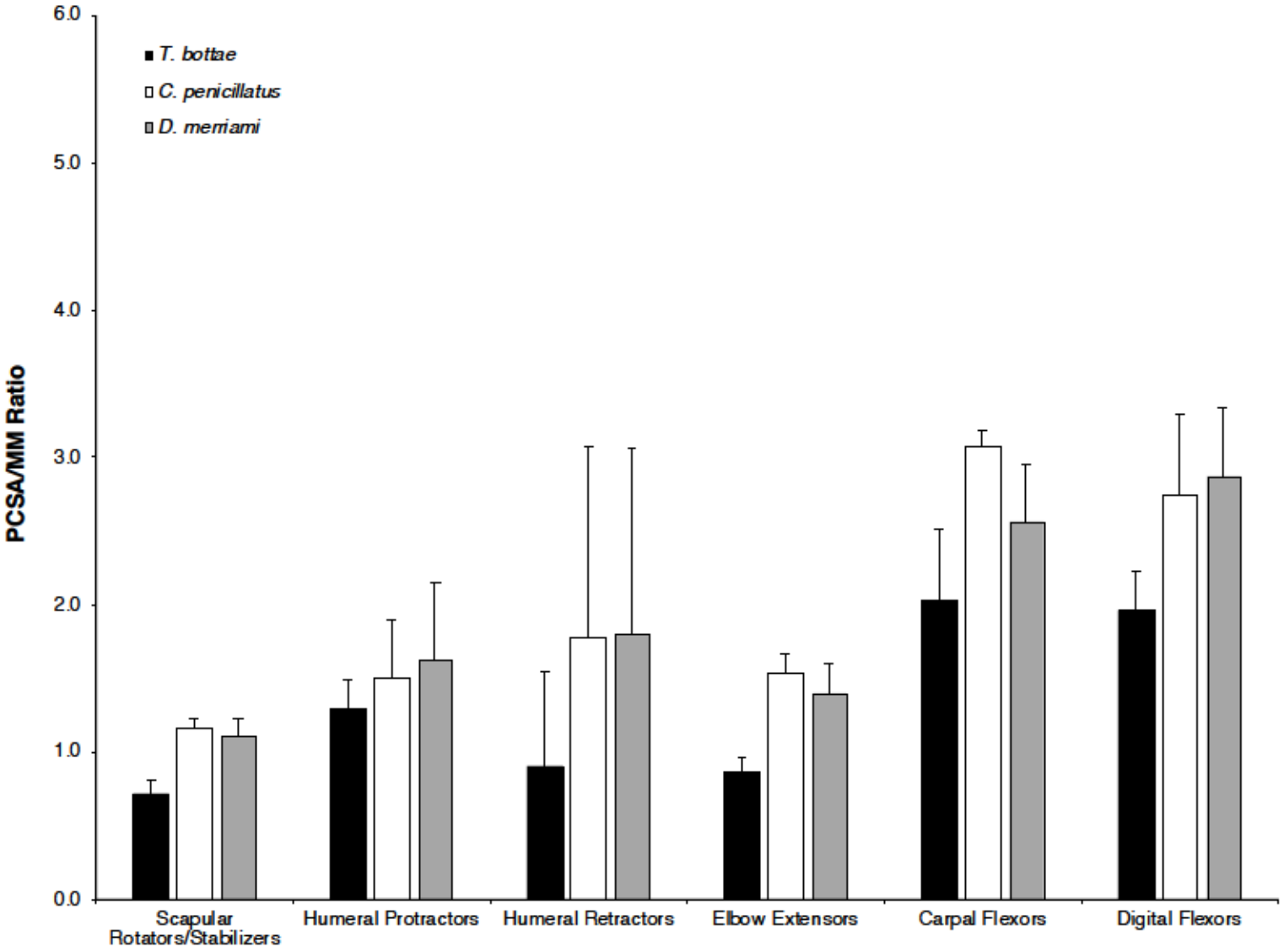
6.0
5.0
4.0
3.0
2.0
1.0
0.0
PCSA/MM Ratio
T. bottae
C. penicillatus
D. merriami
Scapular Rotators/Stabilizers
Humeral Protractors
Humeral Retractors
Elbow Extensors
Carpal Flexors
Digital Flexors

Fig. 5. Architectural index of fascicle length (L_F) to muscle moment arm (r_m) for pocket gopher, pocket mouse, and k-rat functional groups. Ratios greater than 2–3 indicates an ability for muscle contraction to move the joint through a large range of motion. Bars are means±s.d. and are color-coded by species the same as illustrated in Figure 2. The muscles in each functional group are the same as those classified in Figure 3 except for scapular rotators/stabilizers.

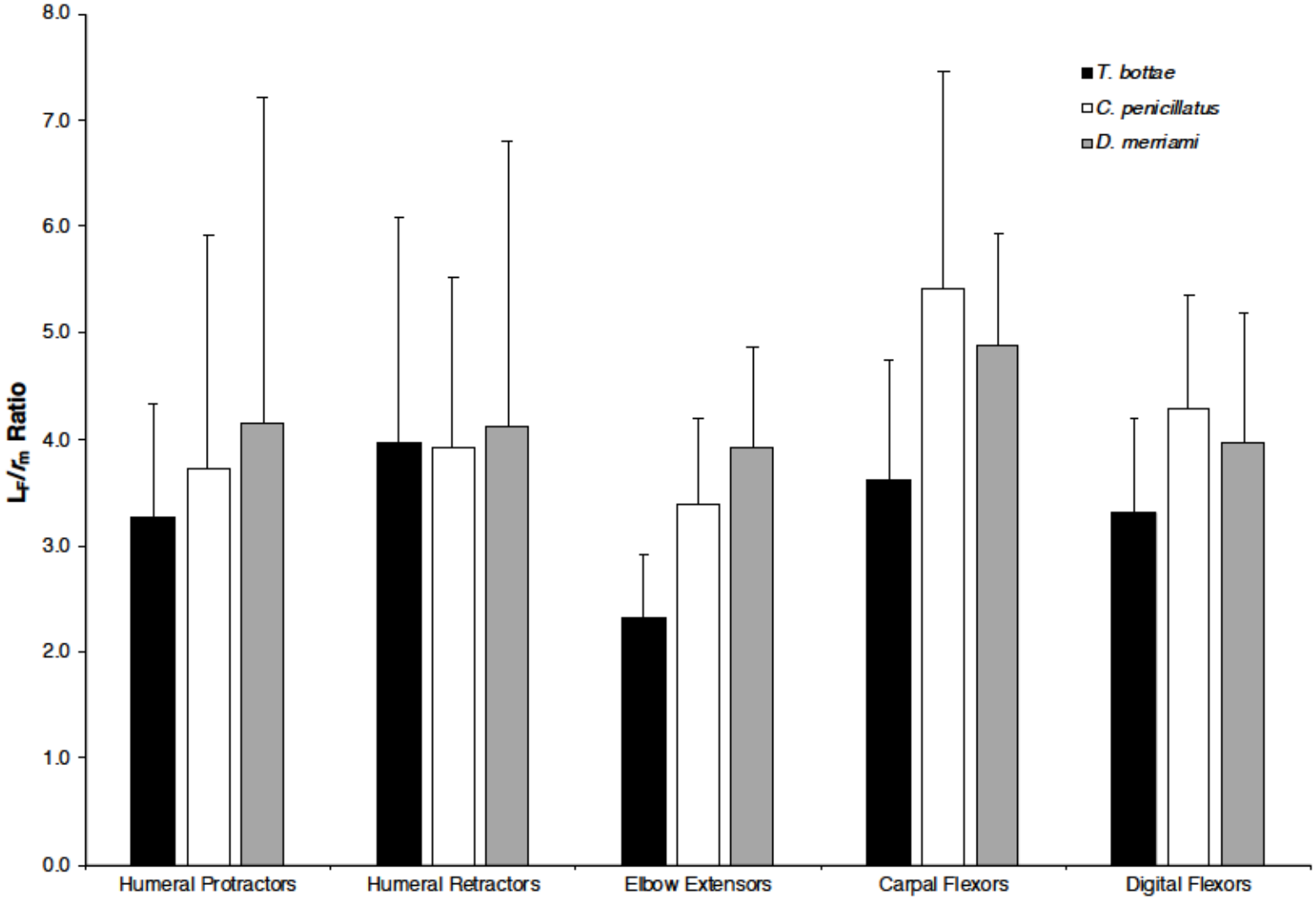
8.0
7.0
6.0
5.0
4.0
3.0
2.0
1.0
0.0
L_F/r_m Ratio
T. bottae
C. penicillatus
D. merriami
Humeral Protractors
Humeral Retractors
Elbow Extensors
Carpal Flexors
Digital Flexors

Fig. 6. Functional space plots for normalized fascicle length (L_F), muscle moment arm (r_m), and physiological cross-sectional area (PCSA). **a.** Normalized PCSA as a function of normalized fascicle length (L_F). PCSA is normalized to body mass $(BM)^{0.67}$ and fascicle length to $(BM)^{0.33}$. **b.** Normalized PCSA as a function of normalized muscle moment arm (r_m). Measurements for r_m are normalized to body mass $(BM)^{0.33}$. **c.** Normalized L_F as a function of normalized r_m. Data *points* are means shown with no *error bars*. Selected muscles are labeled in each panel. Muscles that produce large force (large PCSA) and are capable of large excursion and shortening velocity (long L_F) have the capacity for high power output (upper right quadrant in **a**); both large PCSA and long r_m are muscles capable of applying large joint torque (upper right quadrant in **b**); both long L_F and short r_m are muscles capable of fast joint rotational velocity (upper left quadrant in **c**). Generalized muscles have relatively small PCSA and both short fascicle and moment arm lengths. Only power stroke muscles are plotted. Muscles with large PCSA, long fascicle length, and long moment arm length are primarily those labeled. Muscle abbreviations are defined in Table 3–5. Circle data points are pocket gopher; squares are pocket mice; and triangles are K-rat.

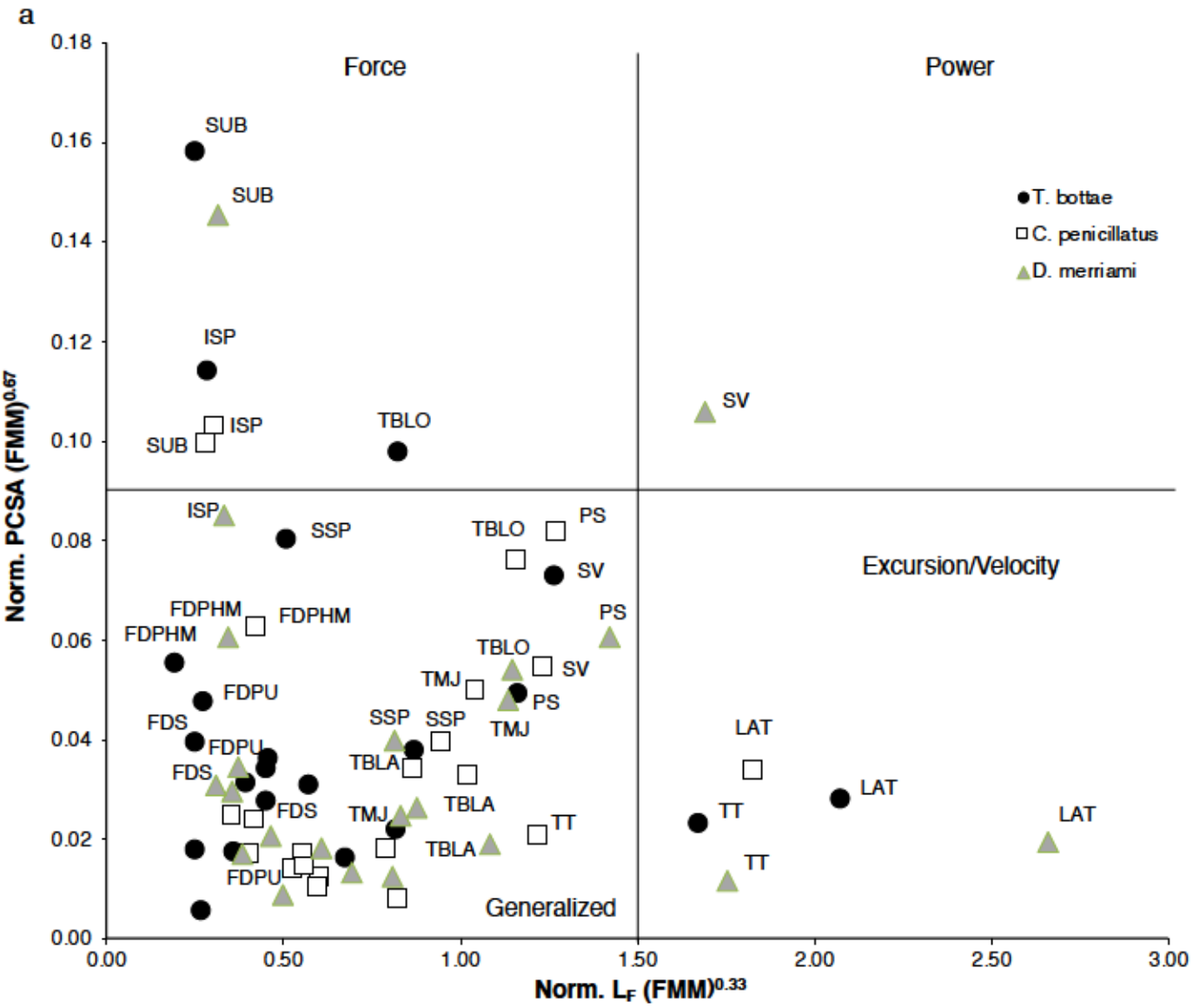
a
Force
Power
Excursion/Velocity
Generalized
T. bottae
C. penicillatus
D. merriami
Norm. PCSA (FMM)^0.67
Norm. L_F (FMM)^0.33
0.00
0.02
0.04
0.06
0.08
0.10
0.12
0.14
0.16
0.18
0.00
0.50
1.00
1.50
2.00
2.50
3.00
SUB
SUB
ISP
ISP
SUB
TBLO
SV
ISP
SSP
TBLO
PS
SV
FDPHM
FDPHM
FDPHM
PS
TBLO
SV
TMJ
PS
FDPU
FDS
FDPU
SSP
SSP
TMJ
FDS
TBLA
FDS
TBLA
TMJ
TT
FDS
TBLA
FDPU
LAT
LAT
TT
LAT
TT

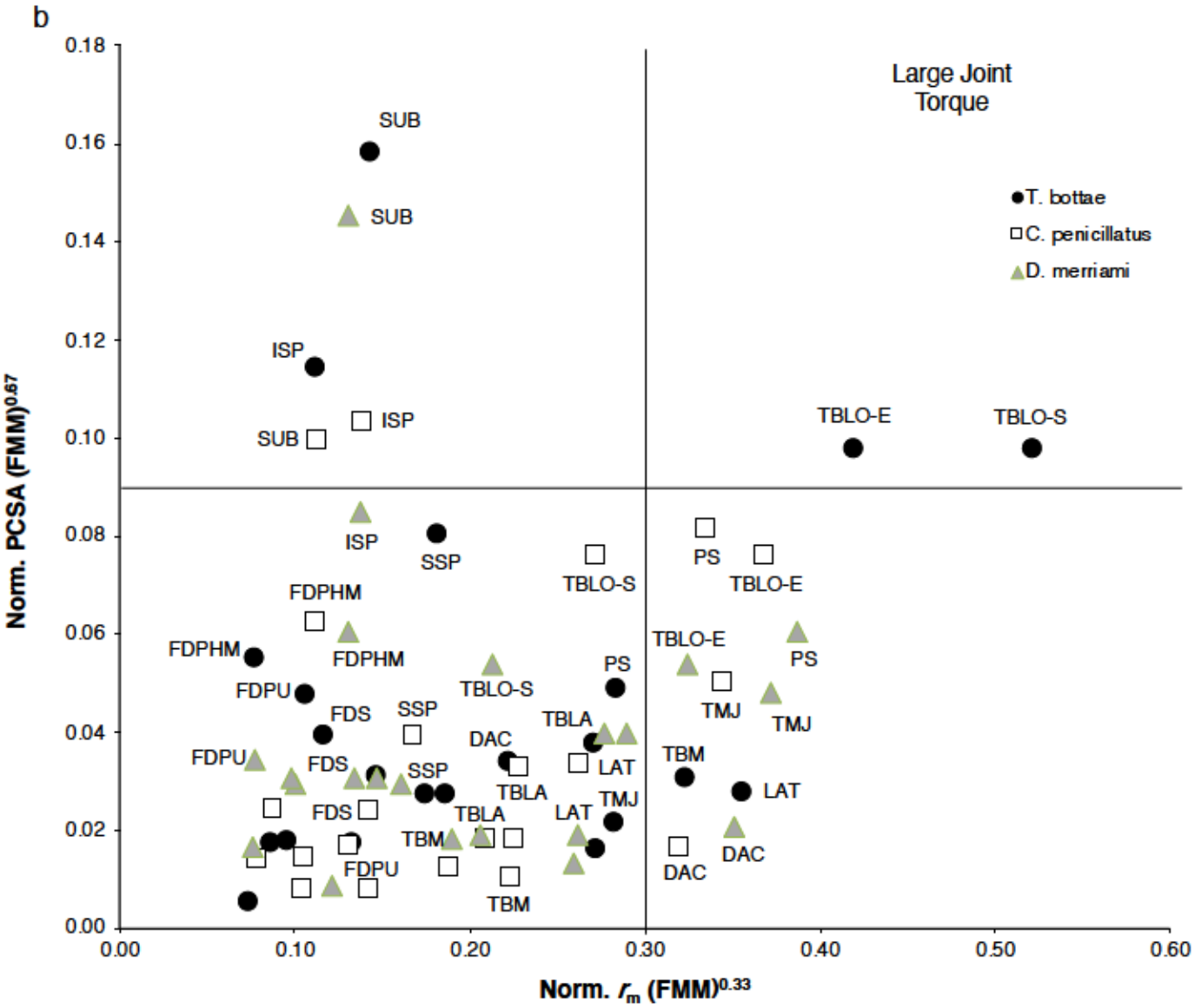
b
Large Joint Torque
T. bottae
C. penicillatus
D. merriami
Norm. PCSA (FMM)^0.67
Norm. r_m (FMM)^0.33
0.00
0.02
0.04
0.06
0.08
0.10
0.12
0.14
0.16
0.18
0.00
0.10
0.20
0.30
0.40
0.50
0.60
SUB
ISP
TBLO-E
TBLO-S
PS
SSP
FDPHM
FDPU
FDS
TBLA
DAC
LAT
TMJ
TBM

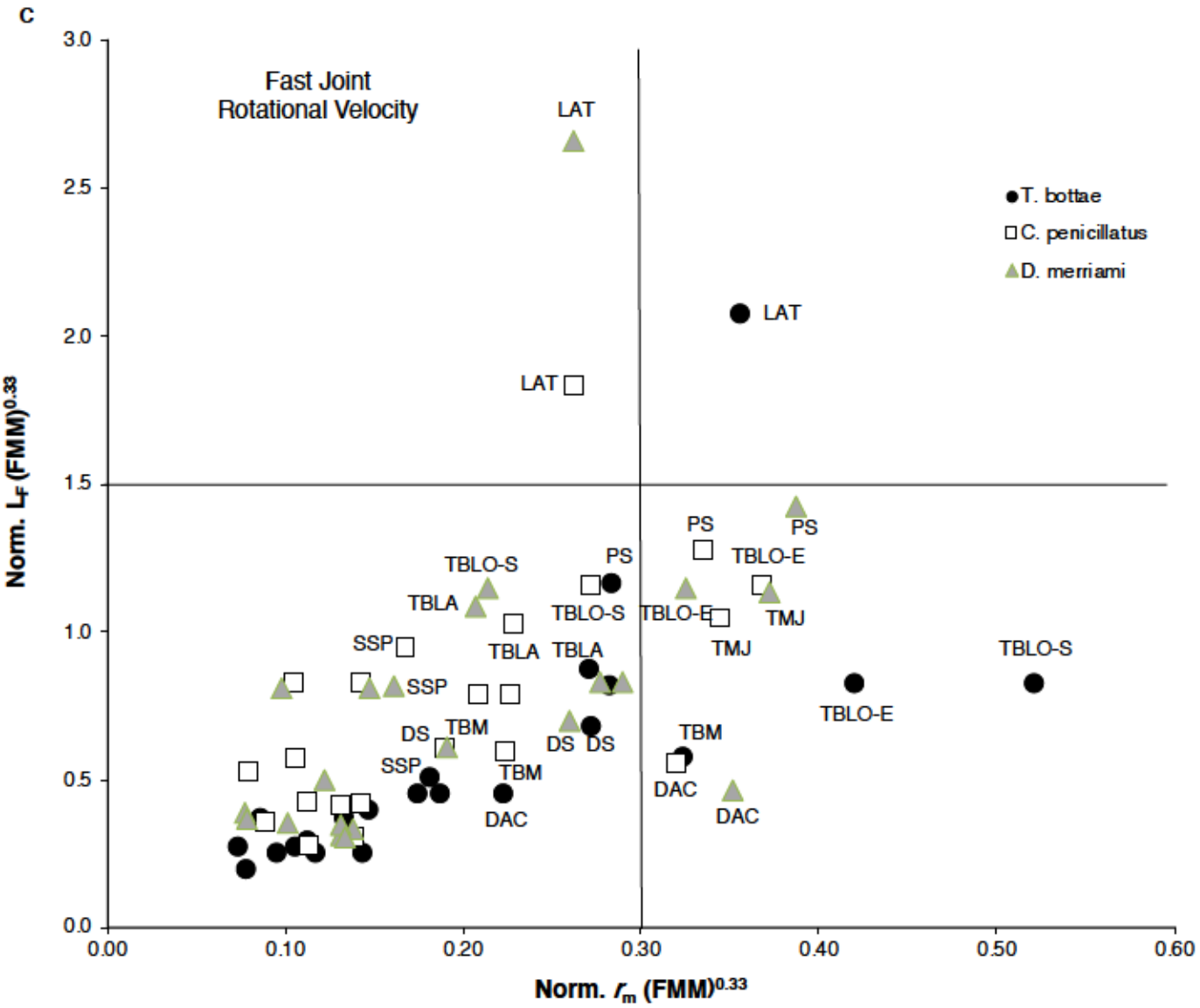
c
Fast Joint
Rotational Velocity
T. bottae
C. penicillatus
D. merriami
Norm. L_F (FMM)$^{0.33}$
Norm. r_m (FMM)$^{0.33}$
3.0
2.5
2.0
1.5
1.0
0.5
0.0
0.00
0.10
0.20
0.30
0.40
0.50
0.60
LAT
LAT
LAT
PS
PS
PS
TBLO-S
TBLO-E
TBLO-S
TBLA
TBLO-E
TMJ
SSP
TBLA
TBLA
TMJ
TBLO-S
SSP
TBLO-E
DS
TBM
DS
DS
TBM
SSP
TBM
DAC
DAC
DAC

Fig. 7. Myosin heavy chain (MHC) isoform composition in pocket gopher, pocket mouse, and K-rat forelimb muscles. Mean percentage composition of MHC isoforms for the major functional muscle groups associated with scratch digging: limb retractors, elbow extensors and carpal/digital flexors for all three species. Data are shown as stacked columns with no standard deviation error bars.

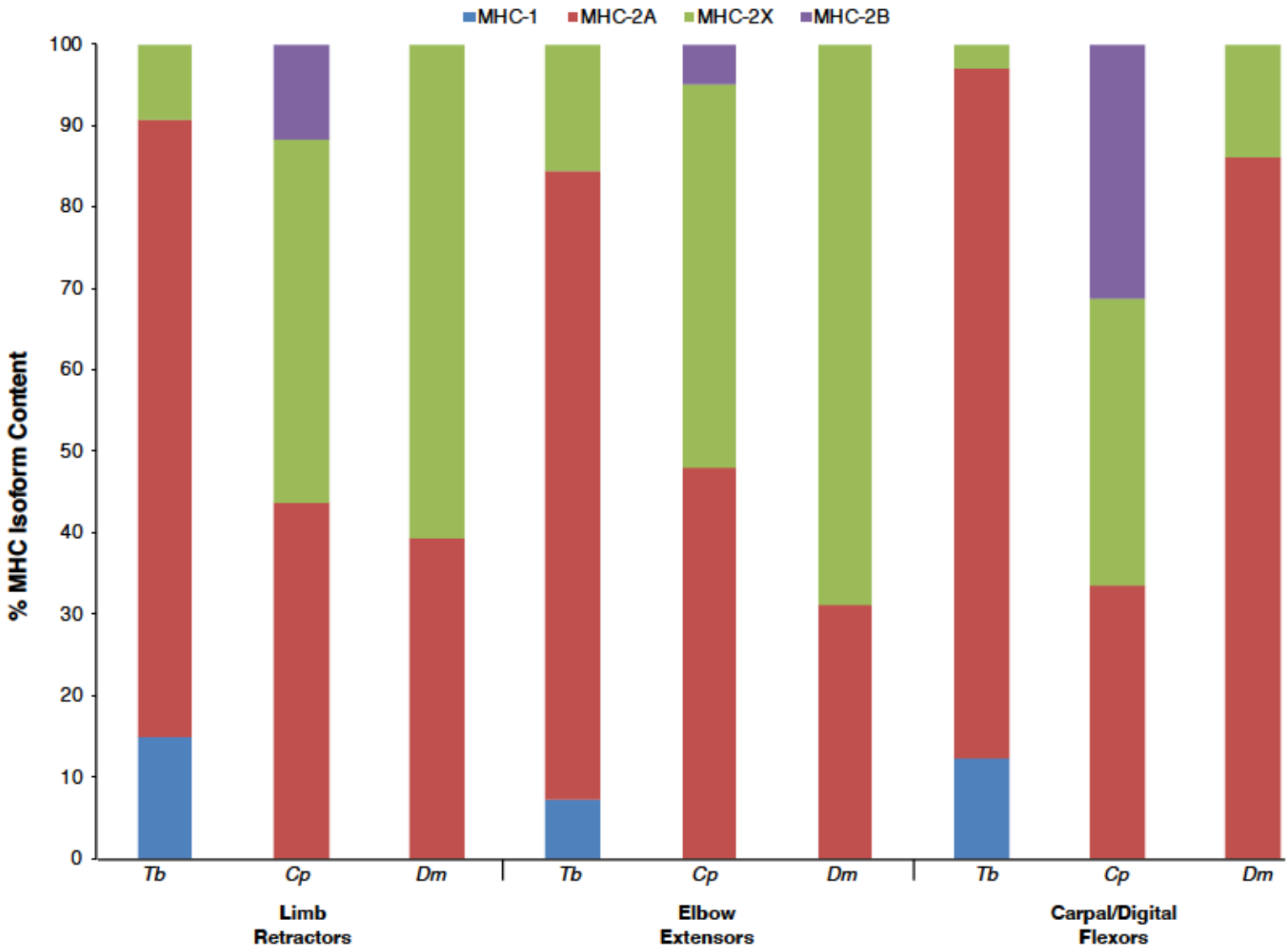
MHC-1
MHC-2A
MHC-2X
MHC-2B
% MHC Isoform Content
100
90
80
70
60
50
40
30
20
10
0
Tb
Cp
Dm
Tb
Cp
Dm
Tb
Cp
Dm
Limb Retractors
Elbow Extensors
Carpal/Digital Flexors

Fig. 8. Regressions of MHC expression and body mass in burrowing rodents. a. Percentage expression of the fast MHC-2A isoform against body mass. **b.** Percentage expression of the fast MHC-2X isoform against body mass. Data for *Ctenomys talarum* (talus tuco-tuco) are from Alvarez et al. (2012).

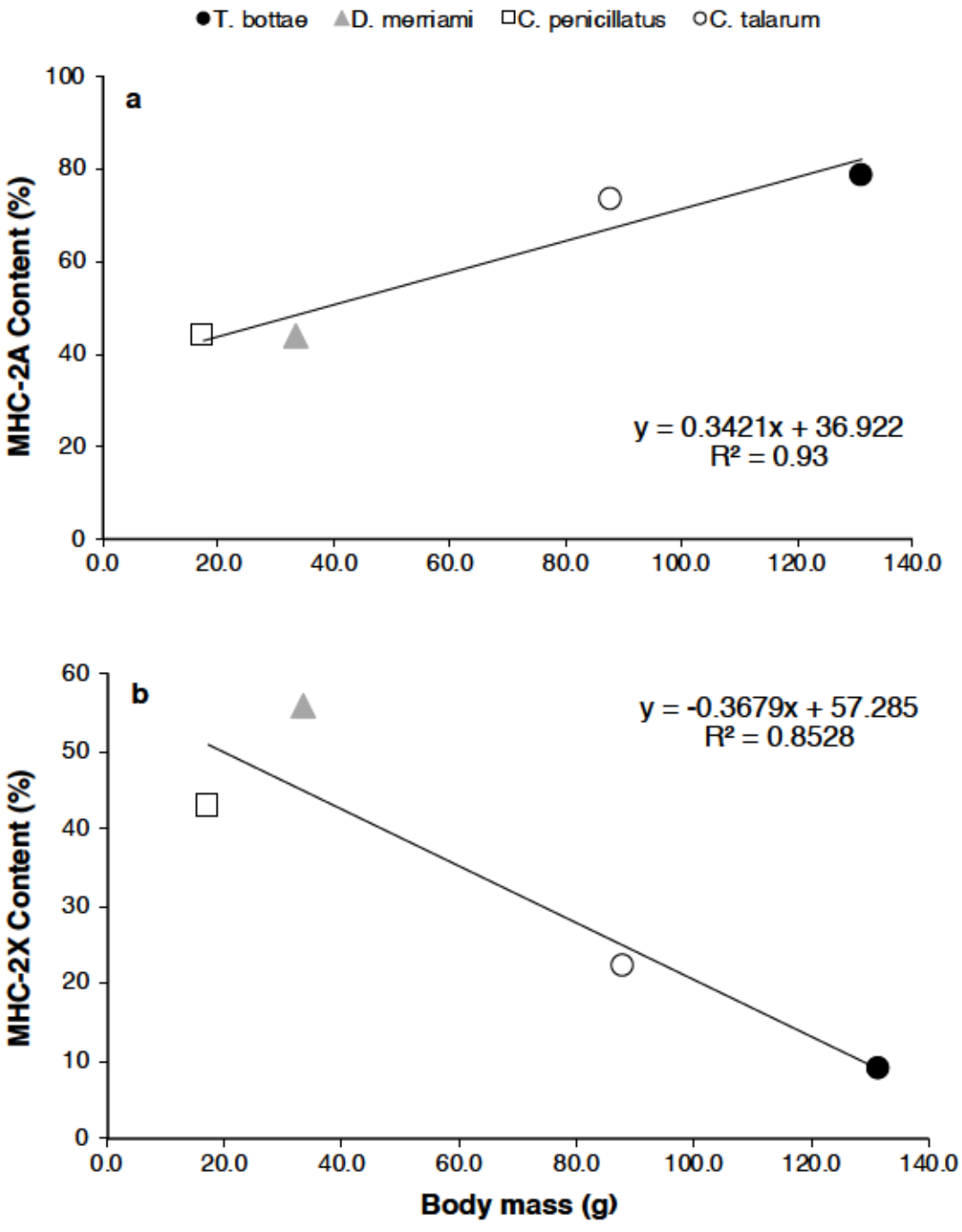
●T. bottae ▲D. merriami □C. penicillatus ○C. talarum
a
MHC-2A Content (%)
y = 0.3421x + 36.922
R² = 0.93
b
MHC-2X Content (%)
y = -0.3679x + 57.285
R² = 0.8528
Body mass (g)

S1. Normalized muscle architectural properties for pocket gopher forelimbs.

Muscle	r_m (mm/ $g^{0.33}$)	Fascicle length (mm/$g^{0.33}$)	PCSA ($mm^2/g^{0.67}$)	F_{max} (N/g)	Joint Torque (N.mm/g)	Power (mW/g)
TC	–	9.6±2.6	3.3±0.5	0.57	–	10.2
TT	–	16.7±3.3	2.3±2.5	0.39	–	13.0
RCP	–	10.3±2.4	2.7±0.6	0.46	–	8.8
RCR	–	6.1±1.9	4.4±1.1	0.75	–	8.3
RT	–	4.6±0.9	3.6±1.0	0.65	–	5.3
SV	–	12.7±2.4	7.3±1.3	1.26	–	29.6
OC	–	5.7±1.5	1.4±0.6	0.24	–	2.4
LAT	3.6±1.4	20.7±5.5	2.8±0.7	0.48	2.79	17.9
PS	2.8±1.0	11.6±2.8	4.9±1.2	0.84	4.19	17.9
PA	2.3±0.5	19.0±5.1	2.0±0.6	0.34	1.31	12.2
PP	2.1±0.8	9.9±2.4	1.5±0.2	0.26	0.99	4.8
DAC	2.2±0.6	4.5±1.0	3.4±1.0	0.59	2.35	4.8
DS	2.7±0.9	6.8±3.6	1.6±0.5	0.27	1.38	3.4
SSP	1.8±0.9	5.1±1.7	8.0±2.8	1.40	4.76	12.1
ISP	1.1±0.4	2.9±1.0	11.4±3.4	1.94	3.91	10.2
TMN	1.8±0.4	3.9±1.6	1.3±0.6	0.22	0.65	1.8
TMJ	2.8±0.6	8.2±1.8	2.2±0.3	0.37	1.85	5.6
SUB	1.4±0.4	2.5±0.9	15.8±3.5	2.71	6.79	12.4
CCB	1.1±0.3	1.9±1.2	1.0±0.6	0.18	0.33	0.5
TBLO-s	5.2±1.9	8.2±2.3	9.8±1.5	1.67	15.40	25.5
TBLO-e	4.2±0.7	8.2±2.3	9.8±1.5	1.67	12.31	25.5
TBM	3.2±0.6	5.7±1.4	3.1±1.0	0.52	2.88	5.5
TBLA	2.7±0.5	8.7±1.6	3.8±0.5	0.64	3.08	10.6
TFA	4.0±0.5	9.1±1.9	0.8±0.2	0.14	0.99	2.3
ANC	1.6±0.6	3.3±1.1	1.4±0.7	0.24	0.79	1.6
BCH	1.6±0.6	6.6±1.4	1.8±0.6	0.31	0.90	3.8
BBL-s	1.9±1.0	4.5±1.9	2.7±1.0	0.47	1.47	3.7
BBL-e	1.8±0.3	4.5±1.9	2.7±1.0	0.47	1.46	3.7

BBS-s	0.9±0.3	3.6±1.8	1.7±0.3	0.30	0.45	2.1
BBS-e	1.3±0.1	3.6±1.8	1.7±0.3	0.30	0.69	2.1
FCU	1.5±0.5	4.0±1.6	3.1±1.5	0.52	1.42	3.6
FCR	0.7±0.3	2.7±1.7	0.6±0.2	0.10	0.12	0.4
PT	–	4.1±1.1	1.5±1.0	0.27	–	2.1
PL	1.4±0.4	6.3±1.5	1.5±0.7	0.27	0.67	3.2
FDS	1.2±0.5	2.5±1.4	3.9±0.9	0.67	1.42	3.0
FDPU	1.1±0.2	2.7±1.3	4.8±2.2	0.82	1.48	3.7
FDPR	1.0±0.4	2.5±0.8	1.8±0.7	0.30	0.55	1.4
FDPHM	0.8±0.3	1.9±0.5	5.5±0.6	0.95	1.31	3.4
FDPHL	0.9±0.4	3.2±1.9	0.9±0.3	0.16	0.27	0.9
ECRL	1.3±0.5	7.4±1.0	1.1±0.6	0.19	0.42	2.7
ECRB	1.0±0.5	7.1±1.1	1.3±0.2	0.23	0.40	3.0
EDC	0.9±0.6	3.2±0.9	1.8±0.5	0.30	0.50	1.8
ED2	1.2±0.1	2.3±1.1	0.5±0.4	0.09	0.24	0.4
EDL	1.3±0.4	3.6±1.7	0.8±0.6	0.14	0.33	0.6
ECU	0.7±0.4	2.3±1.3	2.7±1.3	0.47	0.62	1.7
AD1L	1.3±0.6	1.7±0.7	2.3±0.8	0.39	0.88	1.2
SUP	–	3.0±0.8	0.4±0.1	0.07	–	0.4

Values are mean ± s.d.
For statistical comparison, muscle data were normalized isometrically to total forelimb muscle mass, area (PCSA) and length (fascicle length).

S2. Normalized muscle architectural properties for pocket mice forelimbs.

Muscle	r_m (mm/ $g^{0.33}$)	Fascicle length (mm/$g^{0.33}$)	PCSA ($mm^2/g^{0.67}$)	F_{max} (N/g)	Joint Torque (N.mm/g)	Power (mW/g)
TC	–	10.8±2.6	2.9±0.9	1.02	–	10.7
TT	–	12.2±2.6	2.1±0.5	0.73	–	8.5
RCP	–	10.9±2.9	5.0±2.3	1.81	–	19.4
RCR	–	7.3±1.2	2.4±0.6	0.85	–	5.9
RT	–	8.7±1.8	3.4±0.7	1.20	–	10.0
SV	–	12.3±3.3	5.4±2.7	1.92	–	21.4
LAT	2.6±0.2	18.3±4.8	3.4±1.3	1.19	2.67	20.1
PS	3.4±1.0	12.7±2.9	8.2±1.1	2.91	8.08	35.6
DAC	3.2±0.5	5.5±0.9	1.7±0.8	0.61	1.56	3.1
DS	1.9±0.6	6.0±1.3	1.2±1.0	0.42	0.66	2.5
SSP	1.7±0.3	9.4±1.6	3.9±0.5	1.40	2.01	12.6
ISP	1.4±0.2	3.0±0.9	10.3±3.3	3.72	4.12	10.4
TMN	2.2±0.8	10.3±1.6	2.4±1.5	0.83	1.60	8.3
TMJ	3.5±1.2	10.4±1.4	2.0±0.7	1.78	5.26	17.6
SUB	1.1±0.2	2.8±1.0	9.9±4.0	3.57	3.24	8.9
CCB	0.7±0.1	1.5±0.5	2.1±0.6	0.77	0.70	1.1
TBLO-s	2.7±0.6	11.6±1.2	7.6±0.5	2.72	6.21	30.1
TBLO-e	3.7±1.0	11.6±1.2	7.6±0.5	2.72	8.49	30.1
TBM	2.2±0.4	6.0±1.7	1.0±0.5	0.36	0.70	2.0
TBLA	2.3±0.3	10.2±1.6	3.3±0.6	1.17	2.26	11.4
ANC	1.6±0.5	4.1±0.7	0.8±0.4	0.28	0.39	1.1
BCH	1.4±0.3	6.5±1.5	2.6±0.4	0.92	1.10	5.7
BBL-s	2.3±0.4	7.9±0.8	1.8±0.2	0.65	1.24	4.9
BBL-e	2.1±0.3	7.9±0.8	1.8±0.2	0.65	1.14	4.9
BBS-s	1.0±0.1	8.3±0.8	0.8±0.3	0.28	0.33	2.2
BBS-e	1.4±0.4	8.3±0.8	0.8±0.3	0.28	0.24	2.2
FCU	0.9±0.1	3.6±1.9	2.5±1.2	0.87	0.65	2.4
FCR	0.8±0.1	5.3±1.3	1.4±1.7	0.52	0.39	1.8

PT	–	4.3±1.0	0.8±0.3	0.28	–	1.2
FDS	1.2±0.1	4.2±2.6	2.4±1.0	0.86	0.88	3.3
FDPU	1.3±0.2	4.1±2.1	1.7±0.6	0.60	0.64	2.3
FDPR	1.1±0.3	5.6±1.5	1.4±0.5	0.51	0.46	2.9
FDPHM	1.1±0.2	4.2±2.6	6.3±4.4	2.26	2.12	7.1
ECRL	1.1±0.1	8.1±1.9	1.1±0.4	0.40	0.38	3.0
ECRB	1.1±0.2	8.0±1.3	1.2±0.2	0.43	0.38	3.2
EDC	1.4±0.1	3.1±2.0	2.9±2.1	1.06	1.18	2.3
ECU	±	4.2±2.8	0.9±0.5	0.31	0.20	1.0
AD1L	1.1±0.2	4.0±1.8	1.1±0.5	0.40	0.34	1.3
SUP	–	4.3±1.3	0.2±0.1	0.06	–	0.2

Values are mean ± s.d.
For statistical comparison, muscle data were normalized isometrically to total forelimb muscle mass, area (PCSA) and length (fascicle length).

S3. Normalized muscle architectural properties for kangaroo rat forelimbs.

Muscle	r_m (mm/g$^{0.33}$)	Fascicle length (mm/g$^{0.33}$)	PCSA (mm^2/g$^{0.67}$)	F_{max} (N/g)	Joint Torque (N.mm/g)	Power (mW/g)
TC	–	12.5±2.4	2.6±0.7	0.91	–	9.9
TT	–	17.5±2.7	1.2±0.6	0.41	–	5.9
RCP	–	9.3±2.1	1.5±0.2	0.54	–	4.2
RCR	–	6.6±1.4	2.5±1.5	0.86	–	4.6
RT	–	8.8±2.4	2.6±2.1	0.89	–	5.8
SV	–	16.9±7.9	10.6±3.3	3.66	–	48.1
LAT	2.6±0.5	26.6±1.7	1.9±0.02	0.67	1.51	15.4
PS	3.9±0.3	14.2±2.3	6.1±0.5	2.12	7.04	26.2
DAC	3.5±0.2	4.6±0.9	2.1±0.8	0.71	2.16	2.8
DS	2.6±0.3	6.9±1.9	1.3±0.2	0.46	1.03	2.8
SSP	1.6±0.8	8.1±2.8	4.0±0.3	1.39	1.87	9.8
ISP	1.4±0.4	3.3±1.8	8.5±2.7	2.94	3.60	7.9
TMN	1.5±0.5	4.0±1.4	1.0±0.5	0.34	0.39	1.1
TMJ	3.7±0.1	11.3±1.1	4.8±0.5	1.67	5.34	16.4
SUB	1.3±0.3	3.1±1.2	14.5±4.3	5.04	5.43	13.0
CCB	0.7±0.1	1.3±0.4	1.5±0.1	0.51	0.31	0.6
TBLO-s	2.1±0.3	11.5±1.0	5.4±0.2	1.89	3.45	18.7
TBLO-e	3.3±0.8	11.5±1.0	5.4±0.2	1.89	5.29	18.7
TBM	1.9±0.4	6.1±1.8	1.8±1.0	0.63	1.10	3.1
TBLA	2.1±0.3	10.8±1.9	1.9±0.5	0.65	1.17	6.0
ANC	1.6±0.3	5.1±0.8	1.0±0.4	0.33	0.45	1.5
BCH	1.9±1.2	7.2±1.0	2.2±0.5	0.76	1.21	4.7
BBL-s	2.9±0.2	8.3±0.9	2.5±0.8	0.86	2.11	6.1
BBL-e	2.8±0.5	8.3±0.9	2.5±0.8	0.86	1.98	6.1
BBS-s	1.0±0.2	8.1±0.7	1.2±0.6	0.42	0.37	2.9
BBS-e	1.5±0.6	8.1±0.7	1.2±0.6	0.42	0.61	2.9
FCU	1.2±0.1	5.0±1.8	0.9±0.4	0.30	0.31	1.1
FCR	0.8±0.3	3.8±1.2	1.7±0.4	0.58	0.37	1.9

PT	–	5.7±1.6	0.9±0.5	0.32	–	1.5
PL	1.5±0.1	7.4±1.8	1.4±0.5	0.50	0.64	3.0
FDS	1.3±0.6	3.1±1.3	3.1±1.1	1.09	1.10	2.7
FDPU	0.8±0.2	3.7±0.8	3.4±1.0	1.19	0.83	3.8
FDPR	1.0±0.02	3.6±1.7	3.0±0.3	1.03	0.89	3.1
FDPHM	1.3±0.1	3.4±1.3	6.1±2.0	2.11	2.40	6.1
FDPHL	1.0±0.4	4.2±1.0	0.7±0.5	0.25	0.21	0.9
ECRL	1.4±0.6	10.6±0.9	1.1±0.3	0.39	0.45	3.6
ECRB	1.3±0.7	5.9±1.0	2.4±0.3	0.83	0.92	4.2
EDC	1.2±0.3	3.0±1.7	2.3±1.7	0.80	0.71	2.1
ED2	1.0±0.3	5.1±1.4	0.5±0.4	0.17	0.14	0.7
EDL	0.9±0.3	3.0±1.3	0.3±0.3	0.12	0.08	0.2
ECU	0.8±0.1	3.6±0.9	0.9±0.3	0.32	0.22	1.0
AD1L	0.8±0.1	2.7±1.4	2.6±1.3	0.88	0.63	1.7
SUP	–	4.7±1.6	0.3±0.1	0.09	–	0.4

Values are mean ± s.d.
For statistical comparison, muscle data were normalized isometrically to total forelimb muscle mass, area (PCSA) and length (fascicle length).

APPENDIX

Introduction

Family Geomyidae

Gophers are squirrel-like rodents (sub-order: Sciuromorpha) that consist of nearly thirty-five extant and nine extinct species that are members of the mammalian Order Rodentia. Specifically, pocket gophers are burrowing rodents taxonomically classified in the family Geomyidae, which includes eight genera (Nevo, 1979). Pocket gophers are considered to be true gophers because they have distant relatives in the Family Sciuridae. The ancestors of modern pocket gophers arose in the early Miocene prior to the era of the Megafauna (or giant mammals). At present, pocket gophers are geographically distributed throughout both North and Central America (Nevo, 1979). The genus Thomomys contains nine species, which includes Botta's pocket gopher, *Thomomys bottae* (*T. bottae*: Lessa and Stein, 1992). This species is located throughout North America, but specifically has populations concentrated in the desert ecosystems of California, Texas, New Mexico, and Nevada (Smith, 1998; Wilkins and Roberts, 2007). However, the geographic range of this species in not limited to deserts as they also inhabit mountain valleys or biomes consisting of savanna or grasslands.

The species *T. bottae* is considered to be a fossorial rodent. In this review, the term fossorial is defined as mammals with functional specializations for digging intricate burrows. In addition to their high level of fossoriality, pocket gophers are subterranean. The term subterranean defines the ecology of the animal and these mammals spend most, if not all, of their time underground constructing tunnels where they hide from predators and forage the insects they find in the soil. Therefore, subterranean and fossorial mammals are characterized by primarily living in and constructing elaborate burrow systems underground. Strictly fossorial rodents, however, are characterized as living in burrows but spend appreciable time above ground foraging and mainly use their burrows to evade predators and store food, whereas semi-fossorial mammals construct less intricate burrows than fossorial rodents and display a continuum of morphofunctional modifications for digging habits (Montoya-Sanhueza, 2020).

The diet of *T. bottae* is strictly herbivorous and includes alfalfa, bulbs, and roots within their burrow systems. Foraging both above and below ground requires gophers to use their

ever-growing incisors to cut through tough vegetation; however, it is most typical for *T. bottae* to acquire resources underground. For any forage acquired above-ground, pocket gophers will transport resources into their burrows using multiple methods. For example, *T. bottae* will grip food with its teeth and pull forage into their burrows, pack food into their cheek pouches (a characteristic cranial trait of the family) and transport forage into its burrow system, or tumble food against loose soil (i.e., clearing soil away with vegetation) (Jones and Baxter, 2004).

Within the tunnels of a burrow system, *T. bottae* is typically active for 9 hours per day and it is not specifically limited to diurnal or nocturnal activity (Gettinger, 1984). Burrow systems are not only required for foraging, but also nesting, predator evasion, and rearing of young. Pocket gophers typically live independently in their burrows except when rearing young, which are born as altricial (premature) infant offspring. Nonetheless, young pocket gophers leave the burrow system of their mother immediately after weaning (~40 days). The other instance when more than one animal occupies the burrow system is during the breeding season (Jones and Baxter, 2004). Breeding seasons often dictate the activity of gophers, especially during periods of cooler temperatures in Spring, Fall, and Winter. Specifically, the activity of *T. bottae* is higher during the cooler seasons due to rainfall, whereas activity is less frequent during the Summer due to the higher temperatures and dryness. Rainfall increases moisture in the soil and other materials that *T. bottae* can more easily manipulate compared with dry, compact soil to construct their burrow systems. Thus, burrow construction takes place more frequently during the cooler seasons.

Sympatric relatives – Heteromyidae

The family Heteromyidae is generally classified as the sister group of Geomyids, as it comprises the closest living relatives of *T. bottae* (Lessa and Stein, 1992). Within this family there are three subfamilies; Heteromyinae, Dipodomyinae, and Perognathinae. The genera included within the latter two subfamilies include Dipodymys (*Dipodomyinae*), which consists of Merriam's kangaroo rat (*D. merriami*), and Perognathus and Chaetodipus (*Perognathinae*), that includes desert pocket mice (e.g., *C. penicillatus*) (Randall, 1993). The representative species of *Dipodymys* and *Chaetodipus* are nocturnal and co-inhabit North American climates that are very dry, where they survive as granivores (i.e., seed eating animals). Due to their overall lack of forelimb skeletal specializations, kangaroo rats

(K-rats) and pocket mice are considered to be semi-fossorial rodents, but have hindlimbs that either specialized for ricochetal leaping or more generalized function, respectively. Their habitats range from wind-blown sand and desert shrub to grasslands and chaparral, and these types of biomes are homes to multiple species of geomyids and heteromyids (Randall, 1993). Moreover, the distribution of K-rats and pocket mice ranges from southern Canada to Central Mexico, including regions of Arizona, New Mexico, Texas, California, Nevada, and Utah. K-rats can be found in mostly sand-based habitats (i.e., desert), because deserts have an increased number of seeds available for forage, whereas pocket mice typically reside in habitats of the wind-blown sand, desert shrub, grasslands, rocky hillsides, and chaparral.

Foraging techniques utilized by *D. merriami* and *C. penicillatus* consist of scratch-digging with their forelimbs, which are greatly reduced in K-rats and generalized (or simplified) in pocket mice (Moore-Crisp, 2018). Their foreclaws are used to pierce through soil to gather seeds above ground that are then stored in their external, fur-lined cheek pouches. Yet, feeding takes place underground (out of sight of predators) where they also cache their food. Specifically, seeds are stored by *D. merriami* in either shallow caches, or seeds are hoarded in burrow larders (Randall, 1993). While foraging habits are similar between K-rats and pocket mice, their distinct limb morphologies separate the two species functionally. Beyond reduced forelimbs, K-rats have elongate hindlimbs and hindfeet, and shortened vertebral columns (e.g., neck: cervical vertebrate) (Morgan and Price, 1992). The trait of elongated hindlimbs in *D. merriami* is related to its jumping or leaping locomotor habits (Nader, 1978). Instead of sustained hopping like kangaroos and wallabies (i.e., saltatorial habit), kangaroo rats employ a ricochetal mode of jumping (i.e., ricochetal habit) to leave the security of cover (home burrow) to forage and to quickly vertically leap to evade a predator strike (e.g., rattlesnakes, among other avian natural predators of *D. merriami*; see below). In contrast, pocket mice maintain a typical mouse-like body plan, where *C. penicillatus* in particular, lacks spines on the rump, has short forelimbs, and has grooved upper incisors (Morgan and Price, 1992). Neither species has broad forefeet with well-developed claws. However, also characteristic of *D. merriami* and *C. penicillatus* is their ability to construct complex burrow systems similar to those of their sympatric

relative *T. bottae* as indicated above. Their burrow systems consist of multiple entrances and exits, as well as relatively smaller pits for food storage (Leaver and Daly, 2001).

Burrow System Construction

The digging behaviors of *T. bottae* consist of chisel tooth-digging and scratch-digging. With either habit, the motions of the head/neck or forelimbs excavate earth and move soft/loose materials to construct its burrow systems (Jones and Baxter, 2004). Thus, the structure of its jaws and head/neck, in addition to its forelimbs, requires modification or functional specialization to these two lever systems to increase mechanical advantage (MA) and the out-force that pocket gophers are able to apply to the substrate (see below for mechanical details). The average size of a pocket gopher burrow system is 132 mm in depth and 70 mm in diameter (Jones and Baxter, 2004). The initial construction of the burrow system begins on the surface, which has one or more mounds where soil that has been excavated is stored and the entrance is plugged with additional collected soil. The entrances can be open, but they are typically plugged to limit access by predators such as North American badgers (Jones and Baxter, 2004).

As the burrow system gets progressively deeper from the surface level, with overall structure consisting of a long continuous tunnel (i.e., main burrow) into the main chamber. Throughout the burrow system there are branches off of the main burrow, where shorter branch tunnels typically represent the areas used for foraging. The feeding tunnels run parallel to the surface and these are interconnected to other portions of the burrow systems by down-shafts and ramps. Side tunnels that branch off of the feeding tunnels are used for the disposal of soil that has been excavated. The nesting areas are deep and *T. bottae* lines these areas with vegetation (Jones and Baxter, 2004). Additional branches in the burrow system are utilized as cooling zones, defecation areas, and areas to hide for predator evasion (Wilkins and Roberts, 2007). Collectively, the complexity of the burrow systems of the pocket gophers is quite remarkable. Perhaps even more extraordinary is that the design of burrow system construction for *T. bottae* is similar to that of both *D. merriami* and *C. penicillatus*, which are sympatric species in western desert habitats of the USA, but are taxons that lack the typical morphological specializations for fossorial habit as observed in the pocket gophers.

Predatory avoidance behavior

A critical selective pressure common to all small rodents is predation, and each of the three identified genera/species have unique predatory evasion behaviors. Pocket gophers typically evade predators by the use of their fur coloration patterns as camouflage as well as hiding in their burrowing systems. As the presence of a mound above-ground indicates the burrow system below, it necessitates that pocket gophers plug their entrances making it difficult for predators to enter. They also tend to limit their movement while in the burrow when trying to evade predators (Krupa and Geluso, 2000). Both K-rats and pocket mice are cryptically colored, causing predators to have difficulty locating them at night when they are active. Moreover, K-rats have also been observed to avoid activity when there is direct moonlight, but even when they are not avoiding moonlight, they tend to forage in areas covered with brush and bushes (Randall, 1993). The natural predators of *T. bottae, D. Merriami,* and *C. penicillatus* include birds of prey such as owls (Kotler, 1984), and terrestrial carnivores, including coyotes, foxes, bobcats, badgers, and predatory reptiles such as rattlesnakes, gopher snakes, and whip snakes (Nader, 1978).

For the heteromyids, in particular, when living in diverse open habitats they specifically evade predators by switching their activity patterns from foraging in open habitats to foraging in shrub habitats. As indicated above, K-rats typically escape predators via powerful leaps after they detect low-frequency sounds or ground vibrations that their predator produces when moving, or they use their sense of smell to detect odors given off by a snake. Interestingly, two species of kangaroo rats (e.g., *D. merriami*) also evade snakes by kicking sand and foot-drumming (i.e., striking the feet or head on the ground to create seismic vibrations). The latter is a primitive form of echolocation. When in open habitats, the *D. merriami* use bipedal locomotion to escape predators via zig-zagging patterns of leaps. This is in contrast to when they are in close proximity to a predator where they complete a series of strategic vertical leaps, the trajectory of which depends on which direction a predator is attempting to strike. For example, when under attack by an owl, *D. merriami* leaps perpendicular to the flight path (Longland and Price, 1991), whereas for snakes, it leaps backwards to avoid the strike (Webster, 1962). On the other hand, the predatory avoidance behavior of pocket mice is generalized. Pocket mice move via quadrupedal locomotion and simply use a fast galloping gait (full-bound) to run away from predators and escape to their burrows.

Thermoregulatory behavior

The activity patterns of geomyid and heteromyid rodents are also strongly related to their elevated mass-specific metabolic rates (i.e., energy consumed per gram of tissue) and the ability to maintain a relatively stable core body temperature (Lessa and Stein, 1992). Small mammals have a large surface area to volume relationship (SA:V ratio), thusly taxa such as rodents often display frenetic behaviors to offset rapid loss of body heat as a consequence of small body size (Contreras and McNab, 1990). The species *T. bottae* has a body mass of ~120 g, while *D. Merriami,* and *C. penicillatus* have an average body masses of 45 g and 20 g, respectively, thus pocket gophers are at least three times larger than K-rats and pocket mice. In general, maintenance of endothermic homeostasis in geomyid and heteromyid rodents is due to diligent foraging activity. However, digging is a metabolically costly behavior, which produces excess metabolic heat. This effect is further amplified by substantially elevated ambient temperatures in their chosen desert habitats.

Animals can perform scratch-digging slowly and strongly, or rapidly, requiring greater mechanical power output (and thus greater heat production). Specifically, the large energy demands during burrowing in *T. bottae* account for a substantial increase in its body temperature. Moreover, because rodents are unable to dump body heat via common mechanisms such as sweating and panting, it must burrow deeper into cool earth when its body temperature spikes (Jones and Baxter, 2004). As such, in order to not overheat during active time, pocket gophers, K-rats, and pocket mice alike tend forage at night and construct burrow systems during the cooler seasons.

Functional Morphology

The functional morphology of members of genera Thomomys, Dipodymys, and Chaetodipus is related to their individual behaviors (Samuels and Van Valkenburgh, 2008; Whitford et al., 2017). In general, the small body size of burrowing rodents is necessary because of how these species habituate themselves to life underground across the majority of their lifespan. Despite all three species of desert-dwelling burrowers, however, the overall shapes of their bodies are quite different; pocket gophers have the stereotypical body plan of a fossorial mammal, K-rats have highly reduced forelimbs and elongate long hindlimbs for leaping locomotion as mentioned above, and pocket mice have generalized morphology with fore- and hindlimbs lengths that are even in proportion (Djawdan, 1993).

Moreover, the method and frequency of the digging utilized by *T. bottae*, *D. Merriami,* and *C. penicillatus* is generally representative of strength in their forelimbs and head/neck and jaw. Nonetheless, morphological specialization in the forelimbs will be the main focus of this section. The most well-developed functional muscle groups in the forelimb of digging mammals are the shoulder flexors, elbow extensors, and carpal/digital flexors (Moore et al., 2013; Rupert et al., 2015; Olson et al., 2016). These functional groups include the following muscles as the major musculature activated during scratch-digging: m. pectoralis superficialis/profundus, m. latissimus dorsi, m. deltoideus, m. teres major, m. triceps brachii, m. flexor carpi radialis, m. flexor carpi ulnaris, and m. flexor digitorum superficialis/profundus.

a. Musculoskeletal structure

-T. bottae

One of the main elements that is common in fossorial and semi-fossorial mammals is elongated claws on the manus (forefeet) (Samuels and Van Valkenburgh, 2008). Pocket gophers employ scratch-digging and their well-developed foreclaws are primary structures involved in this behavior (Lessa and Stein, 1992; Stein, 1993). In addition, the distal forelimbs of *T. bottae* are reduced in length (i.e., shorter limb out-lever length), and this feature coupled with large claws, provides enhanced MA for strong burrowing and excavation of soil, respectively. Scratch-digging is performed by two strokes: power stroke and recover stroke (Hildebrand and Goslow, 2001). Briefly, the power stroke involves retraction of the forelimbs paired with the extension at the elbow joint and flexion at the carpus and digits. The recovery stroke recycles the limb by protraction of the forelimb, flexion at the elbow joint, and extension at the carpus and digits. At the end of the full limb cycle, the forelimb is in position to undergo another power stroke and these sequential patterns of limb movement typically alternate between left and right forelimbs as scratch-digging continues (Hildebrand, 1985). During the power stroke, soil is moved ventral and caudal (rearward) relative to the body, and eventually soil is moved out of the burrow tunnels (main burrow) or to specific burrow branches. Pocket gophers perform soil removal by turning 180° (from the direction of burrowing) in the tunnel and then use their forelimbs to push up and out accumulated debris (Moore-Crisp, 2018).

It is noted that the geomyids are also specialized for chisel tooth-digging, which overall,

requires fewer muscles and structural modifications to the jaw relative to those in the forelimbs. For example, the rapidly growing, curved incisors of *T. bottae* have no grooves, leading to one of their common names, the smooth-toothed gophers (Nevo, 1979). This chisel-tooth or head/neck methods of burrowing consists of the animal penetrating soil with their incisors positioned at a high gape angle (i.e., angle at which the mouth is opened) with the head pitched slightly nose-up. The upper incisors hold an anchoring position for the lower incisors to grab soil followed by the extension of their compact, strong neck to move the soil with the lower jaws (Lessa and Thaeler, 1989). One should visualize a backhoe machine and the actions of its scoop being used to excavate soil. The development of their procumbent teeth morphology allows *T. bottae* to be a specialist in tooth-digging; however, forelimb scratch-digging is required by *T. bottae* for stronger burrow construction due to the mechanics of the jaw elevator muscles inserting close to articulation of the mandibular condyle (i.e., jaw joint) (Lessa and Stein, 1992). This mechanical arrangement results in reduced MA at the jaw joint. Thus, the incisors assist in loosening soil and the forelimb muscles excavate and remove earth (Jones and Baxter, 2004). Pocket gophers typically use chisel tooth-digging in compact soil to initially loosen it.

Interestingly, the forelimb muscles of *T. bottae* are larger in quantity but smaller in size than its jaw muscles (Lessa and Thaeler, 1989; Lessa and Stein, 1992), and yet muscle complexes of the forelimb show extensive fusing, especially within the forearm flexor compartment. Pocket gophers also have an extra ligament in their antebrachium that runs between the radius and ulna, proximal to the carpus. In the proximal regions of the forelimb, the insertion of mm. latissimus dorsi and teres major displays extensive fusing. The species *T. bottae* is observed to have only three heads of the m. triceps brachii (uncommon for most digging mammals) with a notably enlarged long head of m. triceps brachii (Lessa and Stein, 1992). Consistent with well-developed musculature are enlarged areas of muscle attachment on the deltopectoral crest of the humerus, medial epicondyle of the humerus, and olecranon process of the ulna (Samuels and Van Valkenburgh, 2008), which are the most typical forelimb skeletal modifications observed in scratch-digging taxa. The complex of extensor muscles that insert at the olecranon process are mm. triceps brachii, dorsoepitrochlearis (m. tensor fasciae antebrachii), and anconeus, while the largest muscle in the antebrachium of *T. bottae*, the m. flexor carpi ulnaris (FCU), originates from

the olecranon (Samuels and Van Valkenburgh, 2008), thus necessitating that this bony landmark be robust.

Along with enlarged muscles and areas of muscle attachment, the shafts of the long limb bones of pocket gophers display additional robustness (i.e., thickness). The humerus and ulna, in particular, must be strong to resist both craniocaudal and mediolateral bending loads acting on these bones during scratch-digging. In addition, limb bones must withstand both bending and torsional (twisting) stresses and strains superimposed on compressive loading involved in body weight support during digging (Samuels and Van Valkenburgh, 2008). The development (and remodeling) of robust long bones in proximal forelimb of *T. bottae* is likely in response to the mechanical loads imposed on them associated with their subterranean and fossorial lifestyle. In contrast, the distal limb bones of the manus in *T. bottae* are reduced in length in order to improve MA of proximal limb muscles (mechanical advantage, MA = greater in-lever to out-lever ratios) (see below subsection b: *Limb lever systems*), although robustness of these bones is retained as the feet are the site of the applied out-force and directly experience the impact of large substrate reaction forces (SRF: Samuels and Van Valkenburgh, 2008). The bones of the forefeet are aptly observed to be stout in many scratch-digging taxa including pocket gophers.

-D. merriami & C. penicillatus

Muscular arrangement for scratch-digging in the K-rats and pocket mice include muscle insertions on a modestly enlarged deltopectoral crest of the humerus, epicondyles of the humerus, and olecranon process of the ulna. For example, the deltopectoral crest in K-rats must be large enough to accommodate attachments of the mm. deltoideus (parts: spinodeltoideus and acromiodeltoideus), pectoralis and latissimus dorsi because a distinct deltoid tuberosity is not observed. Collectively, these muscles have the actions of retracting and adducting the forelimbs as they do in *T. bottae* (Samuels and Van Valkenburgh, 2008). The presence of a somewhat enlarged humeral medial epicondyle is an important skeletal modification for digging. The medial epicondyle is the origin for the carpal/digital flexors, which include the mm. flexor carpi radialis, palmaris longus, flexor digitorum sublimis, and humeral heads of the flexor digitorum profundus. The medial epicondyle is also the origin of the m. pronator teres (Samuels and Van Valkenburgh, 2008). The olecranon serves as the common insertion for the elbow extensors mm. dorsoepitrochlearis, anconeus,

and triceps brachii medial accessory head, as well as the origin of the m. flexor carpi ulnaris.

b. Limb lever systems

The bones and muscles of the forelimbs function as an integrated system to perform scratch-digging. The limb system comprises different classes of levers that are associated primarily with flexion/extension of limb segments via rotations at the limb joints. Briefly, there are three classes (or orders) of lever systems: first, second, and third. A first (1^{st}) class lever is formed by the joint (i.e., fulcrum) located between the applied muscle force (i.e., in-force) and resistance to movement or load (i.e., out-force) (Davis et al., 2010). An anatomical example of a 1^{st} class lever is the m. triceps brachii acting to extend the antebrachium at the elbow joint against the resistance provided by the substrate. A second (2^{nd}) class lever is formed by the out-force positioned in between the joint and in-force. The musculoskeletal anatomy of animals are not naturally composed of 2^{nd} class levers, although they can be formed (as when using a machine) to move a heavy load (e.g., a wheel barrow) (Hildebrand and Goslow, 2001). Last, a third (3^{rd}) class lever is formed by the in-force located between the joint and the out-force. An example of a 3^{rd} class lever is the m. biceps brachii acting to flex the antebrachium at the elbow joint against the mass of the distal limb when recovering the forelimb after a power stroke of scratch-digging (Mondal and Tabassum, 2016). In-force and out-force are related by the torque (i.e., rotation force or moment) balancing equation:

$$F_{in} \times L_{in} = F_{out} \times L_{out}, \qquad \text{EQ. 1}$$

where F is force and L is lever (moment) arm length. Thus, the out-force that is applied by animal limbs has a magnitude that is due to the MA of the lever system, which is determined by the L_{in}/L_{out} ratio. In other words, the resulting out-force applied represents the amount of force that was produced by the limbs muscles amplified by their MA (DeMont, 1996).

Muscle moment arm, which represents the in-lever for muscle torque applied at a limb joint, is a metric of considerable interest as applied to digging or burrowing behavior. It is defined as the perpendicular distance between the muscle line of action and the joint center of rotation, and represents an instantaneous measure of MA with which contractile force produced by a limb muscle (or functional group) can generate a torque at limb joint

(Williams et al., 2008). Therefore, measurement of muscle moment arm (denoted as r_m) is critical for determining one of the most important functional capacities of limb muscles via evaluation of architectural properties (see Materials and Methods, subsection *Architectural Properties/Quantifications*).

Furthermore, the L_{in}/L_{out} ratio determines either force or velocity advantage at a limb joint. A large ratio corresponds with enhanced MA and results in the application of large out-force but at a slow joint rotational velocity. In contrast, a small ratio results in fast joint rotational velocity but with small out-force application. It is for this reason that limb muscles with short r_m can move an elongated limb segment through a large range of motion (RoM) with relatively little muscle shortening, or contractile excursion. However, the limb skeletons of scratch-digging taxa are typically modified for enhanced MA by having large r_m coupled with short distal limb elements. For example, the forelimbs pocket gophers have large MA because an elongated olecranon process (in-lever) and a short radius and ulna (out-lever) producing high out-force (applied joint torque) per unit in-force. As a result, *T. bottae* cycle their forelimbs with slower joint velocities. K-rats and pocket mice, on the other hand, generally have longer out-lever to in-lever arrangements resulting in a low application of out-force, albeit they are capable of cycling their limbs at a higher joint velocity than pocket gophers. By comparison, *T. bottae* has an average digging frequency (i.e., limb cycling frequency) that ranges from 13-17 Hz, whereas *C. penicillatus* average 17–21 Hz and *D. Merriami* and has the highest limb cycling frequency among these three species at 20–24 Hz (Crisp et al., 2019). K-rats and pocket mice appear to compensate for reduced MA by cycling their forelimbs more rapidly during burrowing.

c. Muscle fiber architecture

Muscle architecture is defined as the arrangement of fibers relative to the muscle line of action (Williams et al., 2008). There are two main fiber architectures: pennate- and parallel-fibered muscles. Pennate muscles have fascicles (bundles of muscle fibers) that are attached obliquely to the tendon of insertion or a tendinous inscription(s) that run throughout the muscle belly. The angle at which the fascicles are arranged relative to the long axis fascial plane or intramuscular tendon tissue is known as pennation angle and this metric typically ranges from 0° to 45° under resting conditions. However, when muscles are recruited to produce active force and perform mechanical work, this causes fibers to

rotate about their origin, and thus pennation angle changes as muscles shorten during contraction (Gans, 1982, Azizi et al., 2008). By definition, pennate-fibered muscles have resting pennation angles that range from 15 to 45° (Zajac, 1989, 1992). Assessment of muscle architecture properties involves measurement of the resting pennation angle of the fascicles, in addition to fascicle length, muscle belly length, and muscle belly mass.

In general, the magnitude of force produced by pennate-fibered muscles is larger than that of parallel-fibered muscles. This is because fiber pennation corresponds with shorter fascicles, which in turn, allows for a greater number of muscle fibers per unit area of muscle tissue (Gans, 1982, Azizi et al., 2008). Therefore, pennate muscles typically have greater physiological cross-sectional area (PCSA) than parallel-fibered muscles, and PCSA is proportional to the isometric force production capability of muscles (Alexander, 1984; Williams et al., 2008). Pennation then provides an advantage for large force production capacity per gram of muscle tissue, but pennate-fibered muscles are less capable of performing mechanical work and power (Gans, 1982; Azizi et al., 2008).

Muscle pennation can be identified as one of three fiber architectures: unipennate, bipennate, and multipennate. Unipennate muscles have fascicles oriented in a single plane at some angle relative to the muscle line of action. Pennation angles are relatively low for unipennate muscles ranging from 15 to 25°. Bipennate muscles have fascicles oriented at some angle relative to the muscle line of action on both sides of a central tendon within the muscle belly that is continuous with its insertion. Pennation angles of bipennate muscles are typically larger than those of unipennate muscles (e.g., 20–35°). Multipennate muscles have multiple divisions of fascicles throughout the muscle belly that are separated by numerous tendinous inscriptions. Pennation angles are observed to be relatively high for multipennate muscles and can range from 25 to 45° (Gans, 1982, Zajac, 1989, 1992; Azizi et al., 2008). Multipennate muscles have short fascicles and large PCSA. The m. subscapularis, a scapular stabilizer muscle, is an example of a muscle that is almost universally multipennate in mammals.

Parallel-fibered muscles have long fascicles that run the majority of the muscle belly length (Lieber, 2002), and by definition, have fascicles orientated at low angles from 0 to 15° relative to the long axis of the muscle (Zajac, 1989, 1992). The shape of parallel-fibered muscles can be divided into three categories: strap, fusiform, and fan-shaped (Gans, 1982).

Interestingly, the m. biceps brachii is often described as fusiform by shape and yet it is a unipennate muscle in numerous mammalian taxa. Fascicles that are arranged in parallel to the line of action provide the advantage of shortening ability (i.e., contractile excursion) and velocity of contraction, which is proportional to muscle fascicle and/or fiber length. Generally, parallel-fibered muscles have a larger capacity for performing work and power than pennate-fibered muscles, but they are less capable of producing large force. Parallel muscles with long fascicles are thusly specialized for fast movements or extensive movements requiring a large ROM at the limb joints.

Complete measurements of muscle architectural properties include: muscle moment arm length (r_m), muscle mass (MM), belly length (ML), fascicle length (L_F), pennation angle (θ), and PCSA. Specifically, PCSA is the most important architectural property and it can be calculated with the following equation:

$$(V/L_F) \times \cos \theta, \qquad \text{EQ.2}$$

where V is muscle volume (in g/cm^3), L_F is mean fascicle length, and θ is mean pennation angle in degrees. While PCSA is typically larger in pennate-fibered muscles, it is important to recognize that parallel-fibered muscles with large mass can also have large PCSA due to the use of volume (mass and volume are related by density) in its calculation. Nonetheless, direct calculation of PCSA from measured linear geometric dimensions allows for estimation of several function capacities of muscles including: isometric force (F_{max}), maximal joint torque (at a joint angle of ~90°), and instantaneous muscle power (P_{inst}) (see Materials and Methods, subsection *Architectural Properties/Quantifications*).

Several architectural indices (AI) also provide information on capacities of muscle function. Fascicle length to muscle length (L_F/ML) ratio predicts shortening velocity ability. A L_F/ML close to 1.0 indicates large contractile excursion instead of force due to long fascicles. Another important ratio is fascicle length to muscle moment arm length (L_F/r_m). The smaller the ratio calculated, the greater the MA of a muscle-tendon unit (MTU) at a joint for large force output. In contrast, a L_F/r_m greater than 2–3 indicates greater joint excursion per change in muscle fascicle length. MTU with large L_F/r_m ratios can move joints and limb segments through large RoM.

Burrowing and non-burrowing sciurids have previously been shown to have large PCSA in their proximal limb muscles to act to retract the forelimb during the power stroke of

scratch-digging (Lagaria and Youlatos 2006). Specifically, the massive m. latissimus dorsi was reported to have the largest PCSA among the limb retractors while the well-developed and bi-articular long head of triceps brachii (also a limb retractor/shoulder flexor) had the largest PCSA of the extensor muscles inserting at elbow joint. In the distal forelimb, the m. flexor digitorum profundus had the highest PCSA of the carpal and digital flexors (Lagaria and Youlatos 2006). All three of these muscles are important to out-force (torque) application to the substrate. These findings generally correspond with those of Rupert et al. (2015) which evaluated forelimb architectural properties in groundhogs (*Marmota monax*) and found that most extrinsic muscles of the forelimb were parallel-fibered with long fascicle lengths but had large mass. Thus, the mm. latissimus dorsi and pectoralis superficialis/profundus had large L_F/ML and L_F/r_m ratios indicating contractile excursion to retract the humerus (forelimb) during the power stroke of scratch-digging and could do this with appreciable force because of their elevated PSCA. It was also observed that intrinsic musculature became more pennate in the distal forelimb. For example, m. flexor digitorum superficialis (FDS) and profundus (FDP) were pennate-fibered muscles with the capacity to produce large force to keep the digits flexed while excavating soil (Rupert et al., 2015). Moreover, FDS and FDP can apply appreciable flexor torque at the carpals joint and function could supplement low force produced by the mm. flexor carpi radialis (FCR) and ulnaris (FCU). Similar to Lagaria and Youlatos (2006), the long head of m. triceps brachii in the groundhog was indicated to have a high force production based on its large PCSA, whereas the intrinsic shoulder muscles (e.g., m. subscapularis and m. infraspinatus) of groundhogs were characterized as stabilizing muscles because of their long fascicle lengths, and low PCSA and force capacity (Rupert et al., 2015).

Muscle architectural properties have not been quantified in either pocket gophers, K-rats, or pocket mice. However, the above observations from digging squirrels do provide expectations of muscle performance in burrowing *T. bottae*. With respect to K-rats and pocket mice, previous assessment of muscle fiber architecture in generalized rats and mice also may be insightful. As an example, Mathewson et al. (2012) reported large PCSA (i.e., force capacity) in the flexors and long fiber length (i.e., shortening capacity) in the extensors of the forelimb of the common house mouse (*Mus musculus*). The m. triceps brachii long head (TBLO) notably had a both large PCSA and long fascicle lengths

(Mathewson et al., 2012), which indicates that this muscle would produce more high power output. Hence, the TBLO may be one of the most important muscles in the forelimb of mice by providing propulsion for either running or burrowing. And while the forelimb of rats have not been investigated specifically for their muscle architectural properties, these metrics from laboratory rat hindlimbs were also found to large PCSA and long fascicles in the hip extensors and knee flexors for high power compared to their corresponding antagonist muscle groups (Eng et al., 2008). A similar suite of architectural properties may likewise be expected in rat forelimbs further suggesting that high power output for cycling the limb rapidly is common to rats and mice.

d. Diffusible Iodine-Based Contrast-Enhanced Computed Tomography

The most recent tool that functional morphologists are implementing to perform studies of fine internal tissue anatomy is diffusible iodine-based contrast-enhanced computed tomography (DICE-CT: Gignac et al., 2016; Dickinson et al., 2018, 2019; Nyakatura et al., 2019; Sullivan et al., 2020, Regnault et al., 2020). One of the main advantages of this technique is that it preserves anatomical structure thus allowing study of the entire animal specimen as a non-destructive protocol versus that of traditional dissection methods. A second advantage, and perhaps equally important, is that DICE-CT has the potential of increasing the accuracy of morphological measurements by 'digital dissection' in specimens that are too small or difficult to precisely dissect for quantification of musculoskeletal morphology. The level of resolution (up to 1 nm) of scans produced from DICE-CT can provide visualization of individual fibers from muscles that contribute to specific types of limb movements (e.g., scratch-digging), thus allowing for quantification of architectural properties from single fascicles consisting of fibers that would otherwise only be possible using a microscope and acid-digested (to break down collagen) muscle tissue mounted on slides. A third advantage is that CT (or μ-CT) scans produce relatively rapid, high-resolution 3D images of biological tissues. The 3D renderings of muscles at the levels of resolution possible by DICE-CT are currently allowing for more complete understanding how muscle tissue is organized (e.g., pennation of fascicles) and how it functions to produce force and limb segment movement.

The main parameters involved with DICE-CT are specimen size, density of the tissues to be stained-labeled, concentration of the iodine media, duration of iodine incubation, and

time course for CT scanning (see Materials and Methods, subsection *Digital dissection:* DICE-CT). There are a variety of specimen fixing and staining protocols that can be followed for DICE-CT, and the one chosen is often dependent on cost and availability of materials. Prior fixation of whole animal specimens and/or limbs (or tissue) is standard by use of formalin (or formal-alcohol), but can vary in formulation depending on the taxon being studied and focus of the study. The typical protocol requires concentration of 10% fixative (Gignac et al., 2016). Tissue incubation with iodine can follow either diffusion-based or perfusion-based solution protocols. Lugols iodine is the most commonly used staining-labeling solution as it has the potency to completely permeate a range biological tissues efficiently, as well as its effectiveness for a range of animal body sizes that is can stain. Specifically, incubations in Lugols iodine labels muscle tissue well and at intermediate rates, where it can take hours-to-months to stain an animal depending on the overall size and region of the body being stained (Gignac et al., 2016; Dickinson et al., 2018, 2019; Nyakatura et al., 2019; Sullivan et al., 2020).

Tissue staining protocol requires tinted glass jars and periodic solution exchanges as the color of the Lugols iodine changes to that of a "weak tea" appearance. Tissue shrinkage from staining is common but can be prevented/minimized by adding sucrose to the incubations or by pre-incubating biological tissue in a 10% sucrose solution (Dickinson et al., 2019). Staining must reach the center of the tissue before making final CT scans, although imaging can be done during the staining process to verify that an entire region of tissue has been permeated without over-staining (Gignac et al., 2016). It is also important to note that pre-scans via CT of the specimen or limbs are necessary if imaging of bones is desirable. Completed iodine incubations do very well to contrast levels of tissue (muscle, tendon, connective tissue) but do not permeate bone tissue, and readily mask it on DICE-CT scans.

The resolution of CT scanners is variable and this will determine the total amount of time that the animal or region of its anatomy (e.g., limb) remains in the scanner to obtain images. Size of the whole animal or anatomical specimen also determines the length of time spent in the CT scanner, where scan time can range from minutes to hours. Images at a specified resolution (10-20 μm is most common) are captured in stacks using imaging software. Images can include markers to be displayed at areas of interest (e.g., muscle

attachment sites and joint centers of rotation) in order to make all necessary muscle architectural measurements.

As indicated above, DICE-CT is becoming more ubiquitous because of the advantages of digital dissection, nondestructive protocols, and potentially more accurate measurements due to the muscles remaining in their *in situ* state. Nonetheless, there are some disadvantages to employing this technique for morphometric analyses. Specifically, adjustments still need to be made to the software algorithms coded for the analysis of the muscle architectural properties measured from DICE-CT. But, a recent study on the jaw muscle fascicles of a crab eating macaque compared the results of traditional (or blunt) dissection to muscle geometry assessed from DICE-CT found similar (and reliable) results for fascicle lengths, pennation angles, and PCSA using Avizo 8.0 software for visualization and measurement (Dickinson et al., 2019). In second study (Nyakatura et al., 2019), muscle architecture properties were quantified using DICE-CT on a comparative muscle dataset from the hindlimbs of arboreal-to-fossorial squirrels. The fossorial squirrels had muscle with generally large pennation angles and PCSA thus giving them the capacity for high production, whereas the hindlimb musculature of most arboreal squirrels sampled were found to have long fascicles favoring greater muscle excursion, and coupled with their large volume, these muscles have the capacity for high power output (Nyakatura et al., 2019). Last, a novel report by Regnault et al. (2020) evaluated muscle architecture properties of the shoulder muscles in semi-fossorial short-beaked echidna (*Tachyglossus aculeatus*). Using a combination of DICE-CT and blunt dissection to measure the fascicle lengths and calculate PCSA, they showed that almost all muscles sampled were parallel-fibered and with relatively long fascicles (i.e., simplified and conservative muscle fiber architecture). Accordingly, PCSA of the forelimb musculature was low-to-moderate compared to other sprawling, fossorial taxa previously analyzed (Regnault et al., 2020). For example, scapular stabilizers such as the mm. infraspinatus and supraspinatus were characterized as low force producing over a moderate range of scapular motion in echidnas, which have less scapular excursion compared with fossorial digging rodents. These two muscles in the latter taxa typically have short fascicles and high pennation angles resulting in large PCSA (Regnault et al., 2020).

Using the sympatric species *T. bottae*, *D. Merriami,* and *C. penicillatus*, DICE-CT

would provide high-resolution images for quantification of the linear geometric measurements that can also be measured with traditional (blunt) dissection. Similar high success rates in the accuracy of fine measurements from biological tissues (Gignac et al., 2016), especially from small animals, are expected for the forelimb muscles of these three desert-dwelling rodents as it was shown in the muscles from other mammalian taxa in several recent studies using DICE-CT for quantification of architectural properties.

e. Myosin fiber types/Myosin Heavy Chain

There are four different adult isoforms of myosin heavy chain (MHC) expressed in the skeletal muscles of mammalian limbs and they are primarily identified by their rate of ATP hydrolysis. The following isoforms are listed in order of slowest-to-fastest contracting by their rate of ATP hydrolysis: MHC-1 (slow), MHC-2A (slowest fast), MHC-2X (intermediate fast), and MHC-2B (fastest) (Bottinelli, 2001; Toniolo et al., 2004). These MHC isoforms relate to a specific 'fiber type' by a common name of either slow-twitch (Type I) or fast-twitch (Type II) muscle fibers. Slow-contracting fibers utilize ATP at slow rates whereas fast-contracting fibers utilize ATP at fast rates, thus explaining the slow- and fast-twitch nomenclature. Moreover, by convention, MHC isoform fiber types are beneficial for specific functional roles. For example, slow MHC-I isoform fibers are useful for prolonged contractions (i.e., anti-gravity or postural muscles), whereas fast MHC-2A, -2X, or -2B isoform fibers are necessary for behaviors requiring greater levels of force (e.g., MHC-2A) or power (e.g., MHC-2X or -2B) (Lieber, 2002).

Rodents and humans alike express fast MHC-2X fibers. However, only small rodents and rabbits (the orders Rodentia and Lagomorpha are closely related by phylogeny) and marsupials express the fast MHC-2B isoform in their skeletal muscles (Mascarello et al., 2004). Expression of the fastest MHC isoform is partly dependent on body size and thermoregulation in mammals (Seow and Ford, 1991; Pellegrino et al., 2003). Interestingly, mammals of medium-to-large body size (including humans) have the MYH4 gene (Thomas et al., 2017), although a functional MHC-2B isoform protein is not translated in their skeletal muscles (Chikuni et al., 2004). Therefore, it is a misnomer that humans express Type IIB muscle fibers (Smerdu and Erzen, 2001; Scott et al., 2001). In this instance, 'fiber type' nomenclature and MHC expression are mismatched and Type IIB are MHC-2X isoform fibers, or know commonly known as 'Type IIX' fibers. Also notable is

the inverse scaling relationship fiber shortening velocity with body size, where velocity of shortening decreases for orthologous (i.e., same isoform, different species) MHC isoforms as body mass increases. For example, slow MHC-1 fibers of a rat contract significantly faster than MHC-1 fibers in a horse, and the relationship is most dramatic for the slow-contracting isoform (Toniolo et al., 2007). Indeed, large mammals have a broader distribution of slow-contracting MHC isoforms (Pellegrino et al., 2003) and this is related to their limited ability to dump body heat (i.e., low SA:Vol ratios). Decreases in shortening velocity, however, are more gradual for fast MHC isoforms and contraction and half-relaxation time for MHC-2X fibers are more similar to that of MHC-2A and -2B isoform fiber types across taxa (Schiaffino and Reggiani, 2011).

Intrinsic power generation shares a similar body size dependence with shortening velocity. This is because power is determined as the product of fiber shortening velocity and force. In general, slow MHC-1 fibers generate low force and power, while fast MHC-2A fibers generate modest force and power. MHC-2X fibers generate intermediate levels of force and power and MHC-2B fibers generate high force and power (Lieber, 2009). Power generation is closely related to thermoregulatory abilities because contraction of fast MHC isoform fibers generates more heat as a byproduct, which important to homeothermy and metabolism in small mammals. Hence, rodents can cycle their limbs quickly because of greater intrinsic power from fast MHC isoform expression. Muscle fiber metabolism is also related to 'fatigue resistance.' By convention, slow MHC-I fibers have the greatest fatigue resistance and that of fast MHC-2X fibers is intermediate between MHC-2A and -2B isoform fibers (Schiaffino and Reggiani, 2011). Fatigue resistance, however, is less dependent on MHC isoform expression (Kohn, 2014; Spainhower et al., 2018) and is more dependent on functional use of muscles (i.e., functional adaptation), and how this factor co-varies with specific aerobic (oxidative) and anaerobic (e.g., glycolytic) muscle enzyme activities (Spainhower et al., 2018; in revision). Mitochondrial density is another critical factor in fatigue resistance in skeletal muscles (Lieber, 2009). For example, fast MHC-2X and -2B muscle fibers in rodents have elevated mitochondrial densities comparable to those in slow MHC-1 fibers in other, larger taxa, and thus can sustain high power output important to the mass-specific metabolism in small rodents (Lieber, 2009).

Beyond these considerations, the proportions of slow and fast MHC expressed vary among muscles (and species) and are ultimately dependent on function. A well-known example are distal muscles involved in postural (anti-gravity) activities that typically have larger proportions of slow-contracting fibers with greater oxidative potential, whereas proximal muscles involved in locomotion (i.e., acceleration) may have larger proportions of fast-contracting MHC of the glycolytic fiber type (Alverez et al., 2012; Schiaffino and Reggiani, 2011). Due to both the body size and functional habits of the three species of rodents reviewed herein, as well as the importance of use of their forelimbs for burrowing, the fast-contracting MHC isoforms are of particular interest with respect to rate at which the forelimbs are cycled during scratch-digging.

Several studies have evaluated fiber types in digging rodents (e.g., Goldstein, 1971; Rourke et al., 2004; Alvarez et al., 2012; Rupert et al., 2015). Goldstein et al. (1971) originally studied the heterogeneity of fiber types in burrowing spermophilus (ground squirrels), scapanus (moles), and eutamias (chipmunks). By correlating mass specific metabolic rate (animal with larger mass have lower mass-specific metabolic rates) and slow (red) vs. fast (white) fiber type distributions, larger rodents were expected to have more slow fibers, whereas smaller rodents were expected to have more fast fibers to meet the respective metabolic demands. Almost all the muscles sampled showed heterogeneity of red, intermediate, and white fiber types; however, rodents had predominantly slow-fast fiber types while moles showed a majority of fast fiber types.

South American caviomorphs (genus Ctenomys), in particular, are the most numerous species of all fossorial rodents (Reig et al., 1990) and are convergent with North American pocket gophers. Interestingly, tuco-tucos (e.g., *Ctenomys. talarum*) have relatively low limb MA similar to *D. merriami* and *C. penicillatus*, thus requiring these rodents to rely on a velocity rather than a mechanical advantage for scratch-digging performance. Alvarez et al. (2012) found >90% of muscle fibers in mm. teres major and triceps brachii lateral head of *C. talarum* were the fast, oxidative-glycolytic (FOG = MHC-2A) and fast glycolytic (FG = MHC-2X/2B) fiber types, where the percentage majority of fiber expressed in both muscles were type FOG (Alvarez et al., 2012). It is not uncommon for MHC-2A fibers to have metabolic properties that are more oxidative than slow MHC-1 fibers (Hepple et al., 2000; Ørtenblad, 2018; Spainhower et al., 2018). Similarly, a majority of fast MHC-2A

fibers were also found throughout the forelimb digging musculature of the common groundhog (*Marmota monax*: Rupert et al., 2015). In the limb retractors and elbow extensors of *M. monax*, relatively small percentages (<20%) of slow MHC-1 and fast MHC-2X isoform fibers were expressed, whereas distal carpal/digital flexors had relatively greater slow MHC-1 fibers with the lack of fast MHC-2X expression (Rupert et al., 2015). Notably, neither species expressed the fast MHC-2B, although MHC isoforms were not identified in the study by Alvarez et al. (2012). A final study examining MHC gene expression (mRNA) during hibernation in golden-mantled ground squirrels (*Spermophilus lateralis*: Rourke et al., 2004) conversely reported that MHC-2A had the lowest expression in fibers from the forelimb musculature. Instead, the majority of the forelimb muscles sampled in *S. lateralis* predominantly expressed MHC-2X, and in some muscles, a change in mRNA expression signaling an isoform transition (or shift) from fast MHC-2X to fast MHC-2B was observed due to the environmental stress of hibernation (Rourke et al., 2004).

The above combined results for digging taxa are remarkable considering that large distributions of MHC-2X and 2B isoform fibers are common to the limb muscles of small rodents such as rats and mice. In particular, fast MHC-2X and 2B comprise nearly 85% of the rat hindlimb (Eng et al., 2008) and mouse forelimb (Mathewson et al., 2012) with minimal expression of MHC-1 or appreciable expression in selected muscles only (e.g., m. soleus in rats). Muscle fiber type characteristics, however, have not been evaluated in pocket gophers, K-rats, and pocket mice. Again, the main muscle functional groups that are involved in scratch-digging include the limb retractors (shoulder flexors), elbow extensors, and carpal/digital flexors. Thus, it would be valuable to determine MHC isoform fiber type in extrinsic muscles such as the mm. latissimus dorsi and pectoralis (all heads), as well as that of the major intrinsic forelimb musculature, including but not limited to, m. deltoideus (all parts), m. teres major, m. triceps brachii, m. dorsoepitrochlearis, m. flexor carpi ulnaris, and m. flexor digitorum profundus. MHC expression and fiber type % found in *T. bottae*, *D. merriami*, and *C. penicillatus* is potentially an important factor for determining functional differences among these three species despite their observed similar lifestyles and behaviors (Moore-Crisp, 2018).

Objectives and Hypotheses

Rationale

Similar to pocket gophers, kangaroo rats, and pocket mice each burrow using their forelimbs as an important behavior for their survival in a harsh desert ecosystem. However, whereas *T. bottae* display typical musculoskeletal modifications for scratch-digging, the forelimbs of *D. merriami* and *C. penicillatus* are reduced and generalized, respectively, in their limb form. The fundamental question is how do kangaroo rats and pocket mice demonstrate scratch-digging performance similar or equal to that of pocket gophers? Recent functional data (Moore Crisp, et al., 2019) of digging performance indicate that the muscles of *D. merriami* and *C. penicillatus* may be specialized for short, rapid bursts of scratch-digging while those of *T. bottae* are better suited for prolonged burrowing. Moreover, some pocket mice were found to be capable of producing relatively larger out-force than both pocket gophers and K-rats (Moore-Crisp, 2018). These previous findings are possible only if the intrinsic properties of shoulder flexor and elbow extensor muscles of *D. merriami* and *C. penicillatus* are adapted for larger force and power by their architectural properties and expression of faster MHC isoform fibers compared with *T. bottae*. Thus, greater muscle force can compensate for reduced mechanical advantage (MA) of the forelimbs of *D. merriami* and *C. penicillatus*, and greater intrinsic muscle power would allow these two species to cycle their forelimbs at greater frequencies. The latter is also consistent with reduced MA of K-rat and pocket mice forelimbs, and instead, these taxa have an advantage for fast joint rotational velocity (Hildebrand, 1985; Stein, 2000).

The objective of this investigation is to quantify muscle architectural properties and MHC isoform expression in forelimbs of three burrowing rodents. To this end, diversity in functional use of rodent forelimbs for scratch-digging will be evaluated by a thorough comparative analysis of muscle properties to explain how three sympatric species survive by burrowing while each have marked differences in body form and forelimb size. It is **hypothesized** that the forelimb muscles of *D. merriami* and *C. penicillatus* have fast-contracting muscles related to powerful rapid bursts of scratch-digging that compensate for their overall lack of muscle development, whereas the pocket gophers will have stronger, slow-contracting muscles consistent with large limb MA. Three specific predictions are indicated below.

It is **predicted** that (1) the limb retractors, elbow flexors, and carpal/digital flexors of *D. merriami* and *C. penicillatus* will have a predominant expression of fast MHC-2X and -2B isoform fiber types, whereas those functional groups in pocket gophers will have a broader distribution of fast MHC-2A fibers. It is also predicted that (2) the muscles composing those three functional groups will have long fibers and a large capacity for shortening and excursion in *D. merriami* and *C. penicillatus*. The well-developed muscles of pocket gophers are expected to have greater degrees of fiber pennation with shorter fibers and larger PCSA that than observed in saltatorial K-rats and generalized pocket mice. A final prediction is that (3) there will be good consistency between muscle architectural properties measured using traditional (blunt) dissection versus digital DICE-CT techniques, but with greater accuracy reported via digital measurement, especially in the small muscle bellies of K-rats and pocket mice. With animals as small as pocket gophers, K-rats, and pocket mice, DICE-CT will be most beneficial for taking architectural measurements involving muscle pennation by overcoming limitations posed by obtaining measurements while working under a microscope.

Broad Physiological Perspective

Since pocket gophers, K-rats, and pocket mice all have small body sizes and their muscles must express a large distribution of fast-contracting fibers to maintain their core body temperature (i.e., stay warm). An outcome showing subtle differences among species could be further indicative of function specialization (or adaptation) of rodent limbs. This is especially critical for the requirement of greater intrinsic power to cycle their limbs at a fast rate while excavating their burrows. Along with their low basal (total) metabolic rates that aids in compensating for the high-energy demand in these rodents, the composition of the fast MHC fiber types (and high mitochondrial volume) works similarly to produce maximum efficiency in energy expenditure. This is important for these rodent taxa because the metabolic activity of the limb muscles in small animals is higher when compared to larger animals. Since their limbs are being cycled through the digging motions at a rapid frequency and at a high power output, ATP is consumed much faster and this accounts for the fast MHC fiber type isoforms expressed (Kleiber, 1947). Last, the reduced out-levers (i.e., relative forelimb length) in *T. bottae*, *D. merriami*, and *C. penicillatus* are additionally (equally) inconsistent with a high frequency of forelimb cycling thus necessitating that both

muscle architectural modifications in coordination with the isoform of fast MHC expressed translate into the observed performance.